UNIVERSITY OF PADOVA FACOLTÀ DI INGEGNERIA

PH.D. THESIS

Sede Amministrativa: Università degli Studi di Padova
Dipartimento di Ingegneria dell'informazione

DOTTORATO DI RICERCA IN:
INGEGNERIA ELETTRONICA E DELLE TELECOMUNICAZIONI
CICLO XX

Multiple Description Coding for Non-Scalable and Scalable Video Compression

Coordinatore: Ch.mo Prof. Silvano Pupolin
Relatori: Ch.mo Prof. Giancarlo Calvagno
Ch.mo Prof. Gian Antonio Mian

Dottorando: Ottavio Campana

Gennaio 2008

CORSO DI LAUREA IN INGEGNERIA
DELLE TELECOMUNICAZIONI

DIPARTIMENTO DI INGEGNERIA
DELL'INFORMAZIONE

to the memory of Gian Antonio Mian

Contents

Summary

Multiple Description Coding (MDC) techniques are based on dividing the input signal into several chunks of data called *descriptions*. Whenever all descriptions are correctly received the original signal is reconstructed, while in case some information is lost its content is estimated by exploiting the redundancy shared between all the descriptions and a coarse approximation of the signal is decoded.

Clearly, the main goal of MDC is to provide a method for joint source-channel coding, but it has a major characteristic that makes it different from many other techniques. In fact, many joint source-channel coding techniques rely on joint source channel optimization, thus given the knowledge of the transmission channel packet error rate they optimize the bitrate allocation in source and channel coding so that the quality of the decoded sequence is maximized. MDC techniques do not require the knowledge of the channel and the introduced redundancy is chosen starting from the source coding scheme and not from the channel coding strategy. This duality can be expressed as thinking that in the first case joint source channel coding is obtained starting form channel coding and successively jointly perform source coding, while in MDC attention if first paid to source coding and successively channel coding is taken into account. This aspect is indeed reflected in the channel agnosia that characterizes most MDC schemes.

MDC was proposed at the beginning of the 70s for the speech signal and is has been successively applied to many fields like video coding, data transmission, data storage and wireless sensors networks. The topic of this thesis is the application of MDC to non-scalable and scalable video coding.

In the first chapter, an introduction to MDC is given. This is necessary because basic results in MDC where never published, but they were only written in Bell Labs internal reports. Thus, accessing the basic theory is practically impossible, and most of results are only available in some old papers which not only reference those reports, but also reference their results. The chapter begins with a review of the first MDC scheme, known as the Jayant scheme and

from its performance analysis the MDC problem is formulated. Successively, after an introduction to classic Rate-Distortion theory, the MD Rate-Distortion theory is similarly derived and the Cover and El Gamal theorem is enunciated. Finally, some MD applications to video coding are presented.

In the second chapter, MDC schemes for the H.264/AVC coding standard are presented. The main purpose of this chapter is to summarize all the schemes that have been studied in the Signal and Image Image Processing Laboratory at University of Padova during the last years, because this research can be considered concluded. The proposed MDC schemes involve several aspects of the H.264/AVC encoder, in fact some of them exploit the spatial correlation of video sequences, others rely on temporal correlation and others work on the produced bitstream to generate the descriptions.

The third chapter is focused on Scalable Video Coding (SVC) and MDC. This research was performed while I was visiting the Video Processing Laboratory at University of California, San Diego and was supported in part by a scholarship from the "Fondazione A. Gini" (Padova, Italy). The proposed SVC scheme is not related to any existing standard, but it involves motion compensation of wavelet-decomposed frames to provide spatial, temporal and SNR scalability. The encoder structure is inspired by the *Responses of call for proposal for scalable video coding* of W. J. Han. The codec was completely written from scratch and by implementing the wavelet transform, the temporal prediction strategies, the bitplane coding algorithms and the MDC schemes. Finally the schemes performance are presented and the results are compared.

Sommario

La Codifica a Descrizioni Multiple si basa sulla divisione del segnale in ingresso al sistema di codifica in vari sottoinsiemi di informazioni, detti *descrizioni*. Quando tutte le descrizioni sono correttamente ricevute, il decodificatore è in grado di ricostruire il segnale originario, mentre se si verificano degli errori di trasmissione è possibile sfruttare la ridondanza condivisa tra tutte le descrizioni per stimare i dati persi e ricostruire una approssimazione del segnale originale.

Lo scopo principale della codifica a descrizioni multiple consiste nella trasmissione robusta dell'informazione fornendo delle tecniche di codifica congiunta sorgente e canale, ma ha delle peculiarità che le differenziano da molte altre tecniche di codifica congiunta. Infatti, la maggior parte delle tecniche proposte effettuano una ottimizzazione congiunta e perciò richiedono la conoscenza della statistica che caratterizza il canale di trasmissione. Conoscendo la statistica del canale è possibile decidere il partizionamento ottimo del bitstream tra la codifica di canale e di sorgente per massimizzare la qualità del segnale ricostruito. Al contrario, le tecniche di codifica a descrizioni multiple non richiedono la conoscenza del canale e la ridondanza introdotta dal processo di codifica viene scelta a partire dallo schema di compressione. Questa dualità può essere spiegata considerando che nel primo caso la codifica congiunta di sorgente e canale inizia dalla scelta della codifica di canale per poi ottimizzare la codifica di sorgente, mentre nel secondo caso per prima cosa viene considerata la compressione del segnale e la codifica di canale viene considerata successivamente. Questa inversione nell'approccio alla codifica congiunta si rispecchia nell'agnosia del canale che caratterizza la maggior parte degli schemi di codifica a descrizioni multiple.

La Codifica a Descrizioni Multiple è stata introdotta agli inizi degli anni settanta per la trasmissione del segnale vocale ed è stata applicata successivamente ad altri campi, quali ad esempio codifica video, trasmissioni numerica, archiviazione di dati e reti di sensori wireless. L'argomento di questa tesi è la Codifica a Descrizioni Multiple applicata alla codifica video scalabile e non.

Nel primo capitolo viene introdotta la Codifica a Descrizioni Multiple. Questa introduzione è resa necessaria dalla frammentazione della teoria, che specialmente all'inizio è stata sviluppata e pubblicata nei report interni dei Bell Labs e che quindi è difficilmente accessibile. Di conseguenza la maggior parte dei risultati teorici non sono direttamente accessibili, ma possono essere ritrovati in alcuni articoli che oltre a citare i report interni ne riportano anche i risultati. Il capitolo inizia con la presentazione del primo schema di codifica a descrizioni multiple, conosciuto anche come schema di Jayant, e dall'analisi delle sue prestazioni viene formulato il problema della Codifica a Descrizioni Multiple. Successivamente, dopo un richiamo alla teoria classica di Rate-Distortion, la teoria Rate-Distortion per la Codifica a Descrizioni Multiple viene presentata e viene enunciato il teorema di Cover ed El Gamal. Per finire sono illustrate alcune applicazioni per la codifica video.

L'argomento del secondo capitolo è costituito dalla codifica video non scalabile e dagli schemi sviluppati per lo standard di codifica H.264/AVC. Lo scopo principale di questo capitolo è di riassumere tutti i risultati della ricerca sviluppata nel corso degli anni presso il Laboratorio di Elaborazione dei Segnali e delle Immagini dell'Università di Padova e che si può ormai considerare conclusa. Gli schemi proposti coprono aspetti anche distinti del codificatore H.264/AVC, infatti alcuni sfruttano la ridondanza spaziale delle sequenze video, altri invece si basano sulla ridondanza temporale e altri ancora lavorano direttamente sul bitstream compresso prodotto dal codificatore.

Per finire il terzo capitolo è rivolto alla Codifica Video Scalabile e alla Codifica a Descrizioni Multiple ad essa applicata. Questa ricerca è stata svolta durante il periodo di scambio all'estero presso il Video Processing Laboratory dell'Università della California, San Diego, ed è stata supportata in parte da una borsa di studio della "Fondazione A.Gini" di Padova. Lo schema di codifica video scalabile non è basato su alcuno standard, ma sfrutta la moto compensazione di frame decomposti mediante le wavelet per fornire scalabilità spaziale, temporale e in qualità. La struttura del codificatore è stata ispirata dalla *Responses of call for proposal for scalable video coding* di W. J. Han. Il codificatore è stato scritto completamente in C, a partire dalla trasformata wavelet, la decomposizione per la motocompensazione e gli algoritmi per la codifica a piani di bit e compressione delle immagini e dei residui. Per finire le prestazioni dei vari schemi di codifica a descrizioni multiple per il codificatore vengono presentate e confrontate.

Chapter 1

Introduction

The main goal of *source coding* consists in representing the information with the minimum number of bits, in order to reduce the required bandwidth. Thus, more parallel transmissions are feasible, even without any change to the network, which might not be easily done because of technological limits or economical constraints.

By reducing the bitstream size and by rising the coding efficiency, the major drawback quickly becomes visible: compressed data more likely suffers transmission errors than uncompressed information, because errors propagate in encoded data. As an example, when samples are encoded by using prediction, a valid reference is indispensable for flawless reconstruction.

In order to guarantee the reconstructed signal quality, several *channel coding* techniques were developed. All these techniques add redundancy to enhance transmission robustness with respect to channel errors.

Even though source and channel coding are dual problems, they have been considered as separated topics for many years. Video coding standards such as MPEG-1, MPEG-2, H.263 or the latter H.264/AVC where developed by focusing only on compression efficiency and by abstracting the transport characteristics, relying on an adaptation layer to properly adapt the compressed bitstream for transmission or storage. This strategy was mainly supported by Shannon's source-channel separation theorem.

Definition 1 *Let X be a discrete random variable with alphabet $\mathcal{X}$ and probability mass function $p(x) = P\{X = x\}, x \in \mathcal{X}$. The entropy $H(X)$ of a discrete random variable X is defined by*

$$H(X) = -\sum_{x \in \mathcal{X}} p(x) \log p(x). \tag{1.1}$$

Definition 2 *Consider two random variables X and Y with a joint probability mass function $p(x,y)$ and marginal probability mass functions $p(x)$ and $p(y)$. The mutual information $I(X;Y)$ is the relative entropy between the joint distribution and the product distribution $p(x)p(y)$:*

$$I(X;Y) = \sum_{x\in\mathcal{X}} \sum_{y\in\mathcal{Y}} p(x,y) \log \frac{p(x,y)}{p(x)p(y)} \tag{1.2}$$

Definition 3 *A discrete channel is a system consisting of an input alphabet $\mathcal{X}$, an output channel $\mathcal{Y}$ and a probability transition matrix $p(y|x)$ that expresses the probability of observing the output symbol y given that the symbol y was sent. The channel is said to be memoryless if the probability distribution of the output depends only on the input at that time and is conditionally independent of previous channel inputs or outputs.*

Definition 4 *The "information" channel capacity of a discrete memoryless channel is defined as*

$$C = \max_{p(x)} I(X;Y) \quad , \tag{1.3}$$

where the maximum is taken over all possible input distributions $p(x)$.

Capacity is bounded to the channel statistic, which can be expressed in terms of Signal-to-Noise Ratio (SNR). For example, in case of a binary symmetric channel, it can be shown that $I(X;Y) \leq 1 - H(p)$, where p is the probability of transmission error and depends on the adopted modulation and noise power.

Given these definitions, the Shannon's source-channel coding theorem can be stated:

Theorem 1 *(Source-channel coding theorem): If $\mathcal{X} = \{\mathcal{X}_1, \mathcal{X}_2, \cdots, \mathcal{X}_n\}$ is a finite alphabet stochastic process that satisfies the AEP, then there exists a source channel code with $P_e^{(n)} \to 0$ if $H(\mathcal{X}) < C$.*
Conversely, for any stationary stochastic process, if $H(\mathcal{X}) > C$, the probability error is bounded away from zero, and it is not possible to send the process over the channel with arbitrarily low probability of error.

To guarantee optimality, this theorem requires the channel capacity to be big enough to hold the compressed bitrate. This reflects in SNRs sufficiently high to guarantee the needed capacity. The theorem was stated for unicast channel, but it has been successively extended to the broadcast channel, and in this case the capacity is in general further reduced. Moreover, the theorem result is achieved asymptotically, so it may be possible that a practical joint source/channel coding techniques are preferable to separate schemes

Multiple Description Coding (MDC) [Goy01a] techniques can be generally classified as joint source channel coding, even though they do not often consider the channel statistics. In fact, MDC techniques do not require the knowledge of the channel and the introduced redundancy is chosen starting from the source coding scheme and not from the channel coding strategy. Nevertheless, they try to enhance transmission robustness by dividing the input signal into chunks of data called *descriptions* and by exploiting the channel diversity for transmission. At the receiver, whenever all the descriptions are correctly received, the original signal is reconstructed, while in case of information loss, the correlation between the descriptions is exploited to estimated the lost information and to reconstruct an approximation of the original signal.

By dividing the original signals into several descriptions, only suboptimal compression ratios are achieved, because additional redundancy is introduced. Fortunately, this additional information is exploited to reconstruct the signal in case of transmission errors, and has the same role of channel coding when optimality is guaranteed by the separation theorem. Therefore, MDC techniques represent a strategy that can be exploited when the source-channel separation theorem does not hold or cannot be applied.

1.1 The channel splitting scheme

We do now introduce one of the first known MDC schemes, the channel splitting scheme. Due to its simplicity, this scheme is an easily understandable example, which can be used to introduce basilar concepts necessary to evaluate more complex MDC schemes.

This scheme was developed at the end of the 1970s at the Bell laboratories. In [Ger79] the idea at the basis of the splitting channel scheme is attributed to W. S. Boyle, while in [Mil80] it is referred also to Miller, who also filled a patent for this scheme [Mil83].

The problem that researchers at Bell Labs had to solve was related to the faults of the telephone systems transmission lines. At the time, too many breakdowns in the telephone system were reducing the telephone network reliability. To reduce the number of interrupted calls, a transmission system based on two lines was proposed. After input speech signal sampling, coefficients were split into even and odd ones, thus obtaining a sub-sampling of a factor 2. These two sets of samples were independently encoded by using

Differential Pulse Code Modulation (DPCM) and transmitted to the receiver, as shown in Figure (1.1).

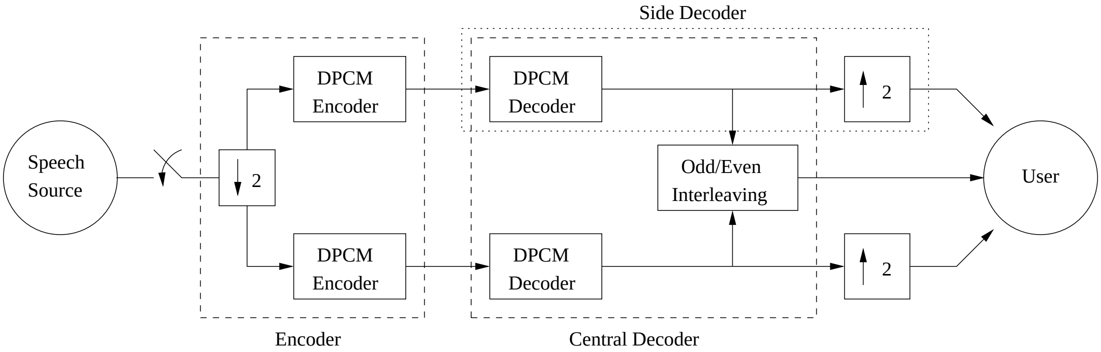

Figure 1.1: Channel splitting scheme: after input signal quantization, two sub-sampled sample sets are generated and independently encoded. The user can receiver the full-rate signal obtained by the central decoder or in case of line fault an approximation of the original signal output by one of the side decoders.

The decoder of the channel splitting scheme consists of three different parts. For each line connected to it, it has a DPCM decoder followed by an interpolator. These two blocks compose the two *side decoders*, which reconstruct the signal by exploiting the information obtained from only one of the two lines. Samples from the DPCM decoders are also fed to Odd/Even Interleaving block, which merges together the two streams and therefore reconstructs the original speech signal. The DPCM blocks and the interleaver compound the *central decoder*, which is the preferred decoder under normal circumstances.

Thus, the decoder can dynamically switch its output between the central and the side decoders, continuously providing the telephone service even when a breakdown happens.

In the scheme proposed by Jayant, the source is sampled at 12 kHz, hence obtaining two sub-sampled streams at 6 kHz, whose aliasing has reduced power, since the speech signal is usually band-limited to 3.2 kHz. Perceptual testing has shown that by using 5 bits/sample the reconstructed signal quality is considered good even in case of errors or faults. Nevertheless, interesting considerations can be extracted from analytical study of the channel splitting scheme.

Suppose that the speech source can be approximated by a Gauss-Markov process defined by the following discrete-time equation

$$x[k] = \rho x[k-1] + w[k] \tag{1.4}$$

where $k \in \mathbb{Z}$, $x[k]$ are the source samples and $w[k]$ are i.i.d., zero mean Gaussian random variables and $|\rho| < 1$. The correlation between two source samples is given by ρ, and by imposing $w \in \mathcal{N}(0, 1-\rho^2)$ we obtain that the Gauss-Markov process has unit power. Under these assumptions, the distortion-rate function for the given process can be easily evaluated and gives

$$D(R) = \left(1-\rho^2\right) 2^{-2R} \;\; for \;\; R \geq log_2\left(1+\rho\right) \tag{1.5}$$

After description generation, the sub-sampled processes can be described by

$$x[k] = \rho\left\{\rho x[k-2] + w[k-1]\right\} + w[k]. \tag{1.6}$$

Hence the new random processes have now a correlation between samples given by ρ^2. Since $\|\rho\| < 1$, the $x[k]$ succession are less correlated and harder to compress. In fact, the distortion-rate function of the central decoder is now given by

$$D_{central}(R) = \left(1-\rho^4\right) 2^{-2R} \;\; for \;\; R \geq log_2\left(1+\rho^2\right). \tag{1.7}$$

The increased temporal distance of the source samples causes an efficiency loss that can easily be evaluated as

$$\frac{D_{central}(R)}{D(R)} = \left(1+\rho^2\right). \tag{1.8}$$

Similarly, the distortion-rate function of the side decoders can be evaluated remembering that when a side decoder is used than half of the samples will be correctly reconstructed and therefore the same distortion as in the central decoder will corrupt them. By reconstructing the missing samples with the average of the two adjacent correctly received samples, the introduced distortion is

$$D_{interpolation}(R) = (1-\rho)^2 + \frac{1}{2}\left(1-\rho^2\right) + \omega D_{central}(R) \tag{1.9}$$

where D_q is the variance of the quantization error and $\omega \in [0,1]$. To evaluate the distortion-rate function it is necessary to average the central and side decoder distortion, obtaining

$$D_{side}(R) = \frac{1}{2}\left[(1-\rho)^2 + \frac{1}{2}\left(1-\rho^2\right)\right] + \frac{1+\omega}{2} D_{central}(R). \tag{1.10}$$

Two terms appear in Equation (1.10), the first is related to the interpolation error, while the second one is related to quantization error. The latter, even in the worst case of $\omega = 1$ is strictly decreasing when the rate increases, while the first does not change by varying the rate. This limitation, imposed by the interpolation filter, heavily reduces the scheme performance.

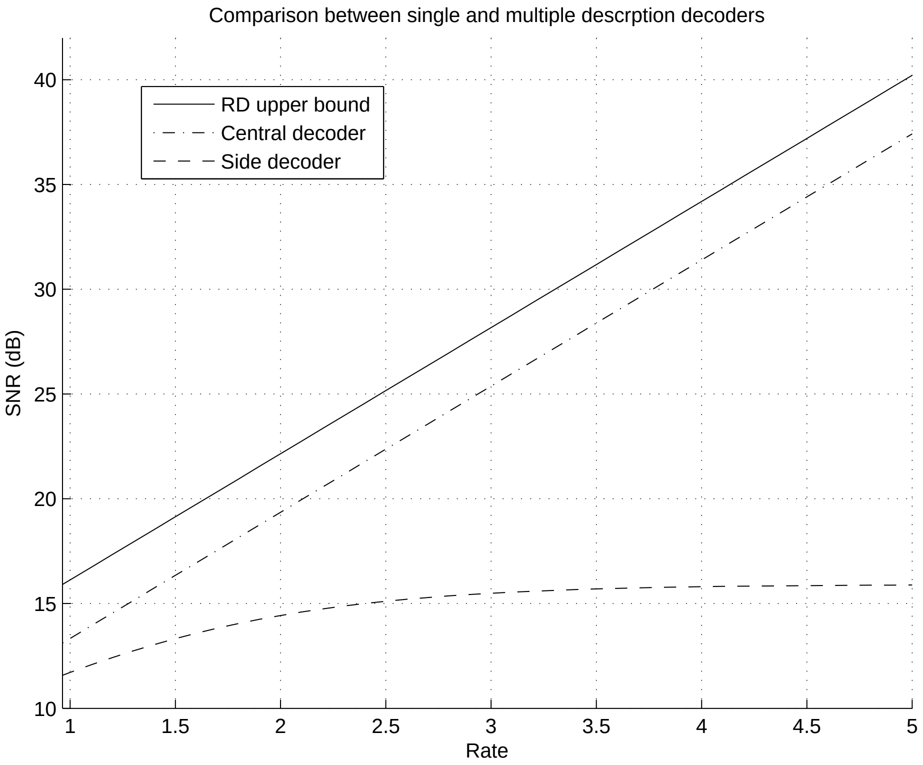

Figure 1.2: Performance of the channel splitting scheme for $\rho = 0.95$ and $\omega = 0.8$. The SNR provided by the central and side decoder is compared to the theoretical bound for the single description encoder. The distance of the curve of the central decoder from the RD upper bound represents the efficiency loss. The distance between the central and side decoder curves shows the quality loss in case of a line fault.

In Figure (1.2), the performance of the single and multiple description encoders is shown. The parameters used in this simulation are $\rho = 0.95$ and $\omega = 0.8$. Source samples in the channel splitting scheme are less efficiently encoded because of their greater distance. This efficiency loss can be seen in the figure, where the multiple description encoder requires one half bit more to obtain the same quality and at the same bitrate loses 3 dB in terms of PSNR. The side decoders performance trend is not able to follow the other curves because of the first term of Equation (1.10).

Further observations can be obtained by comparing the single and multiple description coding scheme in case of line fault. To provide fair comparison, we let the single description encoder work at halved bitrate, even though in case of fault no signal is transmitted. By plotting the performance of the two schemes in terms of SNR, as in Figure (1.3), we can easily see that for low bitrates, i.e. rate $\leq$ 2.7 , the channel splitting scheme gives better performance than the traditional DPCM coding strategy.

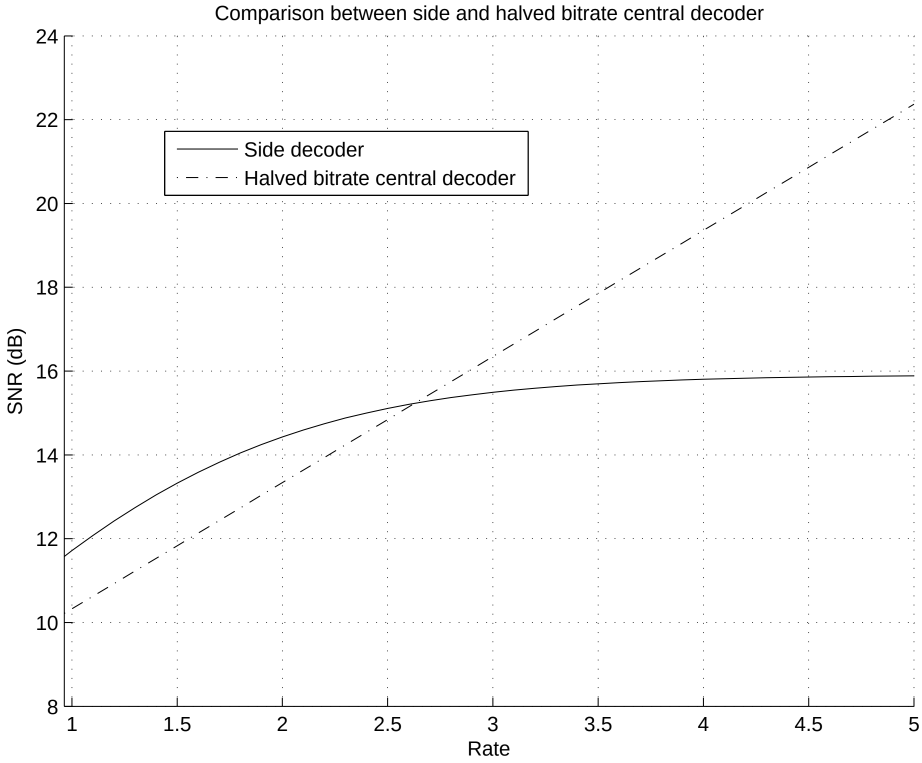

Figure 1.3: Comparison between the channel splitting encoder in case of fault and a halved bitrate single description encoder for $\rho = 0.95$ and $\omega = 0.8$. The multiple description encoder is able to outperform the single description encoder for low bitrates, but its horizontally asymptotic trend gives poorer performance at high bitrates.

This comparison suggests than depending on the available bitrate, different MDC schemes can be the optimal solution. From this latter comparison, we can evince that in case of small bandwidth the decoder is able to better reconstruct the missing samples by averaging those correctly received. Whenever more bandwidth is available, this assumption does not hold any more and the halved precision of each sample leads to better quality. Obviously, even though we can identify in the figure a precise crossing point, this performance overtake is not immediate. In fact, it would require a very efficient quantization scheme where each sample bits could be divided into two sets and carry exactly half of the information. This would imply that no redundancy would be introduced by this hypothetical scheme. Although such a scheme does not exists, Vaishampayan [Vai93b] proposed the Multiple Description Scalar Quantizer, which gives similar results. This quantizer will be introduced in the following chapter, when presenting its application to multiple description video coding for the H.264/AVC coding standard.

1.2 The MD RD region

The last comparison in the previous section poses a very important question: what is the way to compare two MDC schemes? How can coding efficiency and robustness be jointly considered to easily identify effective codecs? In this section we recall some definitions from the rate distortion theory by following [CT06] and successively extend them to the multiple description case.

To be able to define comparisons, in the single description case we usually define a distortion function. Assume that we have a source producing a vector $X_1, X_2, \cdots, X_n$ of independent identically distributed random variables. The encoder describes the source vector X^n by an index $f_n(X^n) \in \{1, 2, \cdots, 2^{nR}\}$, while the decoder represents X^n by an estimate $\hat{X}^n$, as illustrated in Figure (1.4)

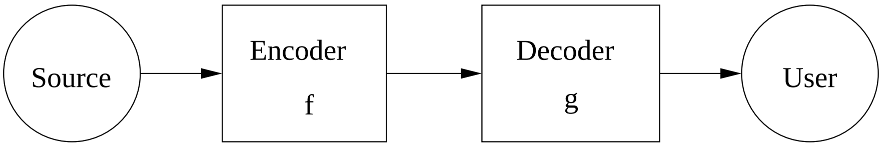

Figure 1.4: Rate distortion encoder and decoder.

Definition 5 *A distortion function is a mapping*

$$d : \mathcal{X} \times \hat{\mathcal{X}} \rightarrow \mathbb{R}^+ \tag{1.11}$$

from the set of (source alphabet, reproduction alphabet) pairs into the set of non negative real numbers.

In other words, the distortion $d(x, \hat{x})$ is a measure of the cost of representing the original symbol x by the symbol $\hat{x}$. The most popular distortion measure for continuous alphabets is the *squared-error distortion*

$$d(x, \hat{x}) = (x - \hat{x})^2 \tag{1.12}$$

because of its simplicity and its relationship to least-squares prediction. This distortion measure can be extended to be defined on vectors of symbols as

Definition 6 *The distortion between the vectors x^n and $\hat{x}^n$ is defined by*

$$d(x^n, \hat{x}^n) = \frac{1}{n} \sum_{i=1}^{n} d(x_i, \hat{x}_i) \tag{1.13}$$

Definition 7 *A $(2^{nR}, n)$-rate distortion code consists of an encoding function*

$$f : \mathcal{X}^n \to \{1, 2, \cdots, 2^{nR}\} \tag{1.14}$$

and of a decoding function

$$g : \{1, 2, \cdots, 2^{nR}\} \to \hat{\mathcal{X}}^n. \tag{1.15}$$

The distortion associated to this $(2^{nR}, n)$ code is

$$D = E\left[d(X^n, g(f(X^n)))\right] = \sum_{x^n} p(x^n) d(x^n, g(f(x^n))) , \tag{1.16}$$

where the set of n-tuples $g(1), g(2), \cdots, g(2^{nR})$, denoted by $\hat{X}^n(1), \hat{X}^n(2), \cdots, \hat{X}^n(2^{nR})$ constitutes the *codebook* and $f^{-1}(1), f^{-1}(2), \cdots, f^{-1}(2^{nR})$ are the associated *assignment regions*.

Definition 8 *A rate distortion pair (R, D) is said to be* achievable *if there exists a sequence of $(2^{nR}, n)$-rate distortion codes (f, g) with*

$$\lim_{n \to \infty} E\left[d(X^n, g(f(X^n)))\right] \leq D.$$

By having defined achievability for a given (R, D) pair, we can finally the rate distortion region and function as follows:

Definition 9 *The* rate distortion region *for a source is the closure of the set of the achievable rate distortion pairs (R, D).*

Definition 10 *The* rate distortion function *$R(D)$ is the infimum of rates R such that (R, D) is in the rate distortion region of the source for a given distortion D.*

Definition 11 *The* distortion rate function *$D(R)$ is the infimum of all distortions D such that (R, D) is in the rate distortion region of the source for a given rate R.*

In the multiple description case, similar definitions can be given. The main difference now lies in the substitution of the (R, D) pair with the $(R_1, R_2, D_0, D_1, D_2)$ quintuple and in defining several encoding and decoding function. In fact, in the MD case a specific rate is assigned to each generated description, and the receiver side chooses to decode the original signal by using all the information or only an approximation of it, by relying on a subset of he transmitted information. In Figure (1.4) an example of MDC scheme with two descriptions is shown. We will obtain for it equations similar to those for the single description case, but they can be similarly obtained for an undefined number of descriptions.

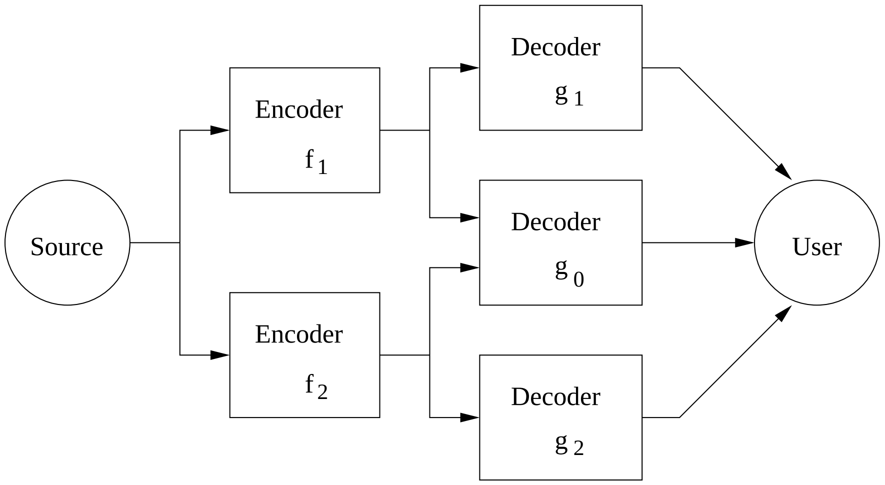

Figure 1.5: Multiple description rate distortion encoder and decoder.

Definition 12 *A $(2^{nR_1}, 2^{nR_2}, n)$-rate distortion code consists of two encoding functions*

$$f_1 \; : \; \mathcal{X}^n \rightarrow \{1, 2, \cdots, 2^{nR_1}\} \tag{1.17}$$
$$f_2 \; : \; \mathcal{X}^n \rightarrow \{1, 2, \cdots, 2^{nR_2}\} \tag{1.18}$$

and of three decoding functions

$$g_0 \; : \; \{1, 2, \cdots, 2^{nR_1}\} \times \{1, 2, \cdots, 2^{nR_2}\} \rightarrow \hat{\mathcal{X}}_0^n \tag{1.19}$$
$$g_1 \; : \; \{1, 2, \cdots, 2^{nR_1}\} \rightarrow \hat{\mathcal{X}}_1^n \tag{1.20}$$
$$g_2 \; : \; \{1, 2, \cdots, 2^{nR_2}\} \rightarrow \hat{\mathcal{X}}_2^n \tag{1.21}$$

where $\mathcal{X}_0^n$ is the central decoder codebook and $\mathcal{X}_1^n$ and $\mathcal{X}_2^n$ are the codewords sets of the side decoders. Since the reconstruction level is not unique any more, three distortion functions have to be defined, one for each possible reconstruction of the sequence:

$$d_0(x^n, \hat{x_0}^n) = \frac{1}{n}\sum_{i=1}^{n} d(x_i, \hat{x}_{0i}) \tag{1.22}$$

$$d_1(x^n, \hat{x_1}^n) = \frac{1}{n}\sum_{i=1}^{n} d(x_i, \hat{x}_{1i}) \tag{1.23}$$

$$d_2(x^n, \hat{x_2}^n) = \frac{1}{n}\sum_{i=1}^{n} d(x_i, \hat{x}_{2i}) \tag{1.24}$$

where $\hat{x}_{0i} \in \mathcal{X}_0$, $\hat{x}_{1i} \in \mathcal{X}_1$ and $\hat{x}_{2i} \in \mathcal{X}_2$. The distortions associated to this code are

$$\begin{aligned} D_0 &= E\left[d\left(X^n, g_0\left(f_1(X^n), f_2(X^n)\right)\right)\right] \\ &= \sum_{x^n} p\left(x^n\right) d\left(x^n, g_0\left(f_1(x^n), f_2(x^n)\right)\right) \end{aligned} \tag{1.25}$$

$$\begin{aligned} D_1 &= E\left[d\left(X^n, g_1\left(f_1(X^n)\right)\right)\right] \\ &= \sum_{x^n} p\left(x^n\right) d\left(x^n, g_1\left(f_1(x^n)\right)\right) \end{aligned} \tag{1.26}$$

$$\begin{aligned} D_2 &= E\left[d\left(X^n, g_2\left(f_2(X^n)\right)\right)\right] \\ &= \sum_{x^n} p\left(x^n\right) d\left(x^n, g_2\left(f_2(x^n)\right)\right) \end{aligned} \tag{1.27}$$

Finally, we can give the last definition before defining the Multiple Description Rate Distortion region.

Definition 13 *A rate distortion quintuple $(R_1, R_2, D_0, D_1, D_2)$ is said to be* achievable *if there exists a $(2^{nR_1}, 2^{nR_2}, n)$-rate distortion code $(f_1, f_2, g_0, g_1, g_2)$ with*

$$\lim_{n\to\infty} E\left[d(X^n, g_0(f_1(X^n), f_2(X^n)))\right] \leq D_0 \tag{1.28}$$

$$\lim_{n\to\infty} E\left[d(X^n, g_1(f_1(X^n)))\right] \leq D_1 \tag{1.29}$$

$$\lim_{n\to\infty} E\left[d(X^n, g_2(f_2(X^n)))\right] \leq D_2 \tag{1.30}$$

Definition 14 *The* Multiple Description Rate Distortion Region *for a source is the closure of the set of the achievable rate distortion quintuples $(R_1, R_2, D_0, D_1, D_2)$.*

Unlike the SD case, where the RD region of many sources is known, the MD Rate Distortion Region is much harder to evaluate. In fact, the Multiple Description Rate Distortion Region is known in closed form only in the case of a Gaussian source and two descriptions. In [Oza80] it is proved that the set of achievable squared distortions $D(\sigma^2, R_1, R_2)$ for a Gaussian source with variance σ^2 is given by the union of all triplets d_0, d_1, d_2 satisfying

$$\begin{aligned} d_1 &\geq \sigma^2 2^{-2R_1} && (1.31) \\ d_2 &\geq \sigma^2 2^{-2R_2} && (1.32) \\ d_0 &\geq \frac{\sigma^2 2^{-2(R_1+R_2)}}{1-\left(\left|\sqrt{\pi}-\sqrt{\Delta}\right|^+\right)^2} && (1.33) \end{aligned}$$

where

$$\pi = \left(1 - \frac{d_1}{\sigma^2}\right)\left(1 - \frac{d_2}{\sigma^2}\right), \qquad (1.34)$$

$$\Delta = \frac{d_1 d_2}{\sigma^4} - 2^{-2(R_1+R_2)}. \qquad (1.35)$$

The sign

$$|x|^+ = \begin{cases} x & ifx > 0 \\ 0 & otherwise \end{cases} \qquad (1.36)$$

does not appear in [Oza80] but it has been introduced in [Zam99]. Since it becomes effective only when $d_1 + d_2 > \sigma^2(1 + 2^{-2(R_1+r_2)})$, i.e. in case of very high marginal distortions, it can be omitted without altering the boundary of the distortion region. Similarly, the expression of the inverse of Equations (1.31), (1.32) and (1.33) is given by

$$\begin{aligned} R_1 &\geq \frac{1}{2}\log\left(\frac{\sigma^2}{d_1}\right) && (1.37) \\ R_2 &\geq \frac{1}{2}\log\left(\frac{\sigma^2}{d_2}\right) && (1.38) \\ R_1 + R_2 &\geq \frac{1}{2}\log\left(\frac{\sigma^4}{d_1 d_2}\right) + \delta && (1.39) \end{aligned}$$

where $\delta = \delta(\sigma^2, d_0, d_1, d_2)$ is defined by

$$\delta = \begin{cases} \frac{1}{2}\log\left(\frac{1}{1-\rho^2}\right), & d_0 \leq d_{0_{max}} \\ 0, & d_0 > d_{0_{max}} \end{cases} \qquad (1.40)$$

$$\rho = \begin{cases} -\frac{\sqrt{\pi\epsilon_0^2+\gamma}-\sqrt{\pi\epsilon_0^2}}{(1-\epsilon_0)\sqrt{\epsilon_1\epsilon_2}}, & \epsilon_1 + \epsilon_2 \leq 1 + \epsilon_0 \\ -\sqrt{\frac{\pi}{\epsilon_1\epsilon_2}} & otherwise \end{cases} \qquad (1.41)$$

$$\gamma = (1-\epsilon_0)\left[(\epsilon_1-\epsilon_0)(\epsilon_2-\epsilon_0)+\epsilon_0\epsilon_1\epsilon_2-\epsilon_0^2\right] \tag{1.42}$$

$$\pi = (1-\epsilon_1)(1-\epsilon_2) \tag{1.43}$$

$$\epsilon_i = \frac{d_i}{\sigma^2},\ fori = 0,1,2 \tag{1.44}$$

and

$$d_{0_{max}} = \frac{1}{\frac{1}{d_1}+\frac{1}{d_2}-\frac{1}{\sigma^2}} = \frac{d_1 d_2}{d_1+d_2-\frac{d_1 d_2}{\sigma^2}}. \tag{1.45}$$

A typical form of the set $R(\sigma^2, d_0, d_1, d_2)$ for $d_0 < d_{0_{max}}$ is shown in Figure (1.6). It is important to note that $\delta, \gamma \geq 0$ and $-1 \leq \rho \leq 0$ for all $d_1, d_2 \leq \sigma^2$ and $d_0 < d_{0_{max}}$.

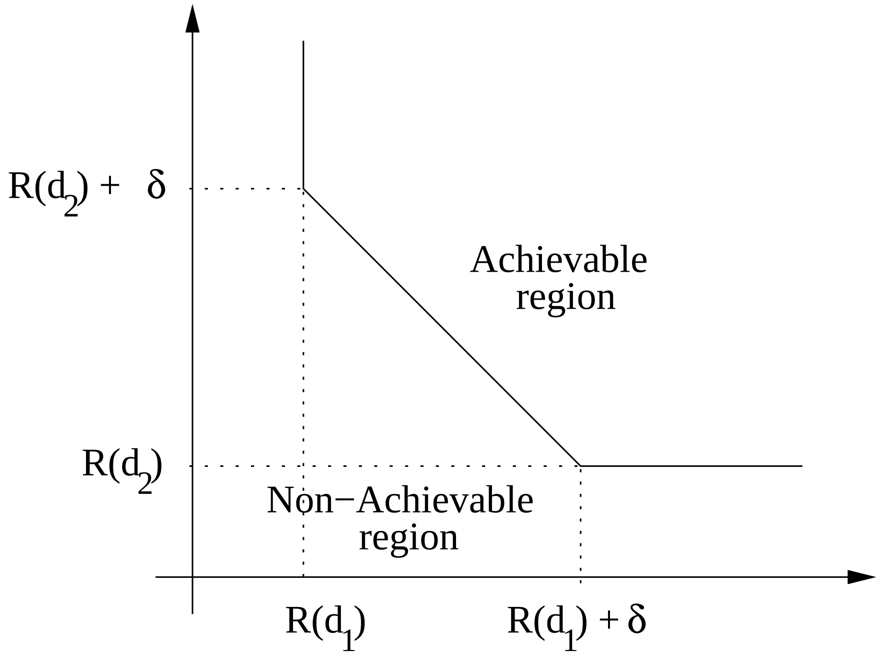

Figure 1.6: The quadrative-Gaussian region for multiple descriptions at some total excess margin rate δ.

The quantity $\delta = \delta_1 + \delta_2 \geq 0$, where

$$\delta_i = R_i - \frac{1}{2}\log\left(\frac{\sigma^2}{d_i}\right),\ i = 1,2 \tag{1.46}$$

represents the Total Excess Margin Rate (TEMR) in the Gaussian case. Some special cases haven been proposed in literature, depending on the TEMR value:

in [Ahl85] the special case of *no* excess rate sum is evaluated, while in [Zam99] the high-resolution case is presented. In general, finding a characterization of the MD RD region is a difficult task and even special cases are hard to handle.

For more general random variable, the MD RD region is not known in closed-form, but only some bounds have been given to approximate it. In [GC82], El Gamal and Cover gave the following bound:

Theorem 2 *Let X_1, X_2 be a couple of vectors of i.i.d. finite alphabet random variables drawn according to a probability mass function $p(x)$. Let $d_i(\cdot,\cdot)$ be bounded. An achievable rate region for distortion $D = (D_1, D_2, D_0)$ is given by the convex hull of all (R_1, R_2) such that*

$$\begin{aligned} R_1 &> I(X;\hat{X}_1) && (1.47)\\ R_2 &> I(X;\hat{X}_2) && (1.48)\\ R_1 + R_2 &> I(X;\hat{X}_0,\hat{X}_1,\hat{X}_2) + I(\hat{X}_1,\hat{X}_2) && (1.49)\end{aligned}$$

for some probability mass function $p(\hat{x},\hat{x_0},\hat{x}_1,\hat{x}_2) = p(x)p(\hat{x_0},\hat{x}_1,\hat{x}_2|x)$ such that

$$\begin{aligned} D_1 &\geq E\left[d_1(X;\hat{X}_1)\right] && (1.50)\\ D_2 &\geq E\left[d_2(X;\hat{X}_2)\right] && (1.51)\\ D_0 &\geq E\left[d_0(X;\hat{X}_0)\right]. && (1.52)\end{aligned}$$

If the random variables are Gaussian, then the closed-form the the MD RD region evaluated by Ozarow is obtained. Successively, Zhang and Berger [ZB87] proved the following theorem:

Theorem 3 *Any quintuple $(R_1, R_2, d_0, d_1, d_2)$ is achievable if there exist random variables $\hat{X}_0, \hat{X}_1, \hat{X}_2$ jointly distributed with a generic source random variable X such that*

$$\begin{aligned} R_1 + R_2 &\geq 2I(X;\hat{X}_0) + I(\hat{X}_1;\hat{X}_2|\hat{X}_0) + I(X;\hat{X}_1,\hat{X}_2,\hat{X}_0) && (1.53)\\ R_1 &\geq I(X;\hat{X}_1,\hat{X}_0) && (1.54)\\ R_2 &\geq I(X;\hat{X}_1,\hat{X}_2) && (1.55)\\ & && (1.56)\end{aligned}$$

and there exist ϕ_1, ϕ_2 and ϕ_0 which satisfy

$$\begin{aligned} E\left[d(X,\phi_i(\hat{X}_0,\hat{X}_1)\right] &\leq d_i,\ i = 1,2 && (1.57)\\ E\left[d(X,\phi_0(\hat{X}_0,\hat{X}_1,\hat{X}_1)\right] &\leq d_0 && (1.58)\end{aligned}$$

Zhang and Berger proved how his bound is strictly stronger than the El Gamal-Cover theorem in the excess rate case.

1.2.1 The MD RD region for the channel splitting scheme

From Equations (1.31), (1.32) and (1.33), we can write the following equation for the channel splitting scheme:

$$\begin{aligned} D_i &\geq \sigma^2 2^{-2R_i},\ fori = 1,2 && (1.59) \\ D_0 &\geq \sigma^2 2^{-2(R_1+R_2)} \cdot \gamma_D(R_1, R_2, D_1, D_2) && (1.60) \end{aligned}$$

where

$$\gamma_d = \begin{cases} 1 & ifD_1 + D_2 > \sigma^2 + D_0 \\ \frac{1}{1-\left(\sqrt{(1-D_1)(1-D_2)}-\sqrt{D_1 D_2 - 2^{-2(R_1+R_2)}}\right)^2} & otherwise. \end{cases} \quad (1.61)$$

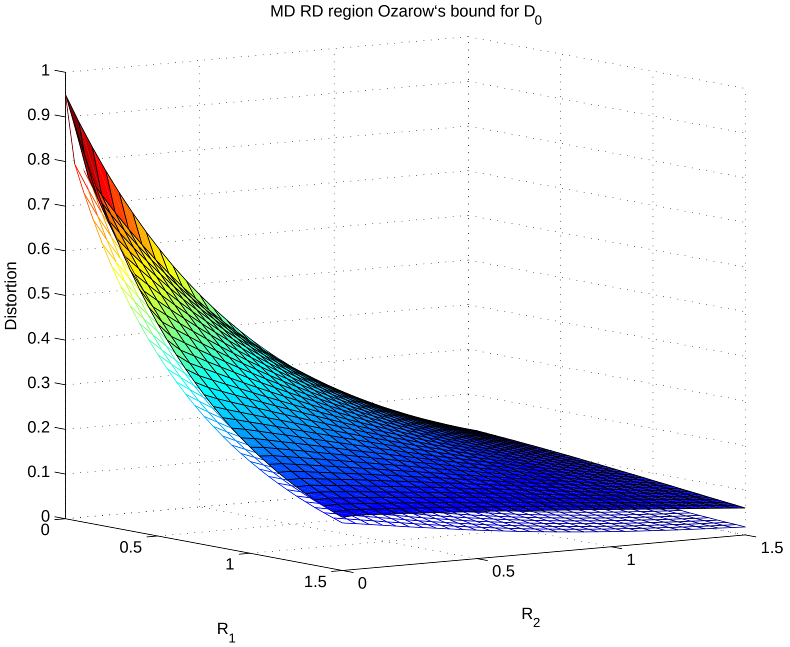

Figure 1.7: Bound for the multiple description rate-distortion region for the channel splitting scheme in case of no redundancy and 50% coding efficiency.

In Figure (1.7), the MD RD region is plotted in two cases: in case of hypothetical no introduced redundancy (lower surface) and in case of 50% redundancy. By losing efficiency, the MD RD region rises and the necessary bitrate to obtain the desired quality becomes bigger. In the corner relative to $R_1 = 1.5$ and $R = 0$ is possible to notice how the surface in case of increased bitrate bends and becomes flat in a small region.

In the *balanced* case, i.e. when $R_1 = R_2$ and $D_1 = D_2$, Goyal [Goy01b] proved that the side distortion for a source with unit variance can be written as

$$D_1 \geq \min \left\{ \frac{1}{2}\left[1 + D_0 - (1 - D_0)\sqrt{1 - \frac{2^{-2(R_1+R_2)}}{D}}\right], \right.$$
$$\left. 1 - \sqrt{1 - \frac{2^{-2(R_1+R_2)}}{D}} \right\} \tag{1.62}$$

under the constraint $D_1 > \sigma^2 2^{-2R_1}$. Written in terms of base rate $r = R(D_0)$ and redundancy $\rho = R_1 + R_2 - R(D_0)$,

$$D_1 \geq \begin{cases} \frac{1}{2}\left[1 + 2^{-2r} - \left(1 - 2^{-2r}\right)\sqrt{1 - 2^{-2\rho}}\right] & for\ \rho \leq r - 1\log_2(1 + 2^{-2r}) \\ 1 - \sqrt{1 - 2^{-2\rho}} & for\ \rho > r - 1\log_2(1 + 2^{-2r}) \end{cases} \tag{1.63}$$

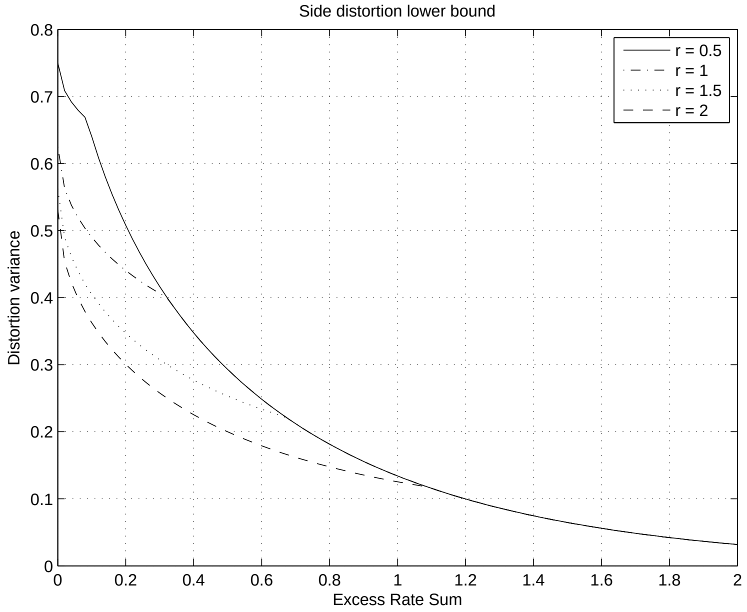

Figure 1.8: Bound for the multiple description rate-distortion region for the channel splitting scheme in case of no redundancy and 50% coding efficiency.

The obtained bound corresponds to the one provided by Ozarow evaluated for the side distortion while keeping fixed D_0. This bound is plotted Figure (1.8), for several excess rate sums. It is interesting to notice that the bound has infinite slope when the excess rate sums is close to zero, then by increasing the rate it flattens and after that starts again to decrease, thus showing a behavior similar to that of the central distortion. The interpretation given by Goyal for the slope variation by increasing the excess rate sum is that at very low bitrates a small additional rate will have more impact if dedicated to reducing the side information that if dedicated to reducing the central distortion. In fact, as it can be seen in Figure (1.7), by increasing the excess rate sum the bound becomes flat in the origin because the bound rises to the maximum distortion, which is the variance of the input signal. Thus there is no gain from allocating the successive bits for the central decoder. These bits can be more efficiently used to reduce the side distortion until also the side distortion bound becomes flat and reducing the central distortion is more effective again. On the other hand, at high bitrates both central and side distortion bounds have the same exponential behavior and therefore the same efficiency is obtained, leaving the freedom of an arbitrary rate allocation.

1.2.2 The Redundancy Rate-Distortion Region

As we have seen in the previous section, even in the case of a Gaussian source and two channels the MD RD region is hard to evaluate. Whenever random variables have a different p.d.f. or more complicated operations such as motion compensation, are performed, giving a full characterization of this region becomes quickly impossible.

In order to describe a MDC scheme, the Redundancy Rate-Distortion Region is evaluated. This region can be defined as the set of achievable side distortion values obtained by varying the introduced redundancy under a fixed quality of the central decoder. By indicating the redundancy r as

$$r = \frac{\sum_{i=1}^{N} R_i}{R_0} \tag{1.64}$$

where R_0 is the rate for the Single Description Coding scheme for a given quality and R_i are the rates of the generated multiple descriptions, a comparison between the SDC and the MDC schemes can be immediately established. An example of RRD Region for the channel splitting scheme is shown in Figure (1.9).

Whenever the MDC scheme has the introduced redundancy as a degree of freedom, the RRD region is a curve. In some schemes redundancy in not tunable and therefore this curve collapses into a point. Although tunable redundancy might seem obvious, in some video coding schemes it does not hold. As an example, MDC schemes based on compressed bitstream division do not

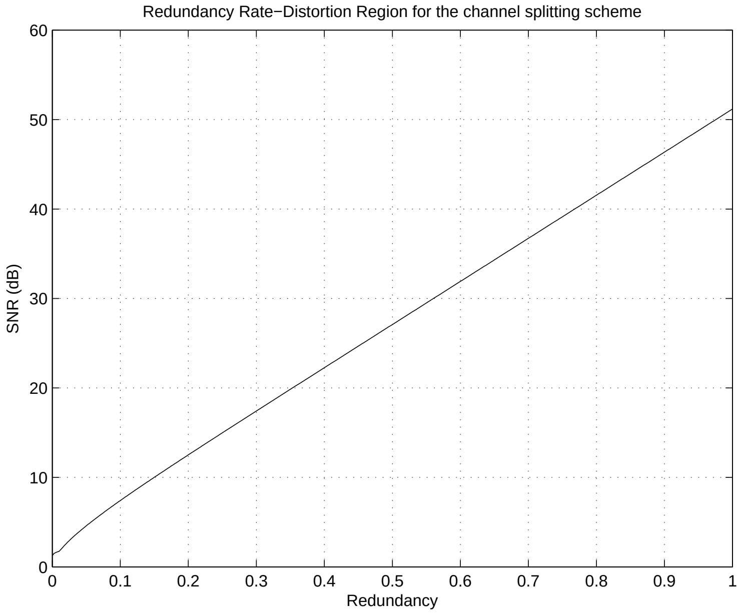

Figure 1.9: Redundancy Rate Distortion region for the channel splitting scheme.

have this possibility because it would be available only by re-encoding the sequence, but in this case transcoding is not allowed.

1.3 Applications to image and video coding

1.3.1 MD coding with Correlating Transforms

Transform-based source coding has been applied to many signal processing problems to obtain coding gain and to enhance the compression quality. Similarly, transforms can be adopted to generate two correlated signals from independent random variables. Correlation reduces coding efficiency, but at the same time allows to estimate lost information from the received one.

A pairwise MD Correlating Transform is defined as

$$\begin{bmatrix} C \\ D \end{bmatrix} = T \begin{bmatrix} A \\ B \end{bmatrix}. \tag{1.65}$$

and its basic application for MDC is shown in Figure (1.10). Obviously, optimal reconstruction can be obtained only if the transformation T maps integer into integer. A way to implement this transform is given by the lifting scheme [CDSY98], which implements such lossless transform by expressing the lin-

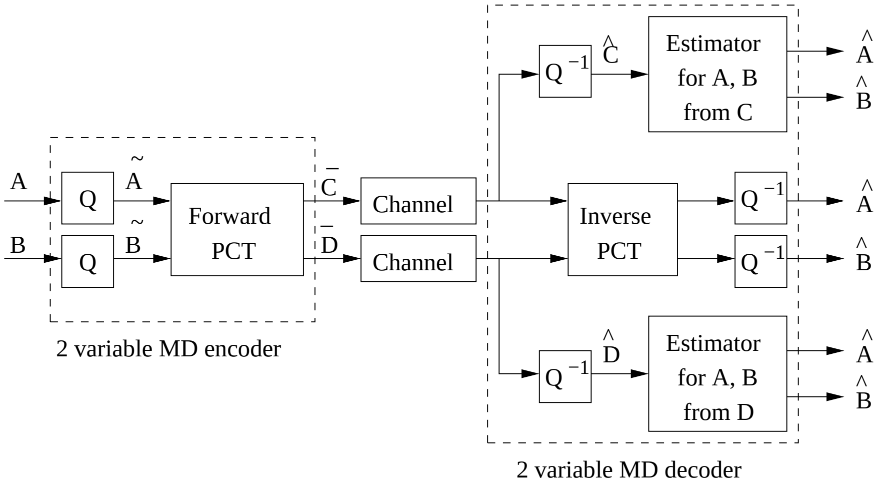

Figure 1.10: Basic scheme of coding and decoding process for a single pair.

ear application T with the LU decomposition. If the quantization step size is denoted by Q, the transform and the quantized quantities can be expressed as

$$T = \begin{bmatrix} a & b \\ c & d \end{bmatrix} \tag{1.66}$$

$$\bar{A} = \left\lfloor \frac{A}{Q} \right\rceil \tag{1.67}$$

$$\bar{B} = \left\lfloor \frac{B}{Q} \right\rceil \tag{1.68}$$

$$W = \bar{B} + \left\lfloor \frac{1+c}{d} \bar{A} \right\rceil \tag{1.69}$$

$$\bar{C} = W - \left\lfloor \frac{1-b}{d} \bar{D} \right\rceil \tag{1.70}$$

$$\bar{D} = \lfloor dW \rceil - \bar{A} \tag{1.71}$$

At the receiver, the original values can be reconstructed by inverting the correlating transform

$$W = \bar{C} + \left\lfloor \frac{1-b}{d} \bar{D} \right\rceil \tag{1.72}$$

$$\bar{A} = \lfloor dW \rceil - \bar{D} \tag{1.73}$$

$$\bar{B} = W - \left\lfloor \frac{1+c}{d} \bar{A} \right\rceil \ . \tag{1.74}$$

In case only one channel is correctly received, reconstruction requires an estimate of the lost coefficient and inversion of the transform. The optimal linear estimator is given by

$$\gamma_{CD} = \frac{\sigma_d}{\sigma_C}\phi \tag{1.75}$$

where ϕ is the correlation angle between C and D. Thus, the approximated reconstructed signal is

$$\begin{bmatrix} \hat{A} \\ \hat{B} \end{bmatrix} = T^{-1} \begin{bmatrix} 1 \\ \frac{\sigma_d}{\sigma_C}\phi \end{bmatrix} \bar{C}Q. \tag{1.76}$$

In [OWVR97] it is suggested to use transforms of the form

$$T = \begin{bmatrix} 1 & b \\ -\frac{1}{2b} & \frac{1}{2} \end{bmatrix} \tag{1.77}$$

while in [GK98] Goyal and Kovacevic extended the family of optimal transforms to

$$T = \begin{bmatrix} a & \frac{1}{2a} \\ -a & \frac{1}{2a} \end{bmatrix}. \tag{1.78}$$

Finally, Wang et al [WOVR01] generalized the correlating transform in a framework to realize MDC. They were able to evaluate the rate distortion analysis for a generic pairwise transform including distortion due to quantization error, they were also able to prove that the family of transforms obtained by Goyal is optimal even in the case of quantization. They summarize their result as *the optimal transform is formed by two equal length basis vectors that are rotated away from the original basis by the same angle in opposite directions*. This result implies that orthogonal transform is not optimal and it has the same performance as the optimal one only when the introduced redundancy is either null or at its maximum possible value.

In case more than two random variables have to be encoded and transmitted over different channels at the same time, the cascade structure proposed in [GK98] can be used. As shown in Figure (1.11) variables are pairwisely transformed and successively another transform is applied to correlate a variable from each previously correlated pair.

Several application of this techniques have been proposed in literature. Most of them aim to protect the transformed values of the DCT coefficients. As an example, in [GKAV98] it is applied to JPEG image coding by applying the following steps

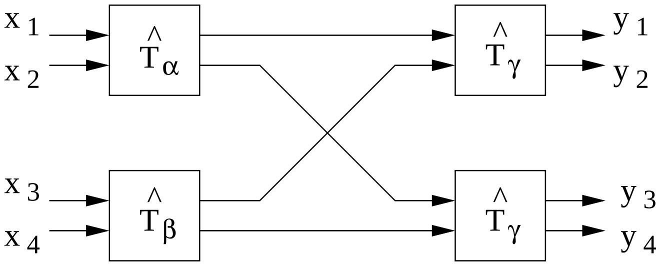

Figure 1.11: Cascade structure allows simple and efficient coding for more than two channels.

- A 8x8 block DCT of the image is computed;
- The DCT coefficient are uniformly quantized;
- Vectors of length 4 are formed from DCT coefficients separated in frequency and space;
- Correlating transforms are applied to each 4-tuple;
- Entropy coding akin to that of JPEG is applied.

1.3.2 MD coding with Frames

Another example of MDC is given by Frames, which are obtained with linear transforms.

The theory of filter banks [Vai93a] and [VK95] provides a framework for a class of signals decompositions in $l^2(\mathbb{Z})$, based on signal analysis through a sliding window by using a set of elementary waveforms. In general, an expansion can be written as

$$x[n] = \sum_{i=0}^{K-1} \sum_{j=-\infty}^{+\infty} c_{i,j}\phi_{i,j}[n] \tag{1.79}$$

where the vectors $\phi_{i,j}[n]$ are the translated versions of K elementary waveforms

$$\phi_{i,j}[n] = \phi_i[n - jN] \tag{1.80}$$

with $N \leq K$. If the family Φ

$$\Phi = \left\{\phi_{i,j} : \phi_{i,j}[n] = \phi_i[n - jN], i = 0, 1, \cdots, k-1, j \in \mathbb{Z}\right\} \subset \mathbb{R}^N \tag{1.81}$$

is a frame, then any signal in $l^2(\mathbb{Z})$ can be represented in a numerically stable way.

The family of vectors in Equation (1.81) is a frame if for any $x \in l^2(\mathbb{Z})$ exist some constants $A > 0$ and $B < \infty$ such that

$$A \,||x||^2 \leq \sum_{i=0}^{K-1} \sum_{j=-\infty}^{+\infty} \left|< x, \phi_{i,j} >\right|^2 \leq B \,||x||^2 . \tag{1.82}$$

If the family Φ is a frame, then there exists another frame

$$\Psi = \left\{\psi_{i,j} : \psi_{i,j}[n] = \psi_i[n - jN], i = 0, 1, \cdots, k-1, j \in \mathbb{Z}\right\} \tag{1.83}$$

such that the coefficients of the expansion (1.79) can be calculated as inner product with its vectors, that is

$$x[n] = \sum_{i=0}^{K-1} \sum_{j=-\infty}^{+\infty} < x, \psi_{i,j} > \phi_{i,j}[n]. \tag{1.84}$$

In case $A = B$, then the frame is said to be *tight* and Φ is equal to Ψ and the expansion formula (1.79) can be written, similarly to orthogonal expansions, as

$$x[n] = \frac{1}{A} \sum_{i=0}^{K-1} \sum_{j=-\infty}^{+\infty} < x, \phi_{i,j} > \phi_{i,j}[n] \tag{1.85}$$

where the term $\frac{1}{A}$ is necessary because the transform is orthogonal but not orthonormal.

If $K > N$, the transform is not a bijection, thus the expansion is a *redundant representation*. Since the transform is no longer injective, its kernel does not consists only of the null element, and therefore only N coefficients are required to be correctly received to reconstruct the signal.

Oversampling of a periodic, band-limited signal can be seen as a frame operator applied to the signal, where the frame operator is associated with a tight frame. Let $x = [x_1, x_2, \cdots, x_n]^T \in \mathbb{R}^N$, with N odd. By exploiting the inverse Fourier transform, a continuous time signal can be written as

$$x_c(t) = x_1 + \sum_{k=1}^{\frac{N-1}{2}} \left[x_{2k}\sqrt{2}\cos\frac{2\pi kt}{T} + x_{2k+1}\sqrt{2}\sin\frac{2\pi kt}{T} \right] \tag{1.86}$$

If we define a sampled version of $x_c(t)$ as $x_d[m] = x_ct\left(\frac{mT}{M}\right)$, assuming $M \geq N$ and by indicating

$$y = [x_d[0]x_d[1] \cdots x_d[M-1]]^T \tag{1.87}$$

than $y = Fx$, with

$$F = [\phi_1 \phi_2 \cdots \phi_m]^T \tag{1.88}$$

and

$$\phi_k = \left[1, \sqrt{2}\cos\frac{2\pi k}{M}, \sqrt{2}\sin\frac{2\pi k}{M}, \cdots, \sqrt{2}\cos\frac{2\pi \frac{N-1}{2} k}{M}, \sqrt{2}\sin\frac{2\pi \frac{N-1}{2} k}{M} \right]. \tag{1.89}$$

It is easy to verify that F is a tight operator, whose columns have norm $\sqrt{N}$. By dividing F by $\sqrt{N}$ the frame is normalized and frame bound corresponds to the introduced redundancy.

Frame expansion from $\mathbb{R}^N$ to $\mathbb{R}^K$ can be considered as a (K, N) block code, where in case up to $K - N$ coefficients are lost perfect reconstruction is possible. Whenever less then N coefficients are correctly received, estimating x can be posed as a simple least-squares problem. Thus, the estimate of the original signal can be obtained by multiplying the received vector with the pseudoinverse matrix of F

$$\hat{x} = F^+ y = F^+ F x \tag{1.90}$$

In [GVT98], a better estimate is proposed, which considers distortion caused by uniform quantization which brings to a Linear Programming problem.

An application of frame expansion to JPEG images is given in [GKAV98], where a 10×8 frame operator F corresponding to a length 10 Discrete Fourier Transform of a length 8 sequence is used. The coding approach proceeds as follows:

- An 8x8 block DCT of the image is computed;
- Vectors of length 8 are formed from DCT coefficients of same frequency, separated in space;
- Each length 8 vector is expanded by left multiplication with F;
- Each length 10 vector is uniformly quantized

1.3.3 MD coding with Motion Compensation

In case of video coding, not only spatial redundancy but also temporal redundancy can be exploited. This additional degree of freedom allows many more schemes, but at the same time makes harder to evaluate theoretically the performance of such MDC schemes.

An example of how temporal redundancy can be exploited is given in [RJW+02], where a video sequence is encoded by using three different prediction loops. Once motion estimation has been performed, the DCT coefficients of the residual information are divided into two descriptions. This two sets are successively used to fill three frame buffers: one obtained by receiving both descriptions and thus operating at full quality and two exploiting only one description information. The X frames is predicted from P_i $i = 0, 1, 2$, where P_0 is the central reference frame buffer and P_1 and P_2 are the side frame buffers. After the central encoder compression, $\hat{F}_1$ and $\hat{F}_2$ are reconstructed respectively from descriptions 1 and 2. By subtracting this value from the difference of the currently encoded frame and the frame buffer, indicated in Figure (1.12) as $G_i = X - P_i - \hat{F}_i$, the decoder mismatch in case of transmission error is evaluated and encoded, so that the decoder drift can be either bounded or even suppressed, depending on the coding strategy.

In this scheme the bits used for G_i $i = 1, 2$ constitute the introduced redundancy, since the decoder will not use them if both descriptions are received.

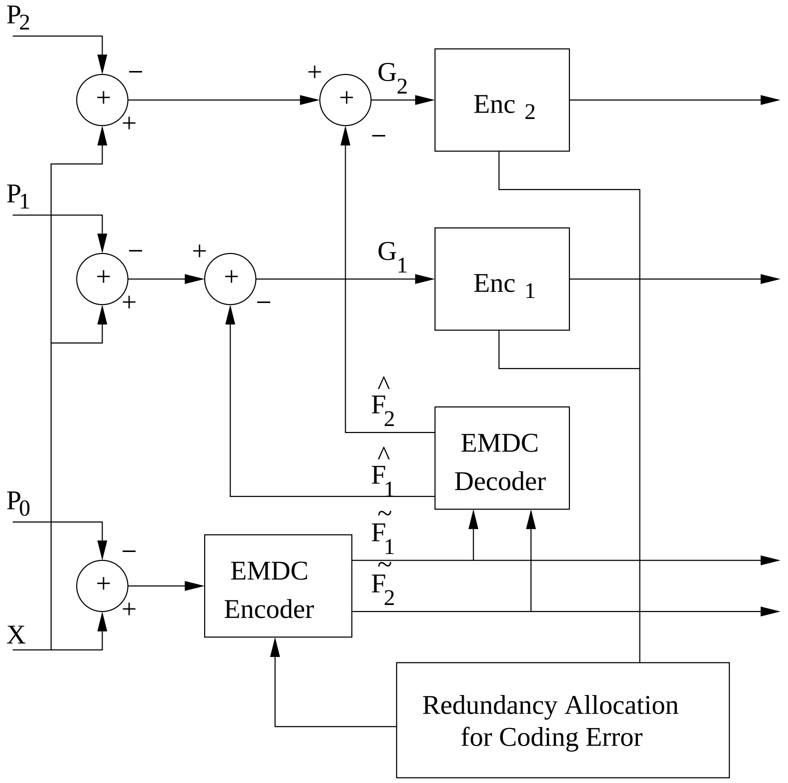

Figure 1.12: MD coding for P mode.

Multiple descriptions are generated in the EMDC by applying a Pairwise Correlating Transform (PCT) to couples of DCT coefficients, in order to reintroduce some redundancy after it has been removed by the DCT. After the PCT, coefficients are split in even and odd and they are encoded with the motion vector field, which is copied in both descriptions, together with the mismatch control signal G_i.

There are several possibilities to generate the mismatch control signal, which bring to different results:

- Full mismatch control: from each description, lost information is estimated by exploiting the PCT. The drift signal G_i is formed by subtracting $\hat{F}_i$, the image reconstructed from only one description, from the original image X and also subtracting the relative prediction P_i. Once G_i has been evaluated, it is encoded as Intra, by applying the DCT and by quantizing with a quantization step size bigger than the step size of the central encoder, thus reducing the introduced redundancy. The main drawback of this approach consists of expanding the original information. In fact, in case of channel fault, only 32 coefficients of the 8x8 block are not received, but the Intra coding in the side encoders works on the full set of 64 values.

- Partial mismatch control: the problem of information expansion is addressed in the side encoders. Rather than completely encoding G_i, only the more important part of the signal is extracted, so that only 32 coefficients are transmitted. The central encoder sends the central prediction error, $X - P_0$, while the side loop sends the difference between a linear estimate of the transmitted image and the side-loop prediction error.

- No mismatch control: in this case no prediction loop is used in the side decoders. Redundancy is no more used to encode the drift signal G_i, but is it used to enhance the quality of each Single Description decoder.

Chapter 2

H.264/AVC-based MDC schemes

2.1 Introduction to H.264/AVC

The H.264/AVC [WSBL03] is a standard for video compression. It is also known as MPEG-4 Part 10, or MPEG-4 AVC (for Advanced Video Coding). It was written by the ITU-T Video Coding Experts Group (VCEG) together with the ISO/IEC Moving Picture Experts Group (MPEG) as the product of a partnership effort known as the Joint Video Team (JVT).

The final drafting work on the first version of the standard was completed in May 2003 and in the successive years it has been extended. In the meanwhile, it has been adopted in always more products.

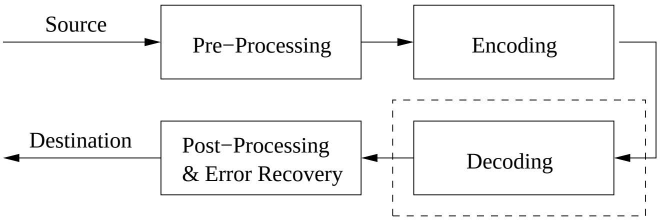

Figure 2.1: Scope of the video coding standard.

The H.264/AVC standard covers the decoder, as shown in Figure (2.1), by defining the bitstream syntax and the decoding operations that have to be performed. The standard follows this approach to specify all the necessary operations to implement a standard-compliant decoder and to give the possibility of implementing only a subset of the standard features in the encoder, which is more complex than the decoder. Thus, features can be selected depending on the project requirements, while the decodability of the output video is guaranteed. As a major drawback, the standard does not guarantee the coding efficiency, whose responsibility is due to the encoder implementation and its coding strategy.

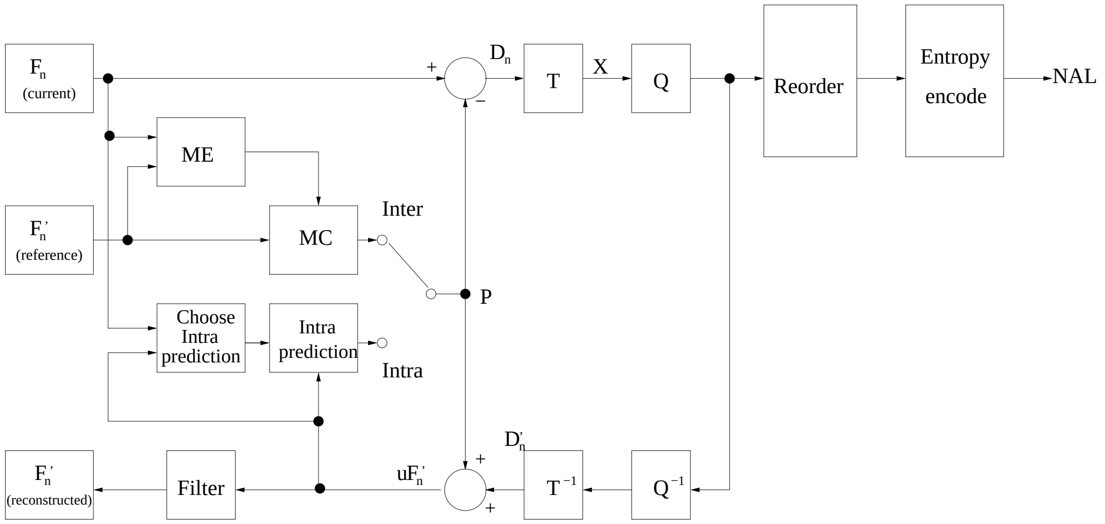

Figure 2.2: Block scheme of the H.264/AVC encoder.

The H.264/AVC encoder is organized in a closed-loop structure. Each frame can be encoded either as Intra or Inter. In the first case, it can be independently decoded, while in case temporal prediction is used, valid reference frames are necessary for motion compensation. After spatial or temporal prediction, the difference signal is transformed and quantized and the obtained values are compressed with entropy coding.

The quantized values are used, together with the information relative to the prediction, to reconstruct the same frame that is decoded at the receiver along the so called reconstruction path, which is the path at the bottom of the block scheme of Figure (2.2). By using the reconstructed frame as reference for the successive ones, the encoder is able to compensate the drift that quantization generates at the decoder and to assure better reconstruction quality. Since the decoder needs to perform both encoding and decoding, it can be easily understood why in the H.264/AVC standard such a freedom of choosing functionalities is given.

2.1.1 Intra prediction

The H.264/AVC standard provides three main Intra prediction modes for the luminance component, which are supported in all slice types.

The Intra 4x4 mode is based on encoding all 4x4 pixel blocks of each macroblock independently. Each 4x4 block is spatially predicted from the already encoded adjacent blocks, by using one of the nine prediction modes, shown in Figure (2.3). With the exception of the DC mode which can be adopted in case of uniform regions, these prediction modes are suited to predict textures with well identified structures.

Spatial prediction in the image domain is a feature that in not present in previous coding standard. In fact, in H.263 and MPEG-4 intra prediction is always performed in the frequency domain. This new strategy is able to provide a better estimate of non smooth regions in the frame.

In case the macroblock is uniform, the Intra 16x16 mode can be adopted. For this type of prediction, only four prediction modes are available: 0 - vertical, 1 - horizontal, 2 - DC, 3 - plane. This four modes are the same available for the two chrominance components, with the difference of the mode number. In this case, mode numbers are 0 - DC, 1 horizontal, 2 - vertical and 3 - plane. The prediction mode is shared between the two chrominance components and if any chrominance block is encoded as Intra 16x16, then both blocks are encoded in this way.

As an alternative to Intra 4x4 and 16x16 is the Intra I_PCM mode, which bypasses prediction and transform coding and directly send the values of the encoded pixels. This mode has the following purposes:

- it offers the possibility of exactly transmitting the values of the frame pixels;
- it provides a strategy to encode parts of the image where excess of details would cause an anomalous bitstream size increment without quality enhancement;
- it provides an upper bound to the bandwidth necessary to encode the block as Intra.

2.1.2 Motion estimation

In comparison to prior video coding standards, H.264/AVC has some features that significantly increase the achievable compression ratio.

In previous coding standards, the size of blocks used for motion estimation is 16x16 or 8x8 pixels. In H.264/AVC, each macroblock can be partitioned in one block of 16x16 pixels, two 16x8 pixels blocks, two 8x16 pixels blocks or four blocks of 8x8 pixels each. In this case each 8x8 partition can be further split in two 8x4, two 4x8 or four 4x4 partitions. Available partitions and sub-partitions are shown in Figure (2.4)

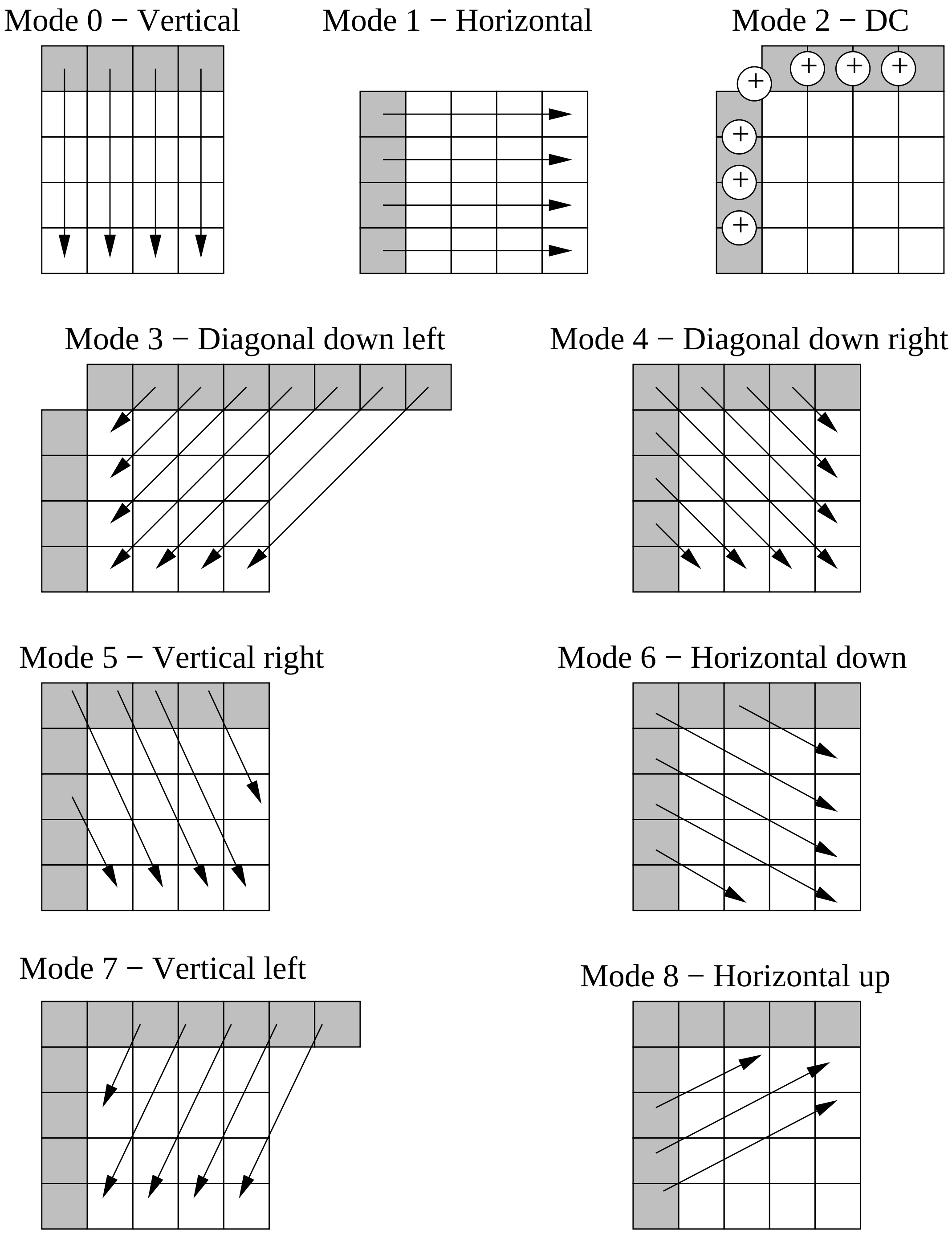

Mode 0 − Vertical

Mode 1 − Horizontal

Mode 2 − DC

Mode 3 − Diagonal down left

Mode 4 − Diagonal down right

Mode 5 − Vertical right

Mode 6 − Horizontal down

Mode 7 − Vertical left

Mode 8 − Horizontal up

Figure 2.3: The nine Intra 4x4 prediction modes.

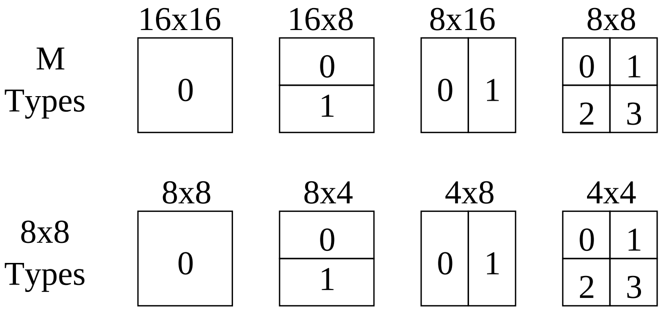

Figure 2.4: Segmentations of the macroblock for motion compensation. Top: partitions of macroblocks. Bottom: possible sub-partitions of 8x8 pixels blocks.

Motion compensation is performed on the luminance component with one quarter of pixel accuracy [Wed03]. To generate sub-pixel values, interpolation is applied twice to the reference frame. In the first step, half pixels values are generated by applying a separable FIR filter, which can be realized as the application of a one-dimensional 6-tap FIR filter horizontally and vertically.

The filter coefficients are

$$h = \{1, -5, 20, 20, -5, 1\} , \tag{2.1}$$

and the final interpolated value is obtained by adding sixteen and dividing by thirty-two, so that its value is clipped to the range 0-255. The quarter pixel values are derived by averaging with upward rounding of the two nearest samples at integer and half integer positions.

Since the chrominance components are low-pass signals, the filtering operation always consists of bilinear interpolations. Furthermore, since the chrominance sampling grid has a reduced resolution if compared to the luminance grid, the displacements used for chrominance compensation have one eight pixel accuracy.

To further increase compression, motion vectors can refer to regions outside the picture boundaries. In this case, non existing pixels are extrapolated by repeating the values of the pixels on the frames edges before interpolation. Moreover, several frames can be used as reference while performing motion estimation, as shown in Figure (2.5). While exploiting this feature, both the encoder and the decoder need to maintain in memory the same multi-picture buffer. Unless the multi-picture buffer consists of only one picture, the reference index parameter has to be encoded for each 16x16, 18x8, 8x16 or 8x8 luminance block. In case a 8x8 block is sub-partitioned, the same reference index is shared between the sub-partitions.

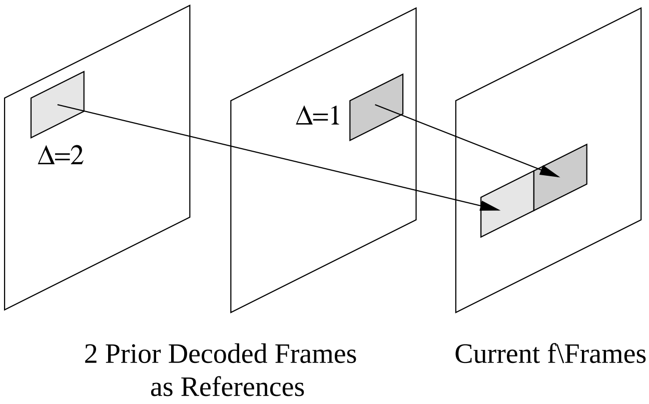

Figure 2.5: Example of multi-picture motion compensation. To correctly identify the reference, the parameter Δ for each 16x16, 16x8, 8x16 and 8x8 is transmitted.

Along to the explained prediction modes, H.264/AVC offers a special mode called P_SKIP. This prediction mode is equivalent to the 16x16 mode with a null motion vector prediction referring to the first image of the multi-picture buffer. This prediction mode leads to extremely high compression ratios, because large areas can be transmitted with only a few bits. Since the motion vector field is differentially encoded by using the median of adjacent motion vectors, the P_SKIP mode can be used not only to encode static portions of the frame, but also zones characterized by slow uniform panning.

The H.264/AVC standard has also the possibility of encoding inter-frames using two reference frames. In case of B prediction, all the features for P frames are available, and the main difference is that B macroblocks can use a weighted average of two distinct motion-predicted frames as references. To make use of multi-picture references in B frames, the encoder and decoder utilize two lists of reference frames, called list 0 and list 1. This two lists are used for four different type of prediction: list 0, list 1, bi-predictive and direct. In the first two cases only one frame is used as reference, while in the bi-predictive case the weighted average of two frames is used as reference. In the direct case, the prediction is automatically inferred from previously transmitted information.

For B frames the B_SKIP mode plays the same role as P_SKIP in P frames: the motion vector is the median of the adjacent partitions and no residual information is transmitted.

2.1.3 Integer transform

As in many coding schemes, the residual signal obtained after prediction is compressed with transform coding. The main differences between the H.264/AVC transform and the transforms adopted in earlier standard consist of its size, which is 4x4 pixels, and of the adoption of an integer transform with properties similar to a DCT.

The transform matrix, given as

$$T = \begin{bmatrix} 1 & 1 & 1 & 1 \\ 2 & 1 & -1 & -2 \\ 1 & -1 & -1 & 1 \\ 1 & -2 & 2 & -1 \end{bmatrix}, \tag{2.2}$$

consists only of integer values of one ad two. This choice has several advantages:

- it does not require a floating point ALU to be executed and it needs only sixteen bits of precision instead of other floating point solutions which need up to thirty-two bits;
- it can be easily implemented as sums, differences and shifts, thus it can be efficiently parallelized;
- it does not suffer from decoder drift, as it happens with fixed point approximation of DCT coefficients across different architectures and CPUs.

The quantization parameter `QP` determines the quantization step size of coefficients in H.264/AVC. The value of this parameter spans from 1 to 52 and each increment of 1 corresponds approximately to a 12% increment of the quantization step size. This reflects approximately in a 12% growth of the encoded bitstream.

In order to keep computational efficiency high, quantization and some scaling products due to the 4x4 transform are performed together, without having to manipulate the coefficients twice.

Successively, with the adoption of the Fidelity Range Extensions [MWG05], the integer transform has been extended to the size of 8x8 pixels. In my tests the size increment did not lead to higher compression ratios, as it could be expected, but it reduced the time needed to encoded each frame. The unchanged coding efficiency is due to the very precise prediction that is at the basis of H.264/AVC performance. The reduced complexity and increased speed make this solution suitable for encoding sequences with very large frames, where big regions are uniform.

2.1.4 Entropy coding

Once coefficients have been transformed and quantized, they are entropy encoded. H.264/AVC offer two coding engines for this purpose: the Context-Adaptive Variable Length Coding (CAVLC) and the Context-Adaptive Binary Arithmetic Coding (CABAC).

In CAVLC, several tables are defined to match the possible coefficients statistics that the encoder might encounter. These tables are used to encode the zig-zag scan of the quantized values of 8x8 blocks, starting from those corresponding to high frequencies and moving towards those at low frequencies. The reason of this strategy is that high-frequency coefficients are often null and their absolute value increases while moving towards low-frequency coefficients. To fully exploit this statistics, CAVLC encodes for each block the number of non-null coefficients and successively encodes the values by using run-length encoding. Moreover, since the initial non null coefficients in the zig-zag scan have a high probability of having absolute size 1, together with the number of non-null coefficients the number of *t*railing ones is saved. This information efficiently indicates the presence of up to three coefficients of absolute value 1 at the beginning of the run-length encoding.

The length of runs is encoded by saving the information of the total number of null coefficients in the zig-zag scan. After that, for each non-zero value the number of zeros before that coefficient is signaled, thus the position of zeros in the zig-zag scan can be reconstructed. In case all the null coefficients have already been encoded in the scan, the number of zeros is omitted to increase coding efficiency, since all the successive runs will have length 0.

H.264/AVC offers the possibility of using arithmetic encoding with CABAC [DMW03], which is based on assigning a not-integer number of bits to each encoded value to further reduce the bitstream size. Two are the key properties of CABAC: coefficient binarization and context adaptivity. Each encoded value is transformed into a string of zeros and ones, where the symbols probabilities are not equal. Thus, the arithmetic encoder is able to fully exploit this statistics to efficiently compress the string of bits. Further more, CABAC contexts are dynamically modeled: previously encoded syntax elements are used to adapt to non-stationary symbol statistics.

By adopting CABAC, the output bitstream size has a reduction between 5% and 15%. On the other hand, complexity and computational requirements are increased, even though the arithmetic coding engine and probability estimation algorithms are specified as multiplication-free operation, in order not to require excessive additional computational power.

2.1.5 In-loop deblocking filter

Block-based compression algorithms often leads to distortion that manifests itself as the production of visible block structures. The main reason of these blocks is the quantization of the transformed coefficients. In fact, each element of the transform basis can be seen as a set small blocks and quantization can be compared to adding a linear combination of scaled elements of the basis functions to the original image.

To reduce this distortion, H.264/AVC defines an adaptive in-loop deblocking filter [LJL$^+$03], whose effect is modulated by the values of several syntax elements. The filter works mono-dimensionally on 4x4 block edges and takes into account up to three pixel in each 4x4 block, as shown in Figure (2.6).

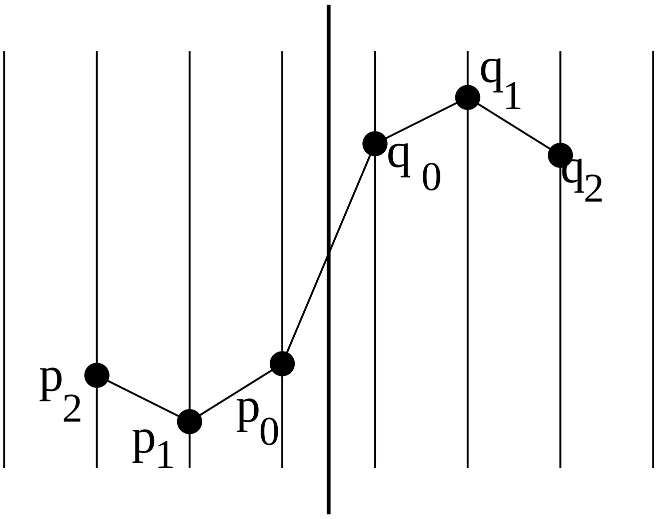

Figure 2.6: Deblocking filter mechanism.

The filter modifies p_0 and q_0 only if all the following conditions are matched:

- $|p_0 - q_0| < \alpha(\mathtt{QP})$
- $|p_1 - p_0| < \beta(\mathtt{QP})$
- $|q_1 - q_0| < \beta(\mathtt{QP})$.

p_1 and q_1 are filtered if the corresponding following condition is satisfied:

- $|p_2 - p_0| < \beta(\mathtt{QP})$

- $|q_2 - q_0| < \beta(\mathtt{QP})$.

The heuristic of this adaptive filter is based on the assumption that a large absolute difference between adjacent samples indicates the presence of blocking artifacts, while small gaps are due to the frame texture and it does not have to smooth them.

As expected, this filter does not reduce sharpness while reducing distortion. This reflects in better subjective quality and in bitstream size reduction between 5% and 10%.

2.2 Test conditions

There are several factors that can influence a MDC scheme performance, especially in case of image and video coding because error concealment techniques can be adopted. In case of video sequences, also the choice of the Group Of Pictures (GOP), its length and the number of P and B frames can significantly change the decoded quality.

In [PA97] and [Per99] three test cases, shown in Table (2.1), are defined to test transmission in error-prone environments. As suggest in other articles, during the development of the MDC schemes based on H.264/AVC we adopted test case number 2 for our test conditions. This case requires the corruption of the bitstream to introduce three 16 to 24 ms long bursts of errors separated by 2 s and 1.5 s far from the beginning of the sequences in order to allow the decoder to correctly synchronize with the stream.

Since at the time we did not have a robust decoder able to deal with a corrupted bitstream and since the worst-case burst is 2 ms long, we decided to approximate the test conditions with the loss of a frame description. In fact, 24 ms corresponds to 41 frames per second. In case of a sequence at 20 frames per second, in case of MDC with two descriptions, 40 packets per second are necessary and therefore the single packet loss is compatible with the test case. Moreover, since the error bursts are separated by two or more seconds, we decided to consider only one error per GOP.

All the H.264/AVC MDC schemes were tested adopting these conditions.

Test case	Residual error conditions	Description	Error interval $[begin, end]$ (s)
1	10^{-3}	High Random BER	$[1.5, end]$
2	3 burst of errors 50% BER within burst Random Burst Length: 16 to 24 ms Random Bursts Separation: > 2s	Multiple burst errors	$[1.5, 8]$
3	Combination of test cases 1 and 2	High random BER and multiple burst errors	$[1.5, end]$

Table 2.1: Error-prone video channel conditions.

2.3 Sub-Sampling Multiple Description Coding

Due to the high spatial correlation within a frame, each pixel may be estimated according to its neighbors. Consequently, a MD scheme can be defined by grouping adjacent pixels into separate descriptions. This operation is represented in Figure (2.7).

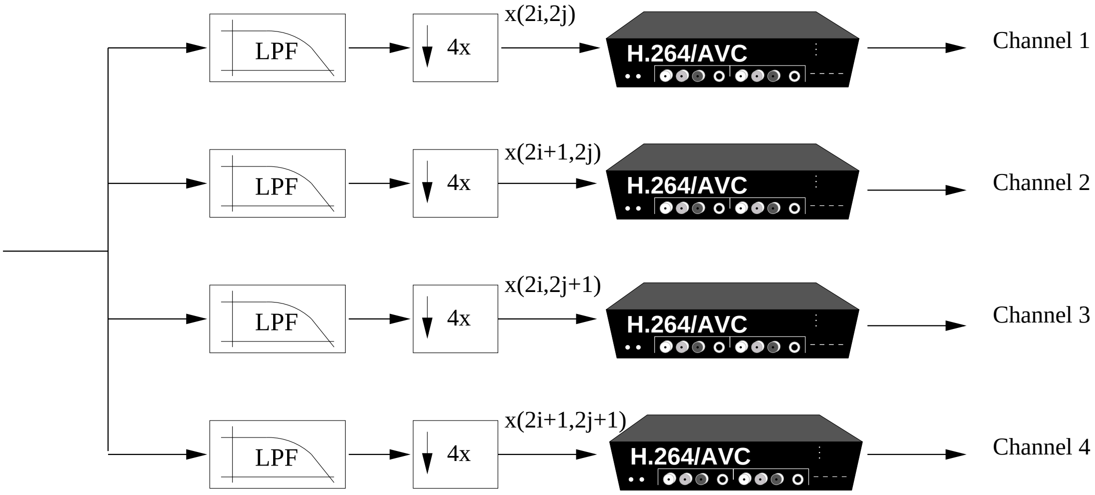

Figure 2.7: Multiple Description transmission using the sub-sampling approach of the SMDC coder.

Each input frame is sampled along its rows and columns with a sampling factor of 2. Let $x(i, j)$ be the luma sample of the current frame at position (i, j), then the four sub-sequences are respectively formed with pixels

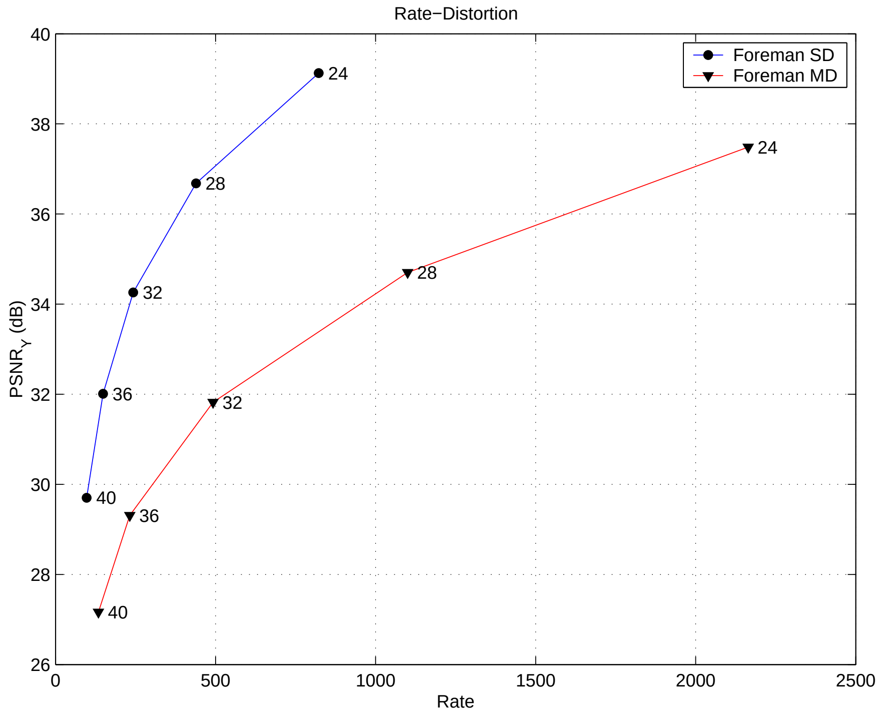

Figure 2.8: SMDC Rate-Distortion functions for the "*foreman*" and "*mobile*" CIF sequences.

$x(2i\,,\,2j)$	first sub-sequence
$x(2i+1\,,\,2j)$	second sub-sequence
$x(2i\,,\,2j+1)$	third sub-sequence
$x(2i+1\,,\,2j+1)$	fourth sub-sequence

In this way, for each input sequence the scheme generates four sub-sequences with halved resolution on both spatial directions, and a size of one fourth of the original sequence size. Figure (2.8) gives an example of the Rate-Distortion functions for sequences "`foreman`" and "`mobile`". The curves are parameterized as a function of the `QP` parameter. From the results shown, it is apparent that the scheme may introduce a considerable redundancy in the case of "hard-to-code" sequences.

Each sub-sequence is sent to a separate H.264/AVC coder, and the output bitstreams are sent to four independent channels. In the case that only one of the descriptions arrives at the receiver, the end-user is able to reconstruct the coded sequence at lower resolution without any artifact or channel distortion. When more sequences arrive, the decoder can estimate the lost information exploiting the correlation among neighboring pixels. In this approach, assuming

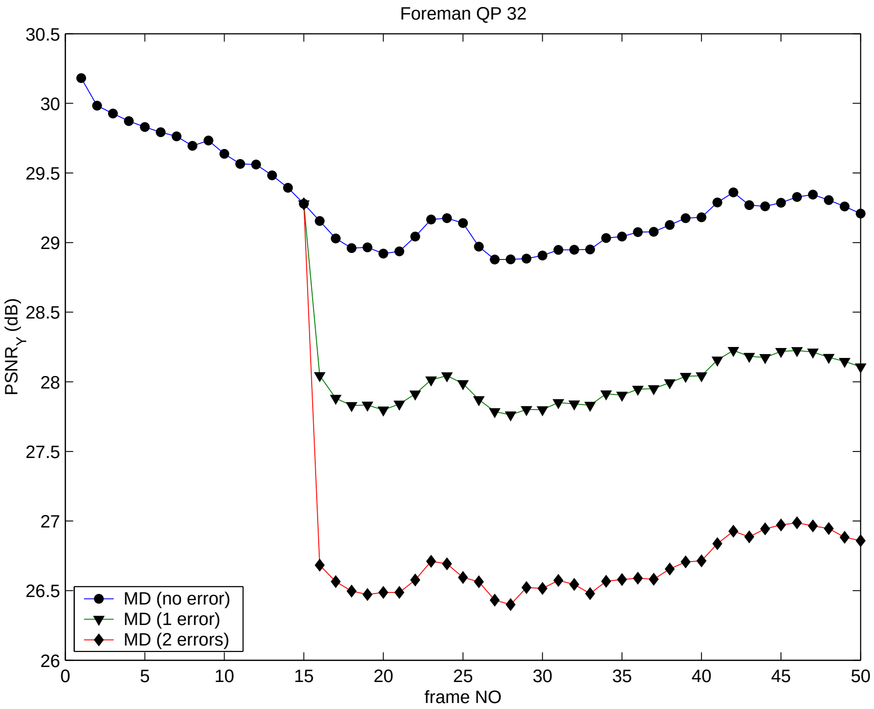

Figure 2.9: PSNR as a function of the frame number when none, one or two descriptions are lost in the "*foreman*" CIF sequence.

that pixel $x(2i, 2j)$ belongs to the lost description, the missing pixel is replaced with the mean of the available pixels.

Figure (2.9) shows an example of the recovering capabilities of the SMDC scheme when one or two descriptions are lost. As a comparison, the results of the no losses case is also given. Note that the PSNR loss is about 1 dB when three descriptions arrive and about 2 dB when two descriptions arrive.

However, it is worth noticing that also when no channel errors occur, the full resolution sequence is reconstructed with some small artifacts. This anomalous behavior is mainly due to small differences of the compression gain between the four encoders which manifests itself as a spatial non-homogeneous quality, visible at low bitrates. Correlating filters were adopted in order to address this problem and to obtain a more efficient reconstruction of the full resolution sequence. However, the performance of such filters was seriously affected by the data intrinsic correlation, and negligible improvements were obtained.

It is worth to note that the SMDC scheme is a particular case of the frame-based MDC scheme where additional descriptions are added with a correlating transform [RMR$^+$04, BRTV04]. However, there is a relevant drawback to this kind of solution, i.e. the high correlation between the coded streams usu-

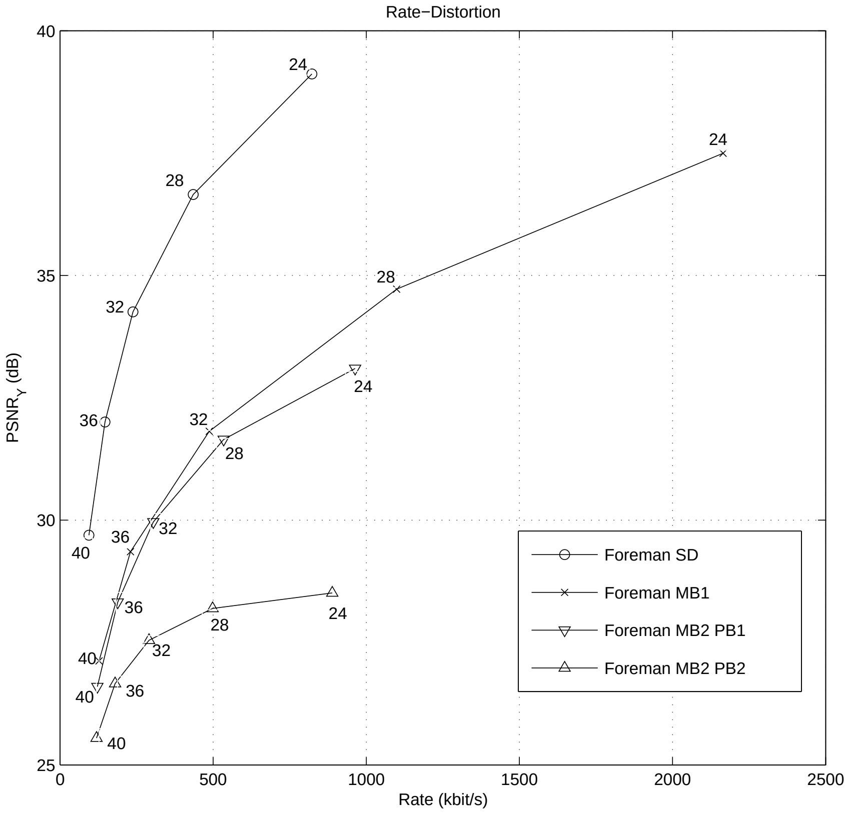

Figure 2.10: Rate-Distortion curves of different sub-sampling schemes for the sequence *"foreman"*.

ally causes a great increase of the bandwidth required by frame-based MDC algorithms. Weaknesses of SMDC are partially addressed by the following alternative MD coding.

2.4 Multiple Description Motion Coding

An interesting multiple description coding scheme based on spatial correlation was proposed by Kim and Lee [KL01] for the H.263 encoder [oII96], namely Multiple Description Motion Coding (MDMC). By following a similar coding strategy, a MDMC-based coding scheme was implemented on top of the H.264/AVC video coding standard [CM04].

The implemented scheme splits the block-based motion vector field in two parts using a quincunx sampling. The obtained motion vector subfields are transmitted to the decoder over separate channels. Then, the residual information of each macroblock is multiplexed on the two streams, by saving it in one description for even macroblocks and in the other stream for the odd ones.

Moreover, some further constraints have been imposed on the design of the scheme. First, each generated description has to be entirely decodable so that in case a whole description is lost, the receiver is able to decode the other one and to reproduce the sequence at a lower visual quality. Second, the computational overhead introduced by the MDC has to be kept as low as possible in order to reduce the computational requirements of the coder and to permit real time execution.

Both these goals have been achieved modifying the scheme of the standard H.264/AVC coder, as shown in Figure (2.11). In the general scheme, we included an additional block, called *Multiple Description Layer* (MDL), between the Network Abstraction Layer and the Transport Layer. The task of the new layer is to divide the bitstream provided by the H.264/AVC coder and to generate the two descriptions. Some information is repeated on both the bitstreams, while some other information is only included in one of them. In this way, the whole motion estimation is performed only once inside the Single Description coder (SDC), and the new layer only needs to split the information and to rewrite some syntax elements.

The descriptions are obtained copying the initial SPS and PPS headers on both streams as well as all the SH headers, while the slice data are divided into two parts. The motion vector information of each macroblock is partitioned using an evolution of the quincunx sampling used by Kim and Lee in [KL01]. This extension is necessary because the H.264/AVC coding standard permits further partitioning into blocks of different sizes, while the previous coding standard H.263 supported only 8x8 pixels blocks. The motion vectors that do not belong to the current description are substituted with null vectors since they require the lowest number of bits per component to be coded, i.e. only one. This substitution allows the system to get a syntactically correct bitstream while the increment of the overall bit rate is reduced to a minimum. The DCT residual information is alternatively included in one of the two descriptions, as Figure (2.12) shows. Whenever the coefficients are not available in the current description, they are considered null by setting the `coded_block_pattern` parameter to zero. In this way, each coded bitstream preserves the H.264/AVC syntax and can be correctly decoded. At the receiver side, whenever both the descriptions are received the MDL merges them together recovering the original bitstream with an operation that is the dual version of the partition performed at the transmitter.

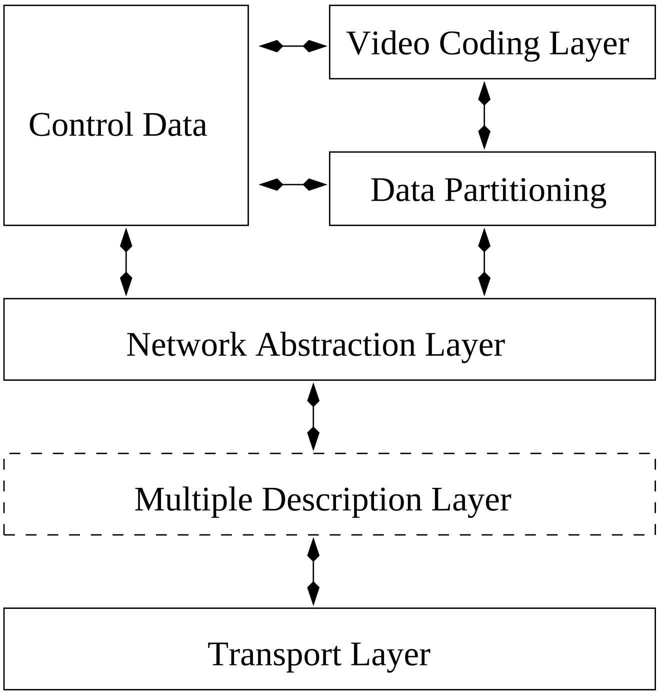

Figure 2.11: Scheme of the proposed coder/decoder. The dotted box represents the new Multiple Description Layer added to the original H.264/AVC scheme.

The splitting process presents some problems due to the context-based entropy coding algorithms, CABAC and CAVLC, which were adopted in the H.264/AVC standard. In the MDL we only support the semantics of the CAVLC because in case of loss of one description, the CABAC-coded bitstream is more vulnerable to errors. In order to provide evidence for the weakness of the CABAC algorithm, we can consider how the motion vectors are coded. The coding context is chosen according to the information of the blocks on the left and above the current one. Whenever a description is not available, lost motion vectors have to be estimated according to the neighboring ones. This operation increases the probability of selecting a wrong context model and can seriously compromise the correct decoding of the rest of the frame. On the other hand, although the CAVLC algorithm can achieve only a slightly inferior performance, it is more robust to errors.

In the splitting process, some problems arise while decoding the residual information. The residual information of every macroblock in H.264/AVC is partitioned into sixteen blocks of 4x4 pixels before the coding process. The CAVLC algorithm uses the number of quantized coefficients different from zero of the blocks on the left and above the current block. Since the coefficients

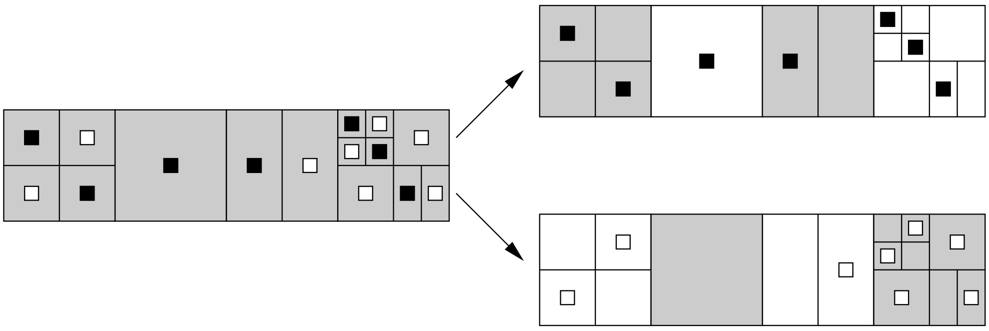

Figure 2.12: Splitting example: quincunx sub-sampling is applied to the motion vector filed of the four macroblocks and residual information is saved for even macroblocks in one description and for the odd ones in the other description.

of adjacent macroblocks are included in different descriptions by the splitting process, the merging routines of the MDL can not decode them correctly unless a transcoding is performed before sending the information over the two channels. In every macroblock, the upper and left 4x4 pixel blocks need to be transcoded, while the other nine blocks can be sent with not changes. The transcoding operation rewrites the `coeff_token`, which is the syntax element that contains the information about the number of quantized block coefficients different from zero. The bit string used to code the `coeff_token` is selected between several VLC tables, and it has to be changed for the upper and left blocks. In fact, during the splitting process the coefficients of the blocks belonging to the adjacent macroblocks have been set to zero, and the MDL needs to change the actual coding context. An example is shown in Figure (2.13). In the same way, a dual transcoding operation is performed at the receiver side during the merging process in order to update correctly the decoding context and to recover the original bitstream.

In case of loss of one description, the lost motion vectors are estimated by the mean of the adjacent ones, while the lost coefficients are not recovered.

The redundancy has been estimated measuring the percentage increment between the overall bit rate of the two MD streams and the original one. In our scheme, the allocated redundancy can not be controlled by reducing the perceptual quality as other MDC schemes do, but it is an intrinsic property of the coded sequences.

Figure (2.14) shows that the added redundancy for sequence "*foreman*" increases with the quantization parameter `QP`, that it is to say that the percentage of redundancy decreases for a video sequence coded at a higher visual quality.

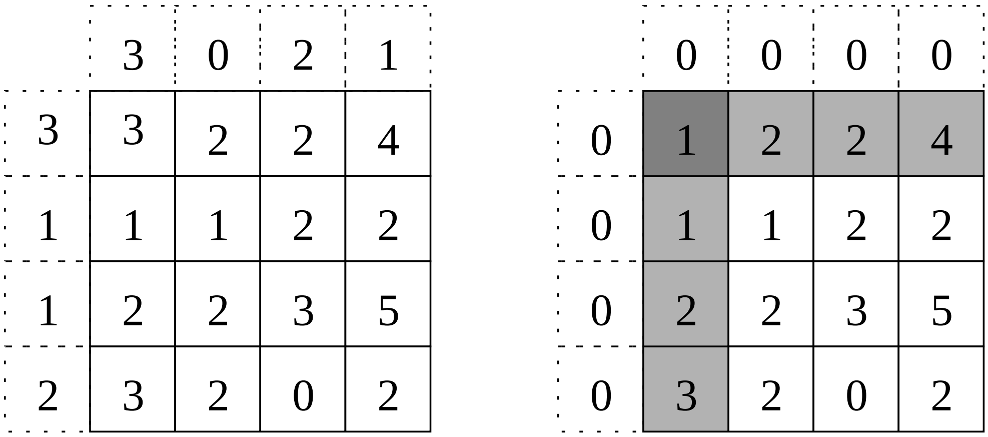

	3	0	2	1
3	3	2	2	4
1	1	1	2	2
1	2	2	3	5
2	3	2	0	2

	0	0	0	0
0	1	2	2	4
0	1	1	2	2
0	2	2	3	5
0	3	2	0	2

Figure 2.13: Example of wrong context after splitting the bitstream. On the left are shown the numbers of non-null coefficients in the 4x4 blocks of a macroblock with their context. On the right the same macroblock is shown as it would be decoded after the splitting process. The upper-left dark gray 4x4 block is wrongly decoded. All the gray 4x4 blocks need to be transcoded in order to get a correct bitstream.

Repeating the same test with other sequences like “*mobile*”, “*news*” and “*akiyo*”, we noticed that the redundancy grows faster for more stationary sequences.

A first explanation is given by the fact that for high-quality and high-motion sequences, most of the bitstream is represented by the residual information because a small `QP` value increases the number of non-null coefficients. Whenever the quality is low or the sequence is more stationary, the number of coded coefficients decreases, and the percentage of bitstream related to the residual information becomes proportionally smaller. On the other hand, the percentage of coded bits associated with the motion vectors and headers increases. This fact introduces more redundancy between the two coded bitstreams since more information is repeated.

The second explanation is related to motion vectors. If the sequence is stationary, then all vectors will be either null or close to zero, and they will be represented with a small number of bits per component. Therefore, the replaced null motion vector is closed to the real one that has to be coded. These two reasons can explain the faster growth of the redundancy for static sequences.

After checking the introduced redundancy, the recovering efficiency was estimated after three transmission errors that cause the loss of the 30th, 51st and 70th frames using 120 Kbit/s for a QCIF video sequences at 30 frame/s. Every error consists of the loss of one third of a description for a frame, which

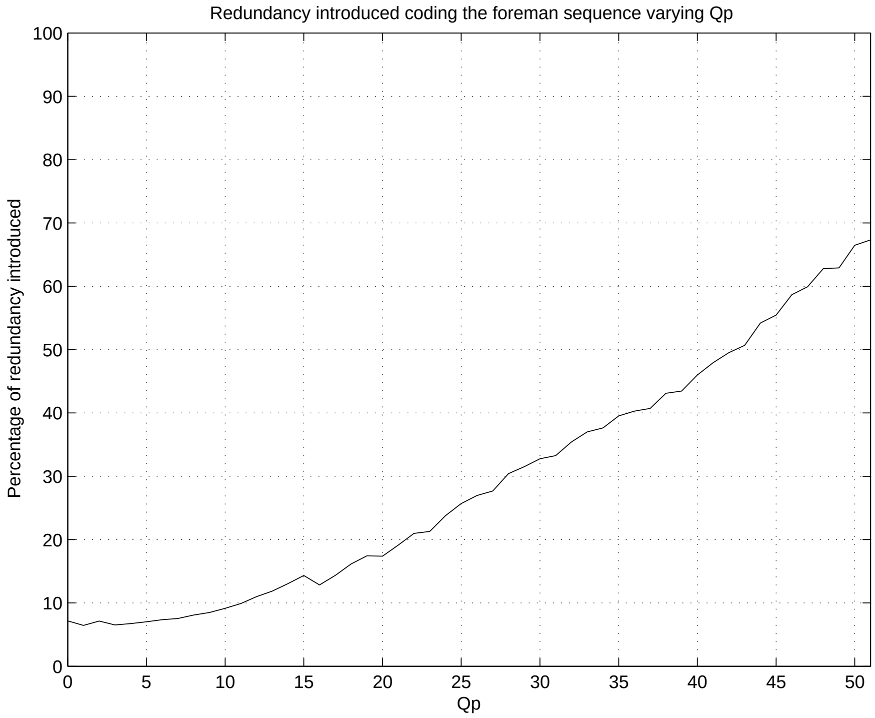

Figure 2.14: Redundancy introduced by the splitting process in the video sequence *"foreman"* QCIF with for all the values of `QP`.

is the same benchmark used by Kim and Lee in [KL01]. In the simulations the aim was to test the proposed scheme with two kinds of errors: errors affecting B frames and errors affecting P frames. The first kind of error can be related to a single frame only, and it does not propagate in the next pictures. On the other hand, whenever part of the information concerning a P frame is lost, the perceptual quality of all the following coded pictures decreases until the transmission of a new I frame since P pictures provide a reference for temporal prediction. A comparison between the obtained experimental results and the data provided in [KL01] shows that the adoption of the new H.264/AVC permits increasing the performance of the scheme with a 4 dB gain in PSNR in an error-free environment.

Whenever an error occurs on a P frame, the loss of quality of the decoded sequence is greater than in the original MDMC and the scheme does not fully recover the previous quality. Anyway, the quality of the reconstructed sequence has a gain of 3 dB compared to the H.263-based MDMC. The fact that the new coding scheme is not able to recover all the lost quality can be related to the lack of the Overlapped Block Motion Compensation (OBMC) in the H.264/AVC coding standard. While lost motion vectors can be correctly

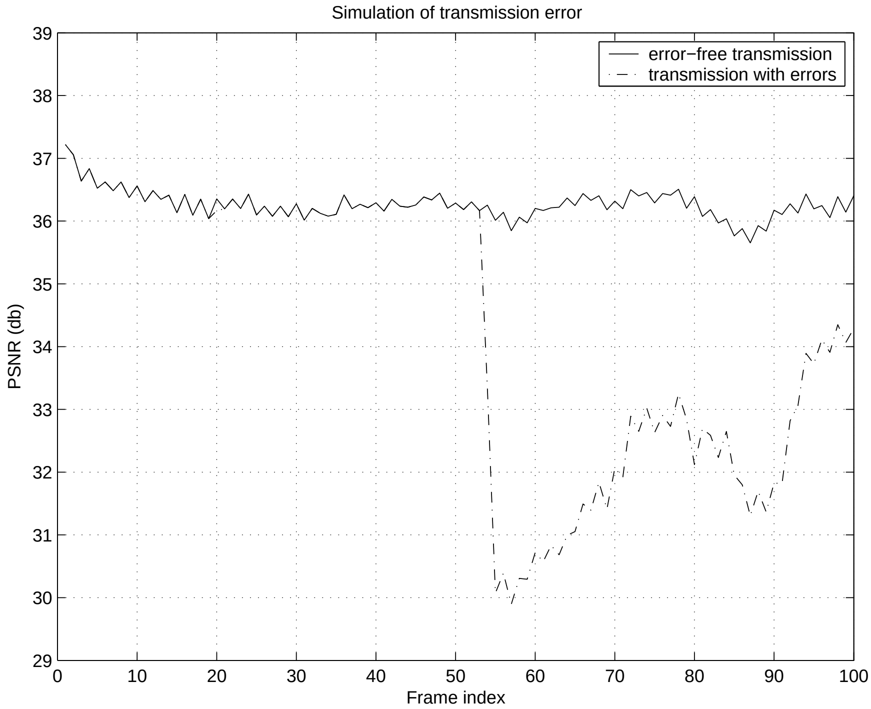

Figure 2.15: Results for a transmission with errors of the video sequence "*foreman*" QCIF with `QP` = cost. = 28.

estimated, the loss of the residual information can not be recovered in any way. The OBMC permits a better motion estimation and reduces the size of the residual information. Since this technique in not available in the H.264/AVC scheme, the loss of the residual information produces a greater quality degradation in the decoded sequence.

An example of transmission for the "*foreman*" sequence with MDMC is given in Figure(2.16).

2.5 Multiple State Video Coder

Depending on the sequence frame-rate and given the high temporal redundancy of the input sequence, each frame slightly differs from the previous ones. From this assumption, two (or possibly more) subsequences may be extracted from the original video sequence by temporal sampling. Each subset of frames is then processed in order to create different video streams. This technique was initially introduced by Jayant [Jay81] for voice transmission over faulty channels, and by Apostolopoulos for video coding [Apo00, Apo01a, Apo01b].

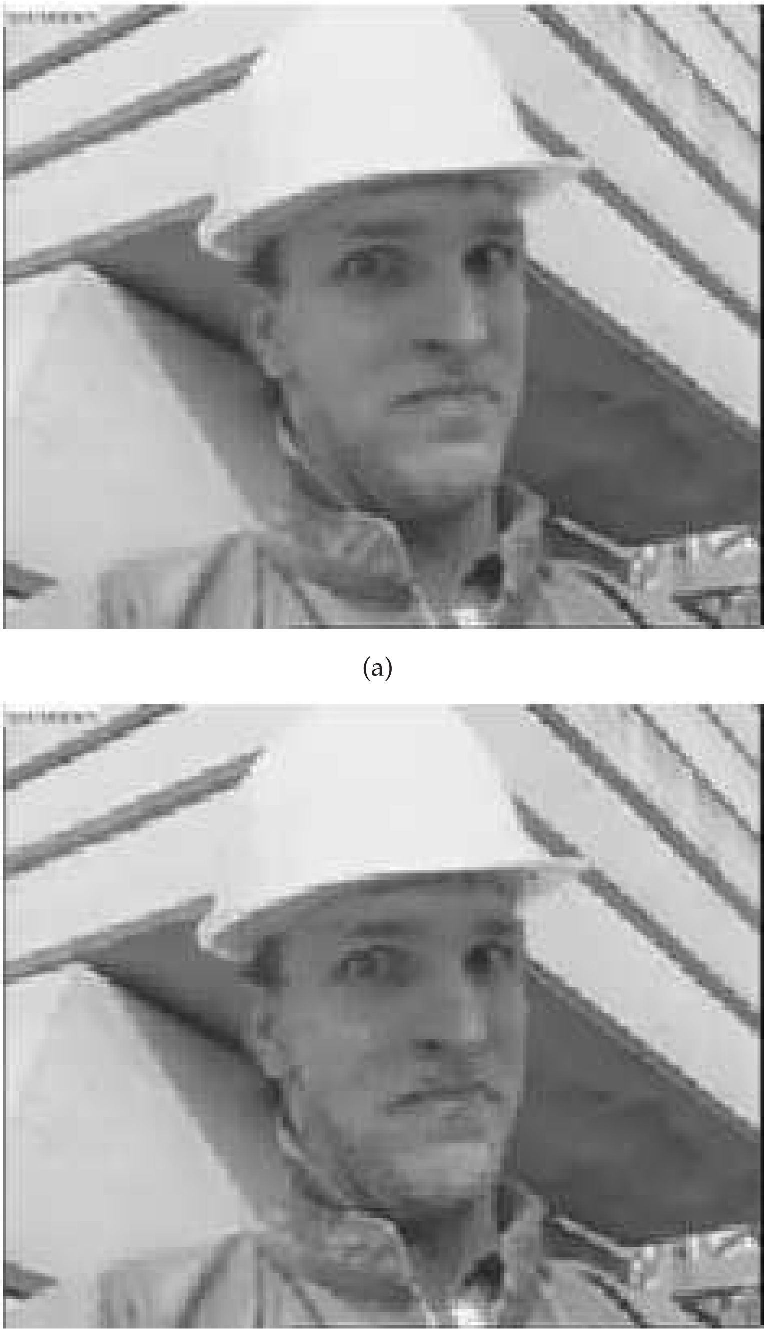

(a)

(b)

Figure 2.16: MDMC transmission example of the *"foreman"* sequence. In (2.16(a)) the correctly decoded frame is shown and in (2.16(b)) the reconstructed frame in case of error is shown. The estimated motion vector field leads to distortion in detailed parts of the image, such as the mouth.

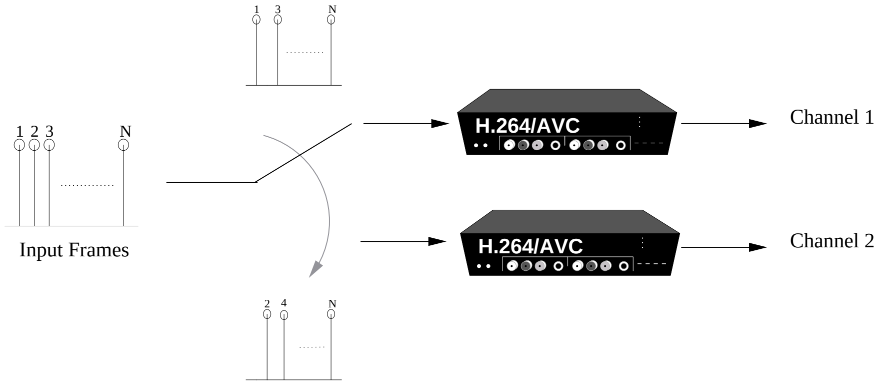

Figure 2.17: MD coding based on temporal sampling. Input sequence is partitioned into even-frame and odd-frame sequences, coded and sent over separate channels.

Given the input sequence[1], odd and even frames are divided into two subsequences $x(2n)$ and $x(2n+1)$. Each subsequence is then independently processed by a H.264/AVC coder, and corresponding output bitstreams are sent over independent channels. This type of MD coder is also known as *Multiple State Coder* since it requires the storage of more than one frame (i.e. state) in order to permit the correct decoding of the whole sequence.

Note that the two streams are perfectly compliant with the syntax defined in the standard. In case the receiver gets both the streams, it can reconstruct the whole sequence at full frame rate. Whenever one of the two streams is lost, a standard H.264/AVC decoder may reproduce anyway the coded sequence at half bitrate. Moreover, if the receiving device implements a MDC decoder, the missing information can be estimated interpolating the only subsequence correctly received as depicted in Figure (2.18).

At this point, a note on the interpolation process should be made. Since the state of the decoder cannot be recovered after a loss of information, the interpolation which estimates the missing frame increases the perceived distortion of the reconstructed sequence. This is mainly due to the mismatch between the reference state between encoder and decoder.

Note also that, despite the scheme of Figure (2.17) reports two distinct video coders and decoders, the whole scheme may be conveniently implemented using a *single* H.264/AVC coder, and keeping up to 16 frames in the motion-compensation frame buffer, because 16 is the maximum size of the H.264/AVC reference list. Hence, this particular implementation could process the two descriptions immediately after the coding operation reducing, in this way, the

[1] Note that in this case n represents the time.

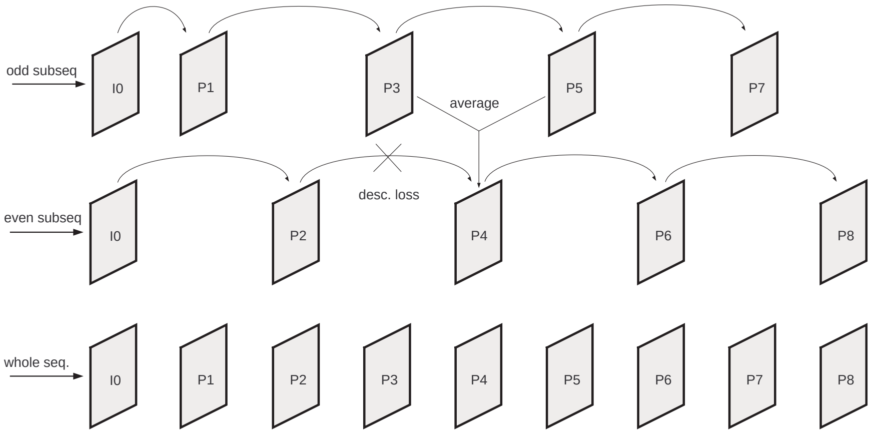

Figure 2.18: Error-concealment for the lost frame using the average algorithm. When a description is lost, the missing frame (P_4) is reconstructed by averaging the previous and successive frames in the sequence (P_3,P_5).

overall computational requirements.

In the case of losses, the quality of the reconstructed sequences is seriously affected by the specific algorithm used for error concealment. A naive solution consists in displaying the coded sequence at half bitrate. This technique, however, yields a less smooth reconstructed sequence with decreased visual quality.

Smoothness may be improved estimating the lost state. During tests, different types of recovering techniques were experimented. In the first state-recovering algorithm, the average between previous and succeeding frames is used as estimate of the lost state. The "average" state was then inserted in the H.264/AVC-decoder frame buffer permitting the decoding of all the following frames in the corresponding subsequence as depicted in Figure (2.18). Unfortunately, the recovered "average" state is poorly correlated with the original state at the receiver. Hence, end users may experiment a perceptually-relevant quality loss resulting in annoying flickering effects. This kind of effects arises from the alternate visualization of frames belonging to the uncorrupted subsequence and frames extrapolated from the recovered state, as shown in Figure (2.19).

Quality variation can be indeed smoothed by taking into account the information on motion vectors leading to the *in-place motion compensation*. Since motion vectors computed in the encoding process are temporally correlated, then a lost frame could be estimated according to the information available from the

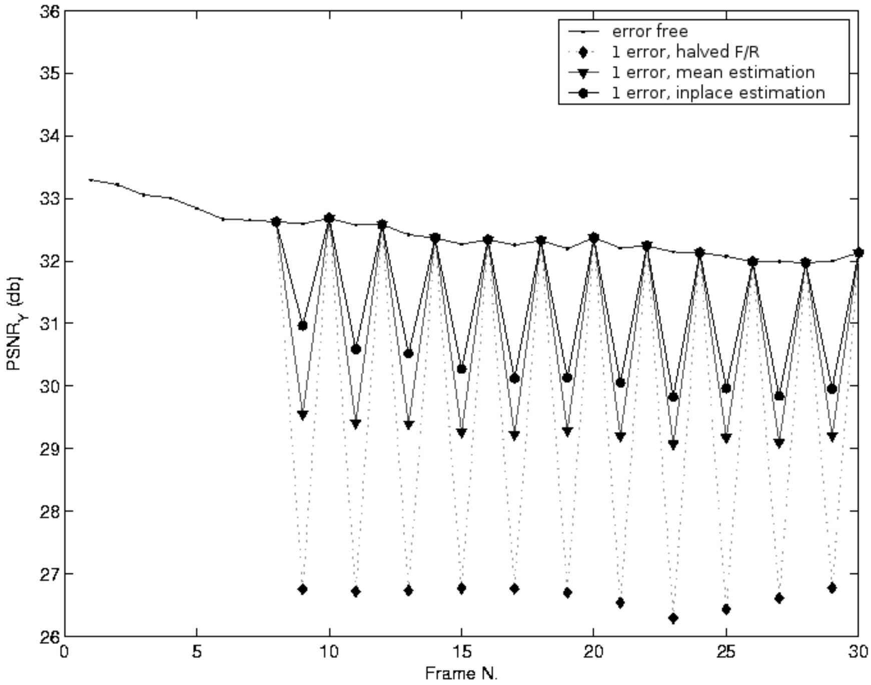

Figure 2.19: PSNR (luma component) for the `foreman` sequence coded at 128 Kbit/s (`QP`=cost). After that a description has been lost, the flickering effect arises as a consequence of the misalignment between the reference state at encoder and decoder.

succeeding one. Let $x(2n+1)$ be the lost frame (odd sequence) and $x(2n+2)$ be the following even frame which is decoded taking the frame $x(2n)$ as reference for motion compensation. A good estimation of $x(2n+1)$ can be made taking the previous frame as $x(2n)$ reference and using the MVs of $x(2n+2)$ halved for motion compensation, as represented in Figure (2.20).

Experimental results showed that the in-place recovering algorithm improves the quality of the reconstructed sequence achieving a 1 dB PSNR gain with respect to the interpolation by frames average. Obviously, the in-place technique has a greater computational complexity since motion compensation is required to reconstruct the lost state. Figure (2.21) and Table (2.2) report a comparison between the different performances obtained by the algorithms described. Finally, Figure (2.21) reports the PSNR behaviors of the three recovering strategies for the *"foreman"* sequence. A one-frame loss has been simulated at the 10-th frame, and, as expected, the simpler is the recovery technique the lower is the recovered quality. Although more complex, the In-place motion estimation is the recovery strategy that gives the best results.

Problems concerning the MSVC scheme are mainly related to a loss of the

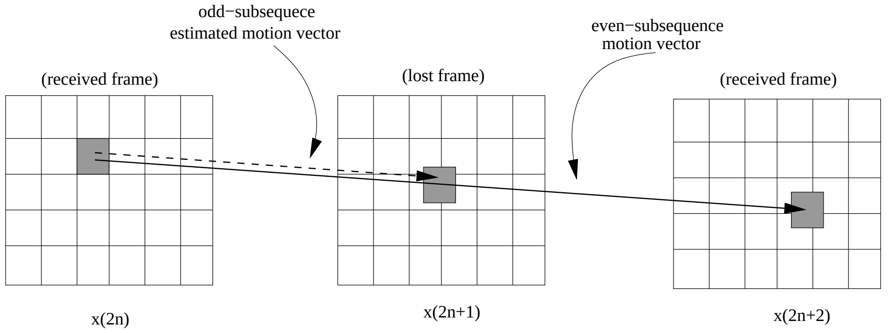

Figure 2.20: Error-concealment using in-place motion compensation. The motion vector of the lost frame $x(2n+1)$ is reconstructed halving the motion vector of the frame $x(2n+2)$.

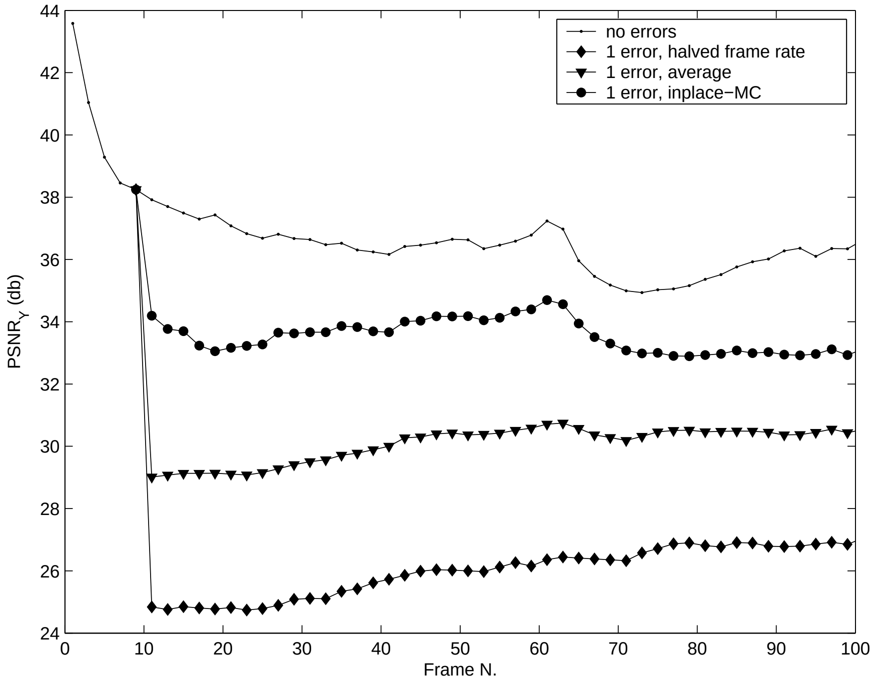

Figure 2.21: PSNR (luma component) of the *odd* frames for the *"foreman"* sequence coded at 128 Kbit/s (QP=cost) using different error-concealment techniques. *In-place* motion estimation outperforms the *halved-frame rate* and the *average* methods, but is more computational demanding.

***"foreman"*, QCIF, QP=cost.**						
Rate	64 (Kb/s)			128 (Kb/s)		
Algorithm	$F_r/2$	Avg.	I-MC	$F_r/2$	Avg.	I-MC
Δ PSNR	1.1	0.6	0.4	1.7	1	0.8
œ$_{\textbf{PSNR}}$	±2.2	±1.2	±0.5	±3.2	±1.9	±1.5

***"foreman"*, QCIF, Rate controlled**						
Rate	64 (Kb/s)			128 (Kb/s)		
Algorithm	$F_r/2$	Avg.	I-MC	$F_r/2$	Avg.	I-MC
Δ PSNR	0.4	0.2	0.2	0.6	0.3	0.3
œ$_{\textbf{PSNR}}$	±0.8	±0.4	±0.4	±1.2	±0.6	±0.6

Table 2.2: Comparison between the different concealment algorithms proposed.

predictive coding efficiency. The temporal correlation which is used to predict a frame from the previous one in a standard H.264/AVC coder may be greatly reduced when we split the sequence into subsequences of even and odd frames respectively, and this behavior is particularly evident for sequences presenting fast motion.

The MDC scheme based on temporal correlation may be improved using two motion vectors to estimate each frame. In fact, motion vectors coding "describe" the correlation between neighboring frames to the receiver. Hence, in the case a frame is lost, the error concealment algorithm can rely on more than one reference for estimating the missing information.

A final graphical example is given in Figure (2.22), where the recovering strategies based on averaging and inplace motion estimation for the lost 285th frame of the "*foreman*" sequence are shown.

2.6 Motion-Compensated Multiple Description Video Coding

In the MCMD scheme [ZMD05, CCD$^+$06], the input sequence is sub-sampled into even and odd frames sequences. The MD encoder is made-up of three dependent coders employing separated frame buffers: a central coder which receives both even and odd frames, and two symmetric side coders which work respectively on even and odd frames. Figure (2.23) shows the encoder scheme with its central coder and one side coder (the other is perfectly symmetric and

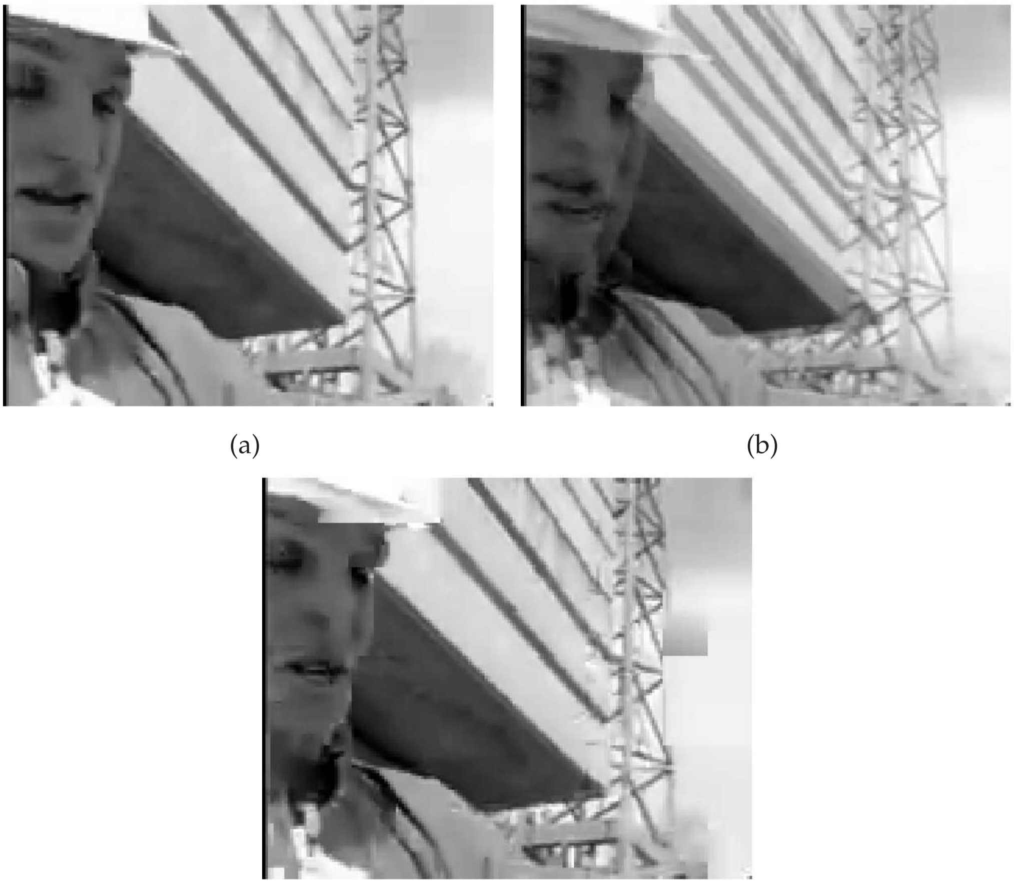

(a)

(b)

(c)

Figure 2.22: MSVC transmission example. In (2.22(a)) the correctly received 285th frame of the "*foreman*" sequence is shown, while in the other two figures the reconstruction of the lost frame is shown. In (2.22(b)) the frame estimated as mean of the two adjacent correctly received frames is shown, while in (2.22(c)) the inplace motion compensation is adopted. It clearly appears that the solution based on averaging frames leads to ghosting artifacts, while inplace motion compensation leads to blocking artifacts, due to motion estimation and lack of the residual signal.

therefore has not been reported).

Let QP_0 and QP_1 be, respectively, the quantization parameters of central coder and side coders. The value set for QP_0 defines the total amount of full-rate distortion D_0 admitted in case of correct transmission. Usually, this is a fixed parameter of the system design. Instead, QP_1 controls the distortion introduced when only one description arrives, and determines the capabilities of the MCMD decoder to reconstruct the lost reference state from only one description. The smaller is QP_1, the greater is the efficiency of side coders to approximate the correct reference state.

The central coder works on the full-rate sequence, and predicts the current frame $x(n)$ from the previous two, $x(n-1)$ and $x(n-2)$, by implementing a second-order linear predictor after the block-based motion compensation in the DPCM loop (MC block) as shown in Figure (2.23).

$$\hat{x}_0(n) \quad = \quad a_1\tilde{x}_0(n-1) + (1-a_1)\tilde{x}_0(n-2) \ . \tag{2.3}$$

The coefficient $a_1 \in [0,1]$ in (2.3) controls the trade-off between coding efficiency and robustness to channel errors. The central prediction error

$$e_0(n) = x(n) - \hat{x}_0(n) \tag{2.4}$$

is quantized (Q_0 block in Figure (2.23) using the quantization step QP_0, and yields the output signal

$$\tilde{e}_0(n) = e_0(n) + q_0(n) = x(n) - \hat{x}_0(n) + q_0(n) \tag{2.5}$$

where $q_0(n)$ is the quantization error under the assumption of granular distortion.

Side coders are two standard-compliant H.264 encoders which process either even or odd frames, respectively. Let $x(2k)$ be the even frame sequence and $x(2k+1)$ the odd one, then the error signals processed by side coders are

$$\begin{array}{rcll} e_1(n) & = & e_1^*(n) - \tilde{e}_0(n) & if\ n = 2k, k \in \mathbb{N} \\ e_2(n) & = & e_2^*(n) - \tilde{e}_0(n) & if\ n = 2k+1, k \in \mathbb{N} \end{array} \tag{2.6}$$

where the signals $e_1^*(n)$ and $e_2^*(n)$ are given by

$$\begin{array}{rcll} e_1^*(n) & = & x(n) - \tilde{x}_1(n-2) & if\ n = 2k, k \in \mathbb{N} \\ e_2^*(n) & = & x(n) - \tilde{x}_2(n-2) & if\ n = 2k+1, k \in \mathbb{N}\ . \end{array} \tag{2.7}$$

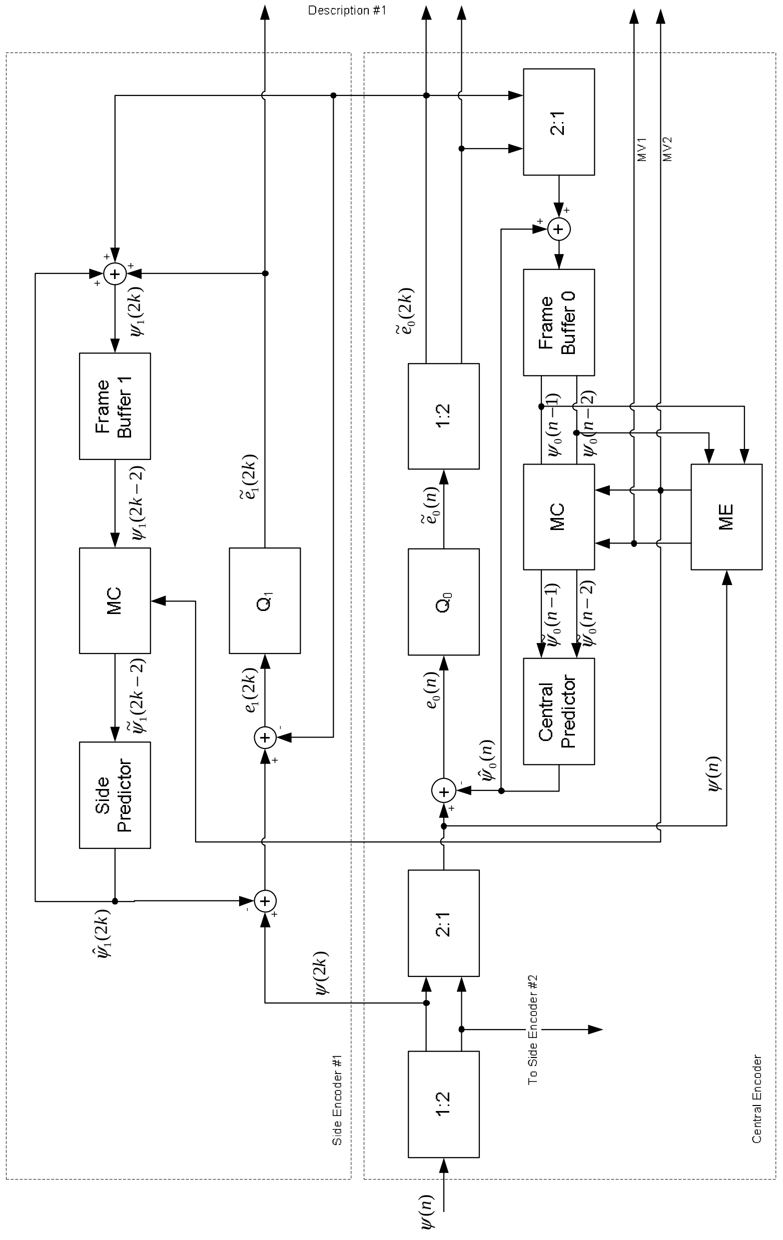

Figure 2.23: MCMD encoder in the H.264/AVC standard. For simplicity, not all signals indexes are expressed in terms of n, some are expressed in terms of k. $2k$ means $n = 2k, k \in \mathbb{N}$, i.e., they are referred only to even frames, since the odd ones are encoded by the other side encoder, which is not included in the block scheme.

After the signals $e_1(2k)$ and $e_2(2k+1)$ are quantized with quantization step QP_1, a distortion signal is added producing

$$\begin{aligned}\tilde{e}_1(n) &= e_1(n) + q_1(n) \qquad (2.8)\\ \tilde{e}_2(n) &= e_2(n) + q_2(n)\ . \qquad (2.9)\end{aligned}$$

It can be easily verified that the following relationships hold

$$\begin{aligned}e_1(n) &= \tilde{x}_0(n) - \hat{x}_1(n) \qquad (2.10)\\ e_2(n) &= \tilde{x}_0(n) - \hat{x}_2(n)\ . \qquad (2.11)\end{aligned}$$

In the original MCMD scheme, motion estimation is performed only once in the central coder for the two reference frames $x(n-1)$ and $x(n-2)$ yielding the two sets of motion vectors MV_1 and MV_2. On the other hand, side coders have no motion estimation, and use the vectors MV_2 computed by the central coder for their motion compensation. Since motion-vectors number and values are necessarily associated to the current partitioning of macroblocks, side coders are forced to take the same macroblock layout of the central coder. This constraint is highly inefficient since side coders must have QP_1 larger than QP_0, and this fact decreases the quality of their reference frames. Constraining a finer side partition increases the bit-rates required to code side motion vectors, and reduces the control over the redundancy allocated in the system.

In the H.263 standard, a constrained side macroblock layout does not affect significantly the MCMD performance since only two types of partitioning are used. Instead, the new coding features of H.264/AVC permit to partition a macroblock down to 4 × 4 sub-blocks. This fact increases the number of different blocks layouts and motion vectors displacements. As a consequence, the resulting side coding bitrates greatly vary according to how the partitioning has been chosen.

In order to bound the increment of redundancy in the H.264/AVC standard, an advanced three-steps motion estimation algorithm was implemented.

Forcing the macroblock partition at side coders increases the additional redundancy. In order to mitigate this effect, we let each side coder to estimate independently its optimal motion vectors and macroblock partitions. Unfortunately, the reconstructed frame at the central coder is not yet available, and therefore, side coders cannot coherently perform motion compensation and provide their mismatch signal. However, under the reasonable hypothesis that the mismatch signal contains mainly high-frequency components, we may assume that the coarse quantization of side coders retains only low-frequency components, allowing us to perform side motion estimation before the central one. The resulting algorithm can be summarized in the following three steps.

1. The motion vectors MV_2 and macroblock partitions for side coders are estimated.

2. The MV_2 set is passed to the central coder, and central motion estimate is performed by computing the MV_1 set. Since this operation may imply a different optimal macroblock layout, the MV_2 vectors need to be adapted to fit it. Adaptation is obtained by splitting the blocks used for motion estimation in the side encoder and replicating the partitioning structure of the central encoder.

3. The mismatch signal is computed as the difference between the reconstructed frames at central and side coders, see Equation (2.6). No motion estimation is performed in this step.

Following this three-step algorithm, the estimate of the MV_2 motion vectors is demanded to side coders rather than the central one. Thus, side bit-rates significantly decrease at the expense of using sub-optimal MV_2 motion vectors in the central coder. Nevertheless, simulations showed that the resulting overall redundancy is acceptable for MDC applications.

Forcing side coders to compute the MV_2 motion vectors instead of the central coder yields a great decrement of side coders bit-rates, at the cost of non-optimal motion vectors used in the central coder. Nevertheless, the resulting overall redundancy is now acceptable for MCMD applications as simulations showed.

The main characteristic of this MDC scheme is its closed-loop structure, which makes possible to control the decoder drift in case of transmission error. Unfortunately, this approach has two drawbacks that pose a serious limitation on its adoption. First, it is extremely heavy: simulations require very long times, because every operation in the encoder is doubled. Therefore, it is impossible to use it on mobile devices, which will not be able to execute it in an acceptable time because of lack of sufficient computational resources. Second, the drift control is slow. Even in case it could run in real-time, the same effect could be achieved by refreshing the decoder status, either by transmitting an Intra frame or by adopting intra-refreshing, which has the main advantage of not increasing the required bandwidth at the cost of requiring longer time to refresh the full decoder status.

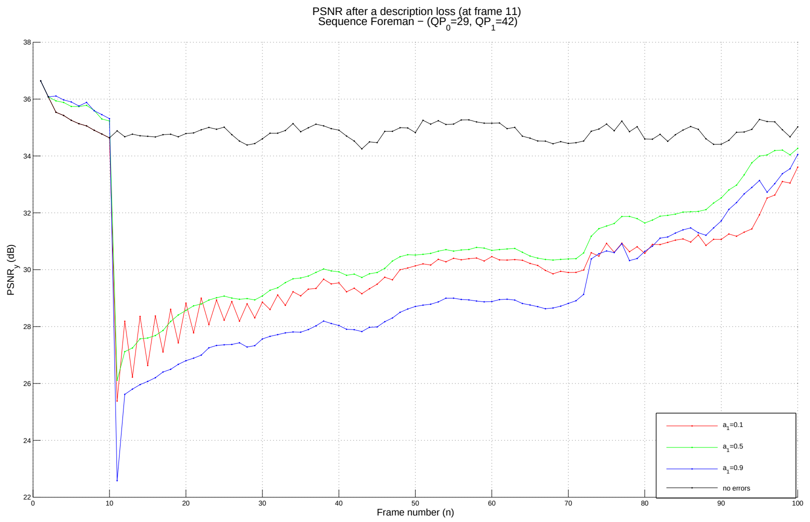

Figure 2.24: Transmission example for the *"foreman"* sequence with $\texttt{QP}_0 = 29$ and $\texttt{QP}_1 = 42$, in case of transmission error at the eleventh frame. The PSNR is plotted for three values of the a_1 parameter, i.e. the weights of the second order predictor.

A final graphical example of error recovery with MCMDC for the *"foreman"* sequence is given in Figure (2.25), where the estimated frame and the error are shown.

2.7 MDSQ-based Multiple Description Video Coding

2.7.1 The Multiple Description Scalar Quantizer

The Multiple Description Scalar Quantizer [Vai93b] (MDSQ) is an extension of the optimal Lloyd-Max Scalar Quantizer (SQ), where the encoder sends the information over two different channels subject to a rate constraint.

Formally, let x be the output of a random process we want to encode. Suppose that the transmission system has two channels with transmission rates R_1 and R_2, that may be in a working or non-working state.

An (M_1, M_2)-level MDSQ maps source samples x onto the reconstruction levels

$$\hat{x}^0 \in \hat{\mathcal{X}}^0 \quad = \quad \left\{ \hat{x}^0_{ij}, (i,j) \in \mathcal{C} \right\} \tag{2.12}$$

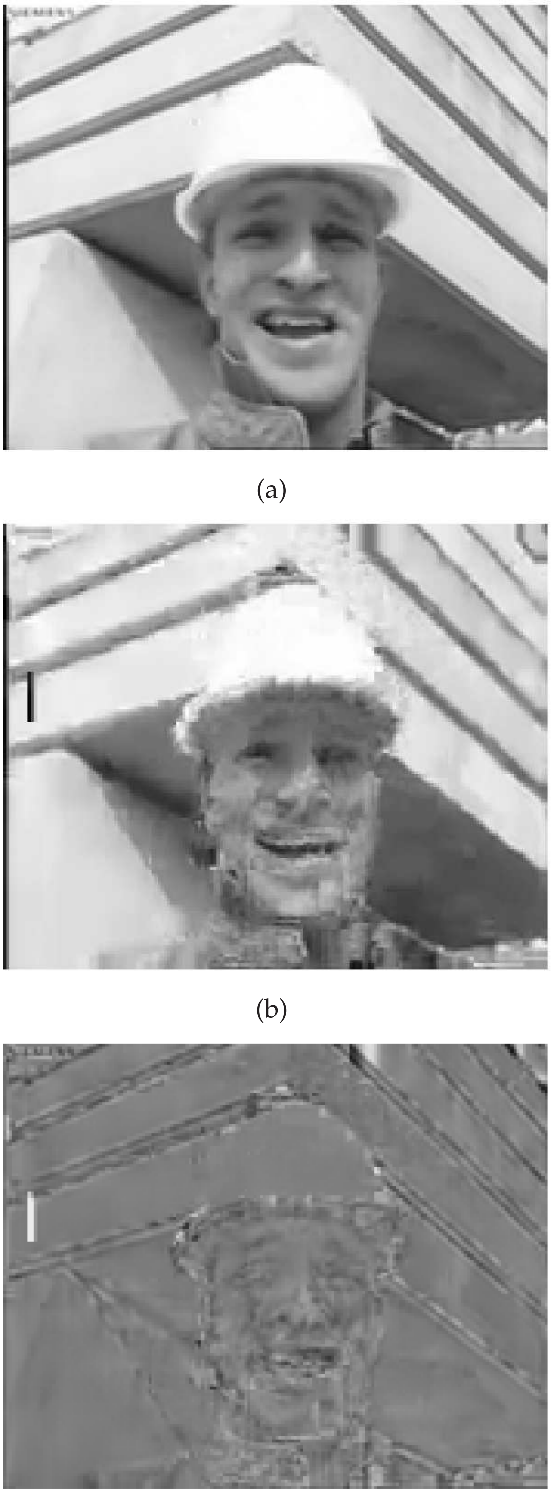

(a)

(b)

(c)

Figure 2.25: MCMDC transmission example of the *"foreman"* sequence. In (2.25(a)) the correctly received frame is shown. Figure (2.25(b)) holds the reconstructed frame in case of transmission error and Figure (2.25(c)) shows the difference of the two previous frames.

$$\hat{x}^1 \in \hat{\mathcal{X}}^1 = \left\{\hat{x}_i^1, i \in \mathcal{I}_1\right\} \tag{2.13}$$

$$\hat{x}^2 \in \hat{\mathcal{X}}^2 = \left\{\hat{x}_j^2, j \in \mathcal{I}_2\right\} \tag{2.14}$$

where $\mathcal{I}_1 = \{1, 2, \cdots, M_1\}$, $\mathcal{I}_2 = \{1, 2, \cdots, M_2\}$ and $N = |\mathcal{C}|$. The set $\hat{\mathcal{X}}^0$ is the central decoder codebook, while $\hat{\mathcal{X}}^1$ and $\hat{\mathcal{X}}^2$ are the codebooks of side decoders.

An MDSQ can be represented as a couple of side encoders $f_1 : \mathbb{R} \to \mathcal{I}_1$ and $f_2 : \mathbb{R} \to \mathcal{I}_2$ working at rates $R_1 = \log_2 M_1$ and $R_2 = \log_2 M_2$ respectively, which select the indexes i and j, and three decoders, $g_0 : \mathcal{C} \to \mathbb{R}$ (central encoder), $g_1 : \mathcal{I}_1 \to \mathbb{R}$ and $g_2 : \mathcal{I}_1 \to \mathbb{R}$ (side decoders) which select the reconstruction levels from their codebooks corresponding to the received indexes.

It is obvious that the encoder functions f_1 and f_2 impose a partition of $\mathbb{R}$ for side decoders, namely $\mathcal{A}^1$ and $\mathcal{A}^2$. They also impose a partition of $\mathbb{R}$ for the central decoder, because its partition must obey to the constraint

$$\mathcal{A}_{ij} = \{x : f_1(x) = i, f_2(x) = j\} \ . \tag{2.15}$$

For this reason, an MDSQ is completely described by the reconstruction levels $\hat{\mathcal{X}}^0$, $\hat{\mathcal{X}}^1$ and $\hat{\mathcal{X}}^2$ and by the encoder functions f_1 and f_2.

Let x be the input of the quantizer and $\hat{x}^m$ be the output of the m-th decoder, where $m \in (1, 2)$; $d_m(x, \hat{x}^m)$ denotes the distortion between the input sample and the m-th decoder output. The average central and side distortions are given by

$$E\left[d_0\left(x, \hat{x}^0\right)\right] = \sum_{(i,j)\in\mathcal{C}} \int_{\mathcal{A}_{ij}} d_0\left(x, \hat{x}_{ij}^0\right) p(x)dx \tag{2.16}$$

$$E\left[d_1\left(x, \hat{x}^1\right)\right] = \sum_{i\in\mathcal{I}_1} \int_{\mathcal{A}_i^1} d_1\left(x, \hat{x}_i^1\right) p(x)dx \tag{2.17}$$

$$E\left[d_2\left(x, \hat{x}^2\right)\right] = \sum_{j\in\mathcal{I}_2} \int_{\mathcal{A}_j^2} d_2\left(x, \hat{x}_j^2\right) p(x)dx \tag{2.18}$$

where $\mathcal{A}_i^1$ is the i-th cell of the partition imposed by f_1 and $\mathcal{A}_j^2$ is the j-th cell of the partition imposed by f_2. They can be obtained evaluating

$$\mathcal{A}_i^1 = \bigcup_j \mathcal{A}_{ij} \tag{2.19}$$

$$\mathcal{A}_j^2 = \bigcup_i \mathcal{A}_{ij} \tag{2.20}$$

For given values M_1, M_2, D_1, D_2, an MDSQ is said to be optimal if it solves the following minimization problem:

$$\begin{cases} \min E\left[d_0\right] \\ E\left[d_1\right] \leq D_1 \\ E\left[d_2\right] \leq D_2 \end{cases} \tag{2.21}$$

In case $M_1 = M_2$, the MDSQ is said to be balanced if $E\left[d_1\right] = E\left[d_2\right]$.

Computing optimal reconstruction levels for a MDSQ is connected to the *index assignment problem*. Since $\mathcal{A}_i^1$ and $\mathcal{A}_j^2$ are tied to $\mathcal{A}_{ij}$ by (2.19) and (2.20), it easy to understand that indexes ij of the central decoder cells impose the shape of side decoders cells and affect side decoders performance. Vaishampayan proposed two different algorithms to solve this problem, namely the *nested index assignment* and the *linear index assignment*. Both algorithms scan the encoders cells as if they were matrix elements lying on the main and its $2k$ neighbor diagonals and associate a progressive number with them. Since each matrix element is associated to a couple of indexes, the scanning algorithms map the central decoder cells indexes to those of the side decoders.

The *nested index assignment* scans the matrix elements in two ways: the east scan and the south scan, which always start from an element of the matrix main diagonal. The east scan starting from element of index (i, i) is given by the sequence $(i, i), (i, i+1), (i+1, i), (i, i+2), (i+2, i), \cdots, (i, i+k), (i+k, i)$ and the south scan is represented by the sequence $(i, i), (i+1, i), (i, i+1)$, $(i+2, i), (i, i+2), \cdots, (i+k, i), (i, i+k)$. In order to obtain two balanced description, these two scanning strategies are pairwise alternately applied.

The *linear index assignment* also consists of two different scan types, namely the U-scan and the D-scan, which are alternately applied as those of the nested index assignment. These methods start from an element of one of the most external diagonals, scan the matrix elements orthogonally to the main diagonal and finish when they reach the opposite external diagonal. Each scan can hold an even or odd number of elements. In case this number is odd, the U and D scans are described by the sequences $\left(i + \left\lfloor \frac{k}{2} \right\rfloor, i - \left\lfloor \frac{k}{2} \right\rfloor\right)$, $\left(i + \left\lfloor \frac{k}{2} \right\rfloor - 1, i - \left\lfloor \frac{k}{2} \right\rfloor + 1\right), \cdots, \left(i - \left\lfloor \frac{k}{2} \right\rfloor, i + \left\lfloor \frac{k}{2} \right\rfloor\right)$ and $\left(i - \left\lfloor \frac{k}{2} \right\rfloor, i + \left\lfloor \frac{k}{2} \right\rfloor\right)$, $\left(i - \left\lfloor \frac{k}{2} \right\rfloor + 1, i + \left\lfloor \frac{k}{2} \right\rfloor - 1\right), \cdots, \left(i + \left\lfloor \frac{k}{2} \right\rfloor, i - \left\lfloor \frac{k}{2} \right\rfloor\right)$ respectively, while a similar expression can be obtained for an odd number of cells.

It can be shown that varying the value of k and therefore altering the number of diagonals used in the scanning process, the behavior of side decoders changes. For small values of k, side decoders work at high bitrate and low distortion, while for big values of k their quality decreases together with the bitrate associated with them.

2.7.2 Implementation of the scheme

We decided to implement a MDSQ based scheme on the JVT H.264/AVC reference code using the base layer with the addiction of B frames and imposing some constraints on its design:

1. the central decoder must reconstruct the same sequence as if it were a standard single description encoder;
2. both descriptions have to be singularly decodable by a standard decoder and;
3. the introduced computational overhead should be kept as small as possible.

All these goals were achieved inserting a splitting block in the standard H.264/AVC scheme after quantization, as show in Figure (2.26). This block generates two descriptions duplicating the control structures like SPS, PPS and SH and information about the motion vectors. Before passing the residual information to the Network Abstraction Layer (NAL), coefficients are divided into two descriptions applying a MDSQ. Since the quantization pass is stored in several places (PPS, SH and the macroblock layer), we decided to set the same `QP` value in the central and side decoders. This non optimal solution reduces the computational overhead but at the same time increases distortion in the side decoders. As subsequently explained, this is not a great problem, because total distortion does not increases too much: DCT coefficients follow a laplacian-like p.d.f. and small values distortion is small.

The decoder can be implemented similarly to the encoder. A merge block has to be added between the NAL and the inverse quantizer. Whenever the decoder receives both descriptions, the original quantized value is obtained from the assignment matrix, while, in case of a channel malfunctioning, the received description identifies the cell of a side decoder and the H.264/AVC decoder works as if it were using a bigger `QP` value. In fact, since many central decoder cells are mapped into the same side decoder index, we obtain the same result as if we would obtain quantizing with a larger `QP`.

The first implementation of the linear index assignment was mainly based on the algorithm proposed by Vaishampayan in [Vai93b]. The only difference consisted in assigning the zero value to the center of the assignment matrix

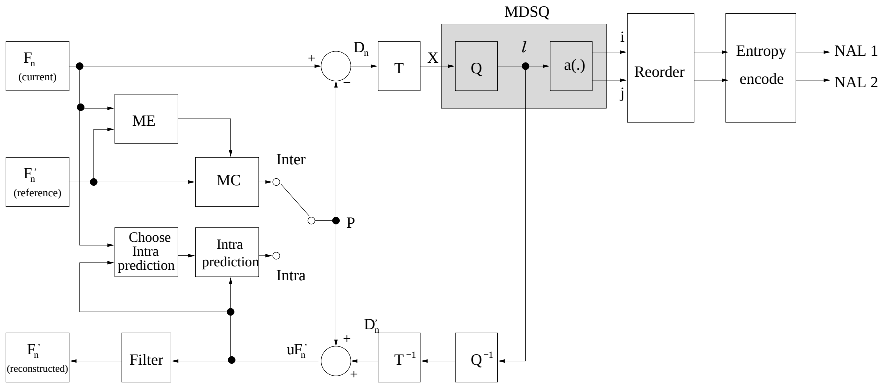

Figure 2.26: Modified H.264/AVC block scheme. MDSQ is obtained adding a splitting function, namely $a(\cdot)$ after quantization and duplicating output blocks in order to generate two distinct NAL units.

and not assigning any other value in the secondary diagonal. During tests, this algorithm behaved quite disappointingly: increasing the number of diagonals used in the algorithm, the introduced redundancy also raised. Analyzing the bitstream produced by the encoder, we noticed that the cause was due to the Context Adaptive Variable Length Coding (CAVLC). Since linear index assignment scans the diagonals orthogonally to them, adding more diagonals caused small values to be mapped onto bigger ones. For example, mapping 0 onto $(0,0)$ and using 7 diagonals, for $k = 3$, level 1 would be mapped onto $(-1,2)$, 2 onto $(0,1)$, 3 onto $(1,0)$ and so on. It is easy to notice that level 2 is mapped onto smaller values than the previous one. This fact leads to CAVLC malfunctioning: MDSQ output values have a not laplacian p.d.f. and therefore CAVLC tables do not fit them. This led us to redesign the assignment algorithm, taking into account both how CAVLC works and coefficients distribution, in order not to translate small input values into big values of the side encoders. Since H.264/AVC uses run length coding to reduce the information that has to be saved, we decided to map as many as possible small values onto zeros to enhance the encoder efficiency. The solution we adopted consisted in excluding some cells from the assignment matrix before executing the algorithm. Considering the cell associated to the value 0 of the central decoder as the center of the matrix, we discarded all the cells of the first and the third quadrant, as shown in Figure (2.27). This assures that coefficients in the interval $[-3,3]$ are always mapped onto zero at least in one of the side encoders for any value of k. Once the coefficients are split and the run-length symbols are recomputed, the Coded Block Pattern (CBP) value has to be recalculated permitting to have a decodable bitstream also when all the coefficients of a 8x8

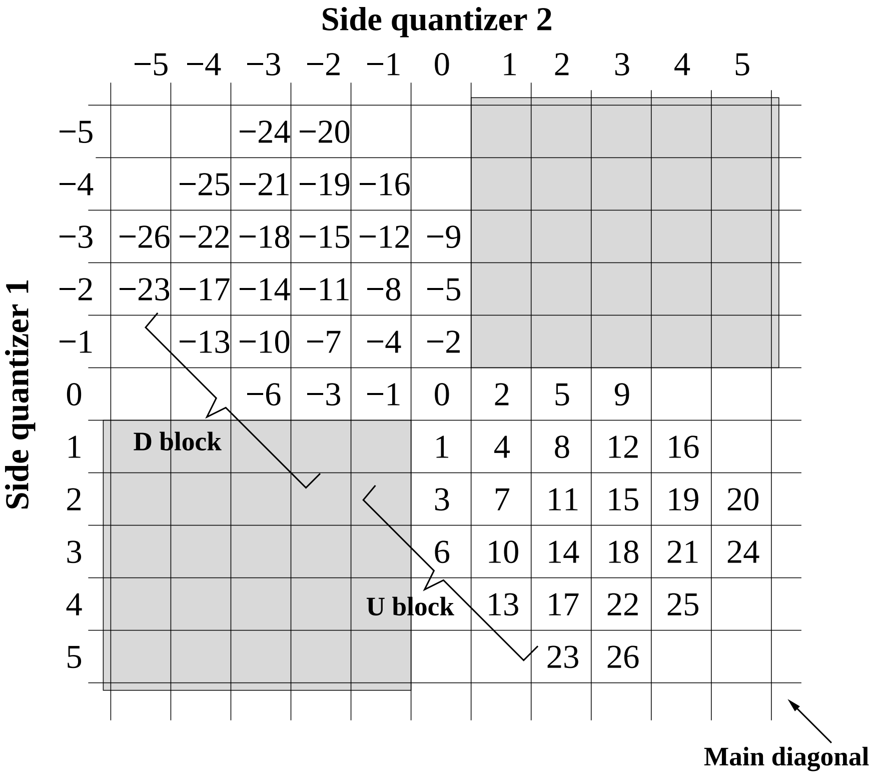

	−5	−4	−3	−2	−1	0	1	2	3	4	5
−5			−24	−20							
−4		−25	−21	−19	−16						
−3	−26	−22	−18	−15	−12	−9					
−2	−23	−17	−14	−11	−8	−5					
−1		−13	−10	−7	−4	−2					
0			−6	−3	−1	0	2	5	9		
1						1	4	8	12	16	
2						3	7	11	15	19	20
3						6	10	14	18	21	24
4							13	17	22	25	
5								23	26		

Figure 2.27: Linear index assignment matrix with $k = 3$ diagonals. The cell numbers represent the scanning order, the axis show the output of the side quantizer. The gray blocks show the invalid quadrants of the matrix.

block have become null after the splitting process.

The nested index assignment was similarly implemented, discarding the cells of the first and third quadrants of the matrix, because it presented the same problem with CAVLC. Two new scanning techniques were added, namely north and west scan, which are symmetrical to south and east scans. These new scans are used in second quadrant, while those proposed by Vaishampayan are adopted for the fourth quadrant.

Figure (2.28) shows that for both methods the redundancy increases with the value of QP. This happens because for low QP values the bitstream mainly consists of high-valued residual coefficients, while for high values of QP motion vectors take most of the bitstream and coefficients have nearly null values. Therefore in the first case the splitting process is very efficient because, although motion vectors are doubled, they do not require too many bits if compared to the residual information and big coefficients are efficiently mapped onto small values that can be efficiently represented by the CAVLC. This does not happen in the second case: motion vectors require a lot of bits when they

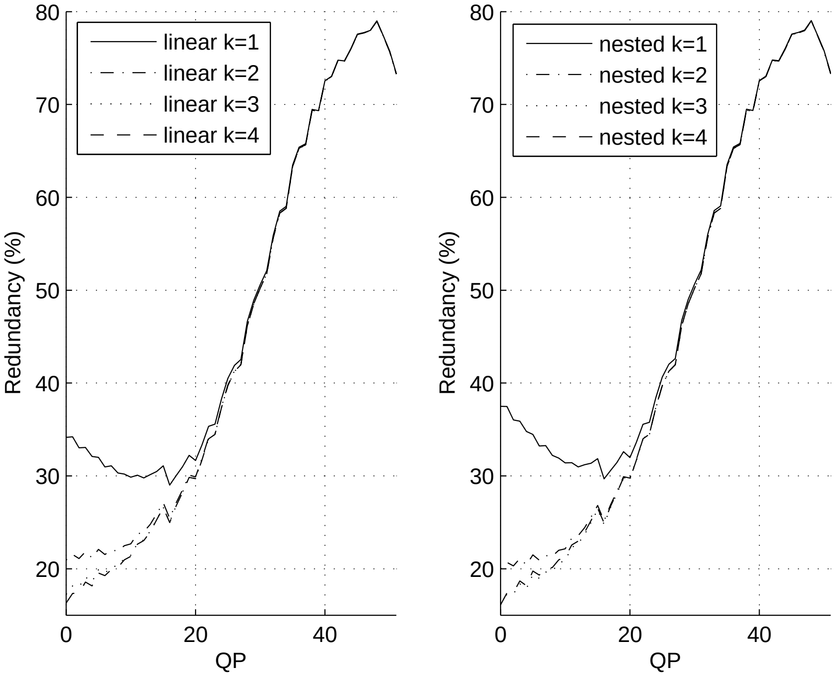

Figure 2.28: Introduced redundancy varying the encoder QP for linear (on the left) and nested (on the right) index assignment method for the CIF sequence "*mobile*". Adding more diagonals to the assignment matrix, both the methods saturate for $k \geq 2$.

are doubled and the splitting process maps low coefficients onto small values and it is not possible to reduce the required bits.

It is also notable that the introduced redundancy reduces until saturation is reached. Adding more diagonals makes more values to be mapped onto 0 level. This can improve compression gain because zeros are efficiently encoded by the run-length coding, but increasing the number of diagonals (k greater than 2) does not improve compression any more. This is due to the laplacian distribution of the coefficients. Even though more values are mapped onto 0, these values are hardly ever used because they are too big and therefore rare.

To simulate a transmission error, we decided to lose a whole frame description. This pessimistic assumption does not occur in real transmission systems. Big frames are usually divided into slices and error bursts or packets loss do not damage the whole image. Being aware of this fact, we chose this loss as a worst case. The corrupted packets belong to the 20th frame, which is a P frame (B frames are not used for motion compensation, therefore errors in B frames do not propagate through the decoded sequence).

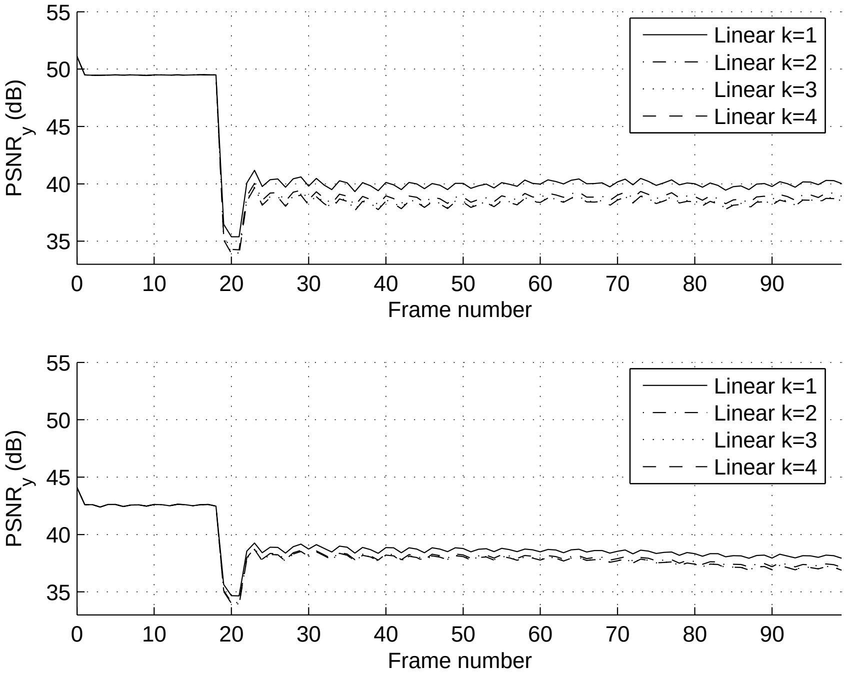

Figure 2.29: PSNR behavior in case of data loss at the 20th frame for sequence “*m*obile”. The upper graph is obtained for $QP = 10$ and $k \in [1, 2, 3, 4]$, while the lower one is attained for the same values of k and $QP = 18$. Since linear and nested method have very close performance, only the first is shown.

During the tests, linear and nested assignment methods gave very similar results, and only for high values of QP and $k = 1$ the nested index assignment outperformed the linear one by 0.5 dB. Hence, Figure (2.29) shows the PSNR behavior only in the linear index assignment case for $QP = 10$ and $QP = 18$. As expected, increasing the number of diagonals the distortion produced by a description loss becomes always higher because the greater is the number of diagonals, the smaller is the redundancy between the descriptions. The proposed scheme has some ability to recover between 4 and 5 dB of PSNR after information loss. Although this might seem to be a small gain, the visual quality of the reconstructed scene is good. In many tests we ran, it was not trivial to identify at sight the difference between correct and the corrupted frames and we had to calculate the difference of the frames and to enhance it in order to notice the errors.

Compared with other MDC solutions proposed for the H.264/AVC encoder [CCD+06], the proposed scheme is able to give better objective and subjective quality requiring slightly more redundancy.

An example of the quality of the reconstructed frame is given in Figure (2.30) for $QP = 12$ and $K = 8$, where the correctly decoded frame, the reconstructed frame in case of transmission error and the difference are shown.

2.8 Performance comparison of the proposed schemes

2.8.1 Schemes comparison

Evaluating a MDC scheme is a complex task, because many aspects should be considered. The Redundancy Rate-Distortion (RRD) region $\rho(D_1, D_0)$, which describes the distortion D_1 achievable by side decoders as a function of the allocated redundancy, and with fixed central encoder distortion D_0, is often used to evaluate the capabilities of MDC schemes. The RRD region comparison of the explained solutions is proposed. However, it should be noted that it does not fit particularly well for the coding schemes where redundancy is not a degree of freedom.

Observe that, in SMDC, MDMC and MSVC the user can not set the amount of introduced redundancy, since it is an inner property of the encoded sequence and not a degree of freedom. In the MCMD and MDSQ-based coding schemes, instead, redundancy can be varied tuning the side encoders rates. For this reason, the RRD region is represented by a curve for these two coding schemes, while it degenerates to a single point for the first three schemes.

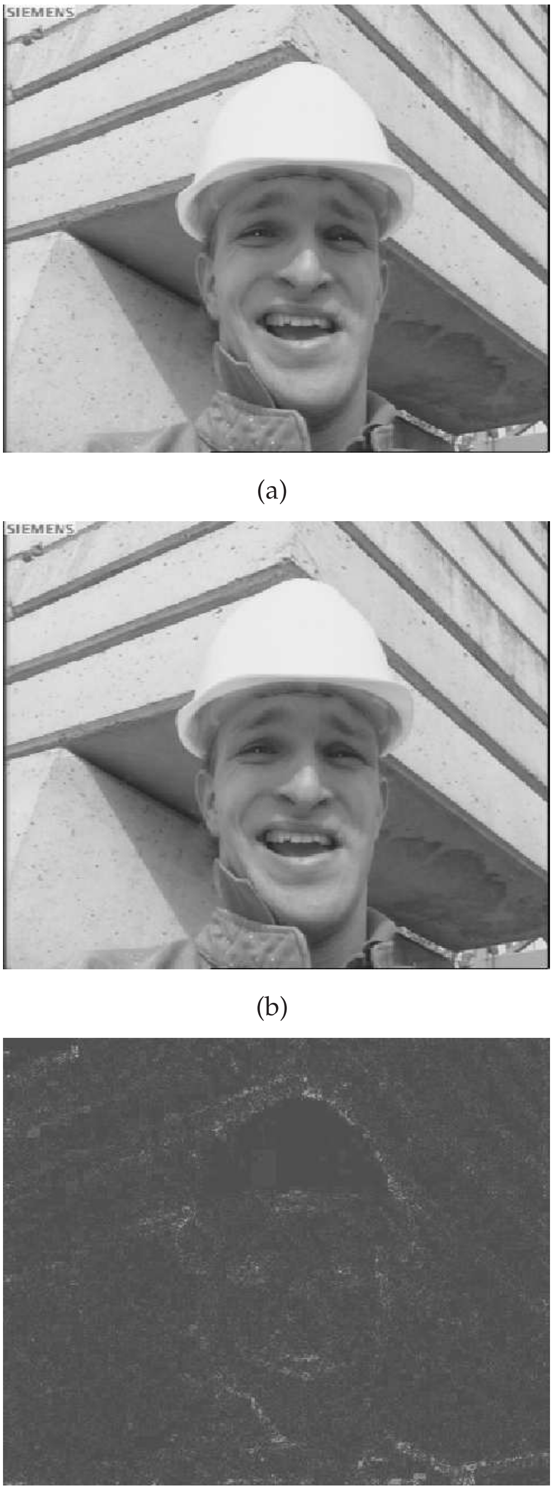

(a)

(b)

(c)

Figure 2.30: Transmission example of the "*foreman*" sequence. In (2.30(a)) the correctly received frame is shown, while in (2.30(b)) the reconstructed frame in case of error is shown. Figure (2.30(c)) holds the difference between the two frames.

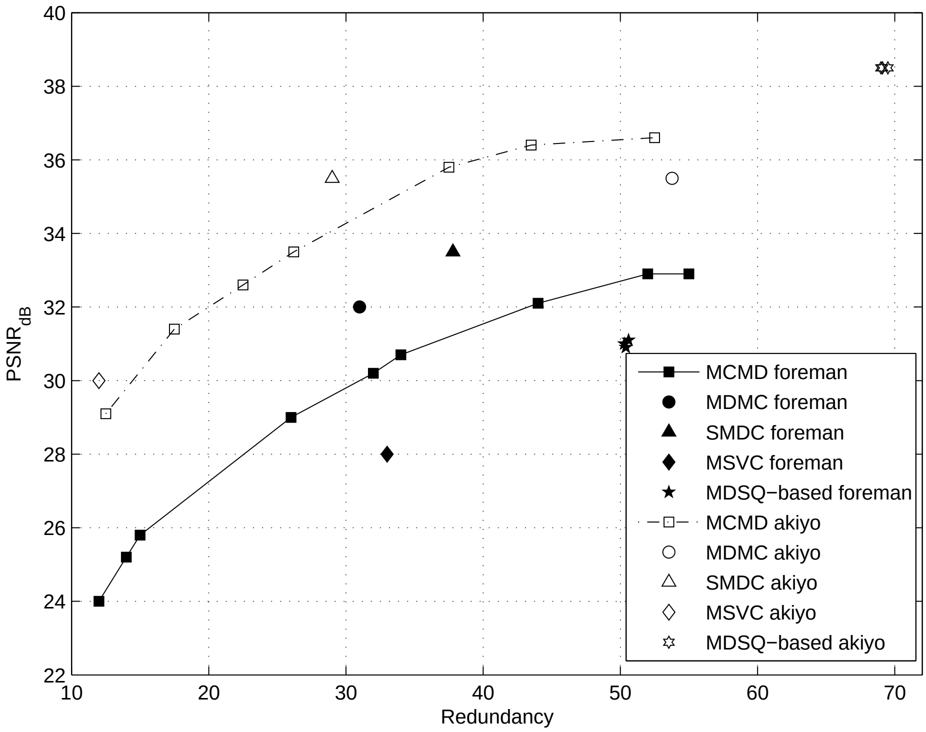

Figure 2.31: Redundancy Rate-Distortion (RRD) regions for the five MD coding schemes for the *"foreman"* and *"akiyo"* QCIF sequences and QP = 29, in case of a whole frame loss.

In Figure (2.31), the five RRD regions have been reported. These results correspond to the coding of the *"foreman"* and *"akiyo"* QCIF sequences using QP = 29, and assuming that one whole frame is lost during the transmission of a description.

Figure (2.31) shows the behavior of the proposed schemes related to the motion complexity of sequences. In this test, *"foreman"* is a fast-varying sequence and *"akiyo"* is a quasi-static one. The SMCD and MCMD techniques are substantially invariant to the characteristics of the scene being encoded. On the contrary, the MDMC, the MDSQ-based and the MSVC algorithms are strongly affected by the amount of motion: MDMC performs well with non-static sequences because the produced bitstream principally consists of the residual information that is not doubled in the splitting process, while the estimate of the lost state in SMCD works at its best on static scenes.

Since PSNR is not the only relevant aspect, but also computational cost and syntax compliance are important, we propose the qualitative comparison of the considered schemes, which is reported in Table (2.3).

	SMDC	MDMC	MSVC	MCMD	MDSQ
Exploited correlation	spatial	spatial	temporal	temporal	quantization
Efficiency	good	good	quite good	variable	variable
Computational Cost	medium	low	medium	high	low
Syntax Compliance	yes	yes	yes	no	yes
Tunability	no	no	no	yes	yes

Table 2.3: Qualitative comparison of the considered MD coding techniques.

Spatial MDC schemes usually demand lower computational complexity than temporal ones. In fact, in temporal MDC algorithms the storage of many reference frames is required, and in the particular case of the MCMD algorithm, there is also an extra computational load due to the double motion estimation required to compute two motion vectors fields. In the MCMD, as for the MSVC, the number of operations is roughly the same of a standard H.264/AVC encoder. However, it requires a double-sized frame buffer. from the computational point of view, MDMC is the lightest solution, because is doe

We must also point out that MSVC, SMDC, MDMC provide fully H.264/AVC-compliant bitstreams which can be, thus, decoded by a standard H.264/AVC decoder. MCMD streams do not correspond to the standard H.264/AVC syntax, and require an ad-hoc multiple-description decoder at the receiver. In addition, we must also observe that the MDMC layer is external to the H.264/AVC core unit, and can be independently developed and optimized since it only depends on the bitstream syntax.

Chapter 3

Scalable Video Coding

3.1 Introduction to Scalable Video Coding

Scalable video coding [Ohm05] allows reconstruction of lower resolution, lower framerate or lower quality sequences from partially received bitstream. Thus, the stream can be dynamically adapted to the network conditions. Moreover, media contents distribution is not going to be bounded only to DVDs, but it is going to be supported by networking applications based both on wireless LANs and cable networks, such as p2p video.

Additionally, video sequences are going to be viewed on several different types of devices, ranging from small handheld devices such as mobile phones or PDAs to widescreen high definition displays. Different networks characteristics, together with all the possible displays, originate a huge set of distinct scenarios that a modern video codec has to be able to deal with.

Scalable video codecs encode the input signal once at highest quality, but allow partial decoding of the compressed information by the user decoder. Thus, flexible transmission over heterogeneous networks and optimal decoding under the constraints imposed by the user hardware limitation are possible. Scalability is usually achieved in three dimensions: spatial resolution, to adapt the encoded sequence to several screens sizes, temporal resolution, to decode the bitstream at the maximum speed allowed by the computational resources of the display and quality-level resolution, which is often referred to as SNR scalability, to match network bandwidth.

In popular motion-compensated prediction and block coding algorithms, inefficiency rises when they are adapted to provide such scalability. The most critical cause of this performance drop is given by the prediction loop. In fact, as soon as some information is lost, the reference frames at the encoder and decoder are no longer the same, and the reconstructed sequence diverges from the reconstructed signal at the encoder used in the closed loop prediction. In the last years, several breakthroughs both in wavelets but also in hybrid video codecs have brought to the proposal of efficient scalable video codecs. As for the JPEG2000 image coding standard [TM02], wavelets can provide spatial and temporal scalability, while innovations in hybrid codec have been applied to the Joint Scalable Video Model (JSVM) [RWS05].

3.1.1 Scalability in existing coding standards

The standards IUT-T H.261 [Rec90] and ISO/IEC MPEG-1 [SR] did not provide any kind of scalability at the time they were defined, because they were designated for very specific applications such as video conference over channels characterized by a fixed bandwidth or storage. The only possible solution to provide scalability is the so called *simulcast*, where two or more streams related to the same sequence but encoded at different qualities are transmitted together on the network. Simulcast is the most inefficient solution for scalability, since it requires independent compressions of the input signal, without being able to exploit the intrinsic redundancy.

Simulcast is also available in ISO/IEC MPEG-2 [EF95], which maintains backward compatibility towards MPEG-1 in order to allow the low-quality stream to be encoded by using MPEG-1 and the high-quality sequences to be encoded with the new standard. MPEG-2 introduced also another tool to provide scalability in the Main+ and Next profiles, based on *layered coding*, where some refinement layers can be added to the low-quality sequence to enhance the quality of the decoded video. Obviously, in case the low-quality sequence is not correctly received and decoded, no information can be extracted from the enhancement layers, which depend on it. The MPEG-2 video scalability modes can be summarized as:

- Spatial scalability: useful in simulcasting, and for feasible software decoding of the lower resolution, base layer. This spatial domain method codes a base layer at lower sampling dimensions (i.e. "resolution") than the upper layers. The up-sampled reconstructed lower (base) layers are then used as prediction for the higher layers.

- SNR scalability: similar to the point transform in JPEG, SNR scalability is a spatial domain method where channels are coded at identical sample rates, but with differing picture qualities (through quantization step sizes). The higher priority bitstream contains a base layer data that can be added to a lower priority refinement layer to construct a higher quality picture.

- Temporal scalability: the first, higher priority bitstream holds a video at a lower frame rate, and the intermediate frames can be coded in a second bitstream using the first bitstream reconstruction as prediction. As an example, in stereoscopic vision the left video channel can be predicted from the right channel.

- Data partitioning: it is similar to frequency progressive mode of JPEG [DIS91], where the slice layer indicates the maximum number of block transform coefficients contained in the particular bitstream (known as the "priority break point"). Data partitioning is a frequency domain method that breaks the block of 64 quantized transform coefficients into two bitstreams. The first, higher priority bitstream contains the more critical lower frequency coefficients and side informations (such as DC values, motion vectors). The second, lower priority bitstream carries higher frequency AC data.

Frequency scalability was also proposed for the MPEG-2 standard, but it was dropped because of its complexity and not excellent quality.

The MPEG-4 [Ric03] standard has similar tools, which are organized in a more flexible framework at the level of *Video Objects* (VO), i.e. areas of the video scene that may occupy an arbitrarily-shaped region and may exist for an arbitrary length of time. An instance of a VO at a particular point in time is a *Video Object Plane* (VOP). This definition encompasses the traditional approach of coding complete frames, in which each VOP is a single frame of video and a sequence of frames forms a VO. However, the introduction of the VO concept allows more flexible options for coding video.

In case of spatial scalability, an I-VOP in an enhancement layer is encoded without any spatial prediction, i.e. as a complete frame or object at the enhancement resolution. In an enhancement layer P-VOP, the decoded, up-sampled base layer VOP at the same position in time is used as a prediction without any motion compensation. The difference between this prediction and the input frame is encoded using the texture coding tools, i.e. no motion vectors are transmitted for an enhancement P-VOP. An enhancement layer B-VOP is predicted from two directions. The backward prediction is formed by the decoded, up-sampled base layer VOP at the same position in time, without any motion compensation and hence without the motion vector field. The forward prediction is formed by the previous VOP in the enhancement layer even if this is itself a B-VOP, with motion-compensated prediction and hence motion vectors.

In temporal scalability, an enhancement I-VOP is encoded without any prediction. An enhancement P-VOP is predicted from the previous enhancement VOP, the previous base layer VOP or the next base layer VOP. An enhancement B-VOP is predicted from the previous enhancement and previous base layer VOPs, the previous enhancement and next base-layer VOPs or the previous and next base-layer VOPs.

SNR scalability is obtained by adopting Fine Granular Scalability (FGS) [Li01], which is based on encoding the sequence as a base layer and an enhancement layer. The enhancement layer is *embedded*, i.e. it can be truncated during encoding or during transmission by a bitstream extractor, assuring that the decoded quality is maximum at any truncation point. A typical application example is given by a server streaming the base layer and a part of the enhancement layer to the client. The amount of truncation is chosen depending on network conditions and available bandwidth, thus maximizing the quality without having to re-encode the input signal.

A final remark has to be given to H.264/AVC. In fact, an SVC amendment for this standard has been approved [HPCH07], which adds several new techniques to the non-scalable standard:

- hierarchical B structure;
- adaptive interlayer prediction techniques, to exploit correlation between spatial and SNR coding layers;
- use of the enhancement layer information in the prediction loops;
- Adaptive Reference FGS, which makes use of leaky prediction by selecting a leaky factor at transform coefficient level to deal with drifting errors.

The hierarchical B structure, as well as interlayer prediction techniques and leaky prediction will be successively explained, because they are not only referred to the H.264/AVC standard.

3.1.2 Wavelets and wavelet-based spatial scalability

The Fourier synthesis theory asserts that a 2π-periodic function $f(x)$ can be written as

$$f(x) = a_0 + \sum_{k=1}^{\infty} (a_k \cos kx + b_k \sin kx) \tag{3.1}$$

where the coefficients a_0, a_k and b_k are calculated by

$$\begin{aligned} a_0 &= \frac{1}{2\pi} \int_0^{2\pi} f(x) dx && (3.2) \\ a_k &= \frac{1}{2\pi} \int_0^{2\pi} f(x) \cos(kx) dx && (3.3) \\ b_k &= \frac{1}{2\pi} \int_0^{2\pi} f(x) \sin(kx) dx. && (3.4) \end{aligned}$$

Successively the Fourier transform has been defined on non-periodic functions, but it does not take into account local information. The first attempt to deal with not-periodic signal and multi-scale analysis was proposed by extending the Fourier transform adding a windowing operation, thus obtaining the Windowed Fourier Transform (WFT). In the WFT, the input signal is chopped into portions, which are independently analyzed for their frequency contents. The choice of the windows profile influences the analysis quality because it introduces distortion

$$\mathcal{F}\left[f(x) \cdot w(x)\right] = \mathcal{F}\left[f(x)\right] * \mathcal{F}\left[w(x)\right]. \tag{3.5}$$

Thus the frequency profile of the signal is convolved with the frequency response of the window $w(x)$. This leads to reduced resolution, due to the width of the main lobe of $\mathcal{F}\left[w(x)\right]$, and spectral leakage, which is related to the side lobes of the frequency window profile. As an example, the rectangular window, whose Fourier transform is the sinc function, has the narrowest main lobe for a given windows length, but it has the largest side lobes of all the commonly used windows [OS75].

The trade-off between the main and side lobes width can be quantified by looking for a window function that is maximally concentrated around $\omega = 0$ in the frequency domain. Kaiser [Kai74] proposed a near-optimal solution to this problem by using a zeroth-order modified Bessel function of the first kind.

The successive step in multiscale frequency analysis, was the proposal of a new kind of transform, the wavelet transform. Wavelets [Gra95] are mathematical functions that divide the input signal into frequency components and analyze each component with a resolution matched to its scale. As in many other other transforms, the input signal is decomposed as the superposition of basis functions, however in wavelet analysis a very important role is played by the *scale*, i.e. the resolution used to inspect the signal. Whenever a small window is used, small features are examined, while larger windows scan gross details.

Given a *mother function* or *analyzing wavelet* $\Phi(x)$, an orthogonal basis can be defined as

$$\Phi_{(s,l)}(x) = 2^{-\frac{s}{2}}\Phi(2^{-s}x - l) \; , \tag{3.6}$$

where the variables s and l are integers that scale and dilate the mother functions Φ to generate the other basis functions. Particularly, s is the index scale that modifies the wavelets width and l is the location index. Since s and l are integers, the functions are scaled by powers of two and translated by integers, so thanks to the self-similarity it is necessary to know only the scaling function to describe the whole basis. To span the input signal at different resolutions, the analyzing wavelet is used in a scaling equation

$$W(x) = \sum_{k=-1}^{N-2} (-1)^k c_{k+1}\Phi(2x + k) \; , \tag{3.7}$$

where $W(x)$ is the *scaling function* for the mother function Φ and c_k are the *wavelet coefficients*, which have to satisfy linear and quadratic constraints of the form

$$\sum_{k=0}^{N-1} c_k = 2 \;\; , \;\; \sum_{k=0}^{N-1} c_k c_{k+2l} = 2\delta_{l,0} \; . \tag{3.8}$$

The coefficients $\{c_0, \cdots, c_n\}$ can be thought as the coefficients of a low-pass filter. By reversing the taps order and by multiplying them by the sequence $(1, -1, 1, -1, \cdots, 1, -1)$, an high-pass filter is obtained, which has a frequency response specular to the one of the low-pass filter. The two filters are said to be *quadrature mirror filter pair* and enable aliasing-free analysis. A couple of synthesis filters can be derived by imposing perfect reconstruction, so that the inverse transform can be realized.

These filters pair is applied several times to the input signal, each time to the smoothed data: each time they are applied to the low-pass output of the previous iteration, or to the whole signal in case of the first application, a new sub-band is created, and part of the frequencies extracted from the input signal, so that it can be sub-sampled and be fed as low-pass input to the following step. Clearly, the more filtering operations are performed, the more sub-bands are available. To each sub-band is associated a spatial resolution of the input signal, because the inverse transform can be truncated at any sub-band and a scaled, aliasing-free subsampled version of the original signal is reconstructed.

An example of local analysis with wavelets is shown in Figure (3.1), where the input signal $f(x) = \sin(x^2)$ is analyzed with the Daubechies 4 wavelet. The signal doesn't have a constant spectral profile, but high frequencies become more and more important when x increases. Thus, local analysis at values of x close to 0 shows the predominance of low frequency components, but by increasing x these elements vanish while high frequencies appear.

Since the wavelet transform is a subband transform, it can be implemented with a filter bank [Mal89], as shown in Figure (3.2), where the forward transform uses two analysis filters h and g followed by sub-sampling. In reconstruction after up-sampling the output of two synthesis filters $\hat{h}$ and $\hat{g}$ are summed together to reconstruct the original signal.

To assure perfect reconstruction, two conditions have to be satisfied

$$\begin{cases} h(z)\hat{h}(z^{-1}) + g(z)\hat{g}(z^{-1}) = 2 \\ h(z)\hat{h}(-z^{-1}) + g(z)\hat{g}(-z^{-1}) = 0 \end{cases} . \tag{3.9}$$

When $h = \hat{h}$ and $g = \hat{g}$, $\{h, g, \hat{h}, \hat{g}\}$ forms an orthogonal wavelet transform. By using the polyphase representation of a filter, h can be written as $h_e(z^2) + z^{-1}h_o(z^2)$ where $h_e(z)$ contains the even coefficients and $h_o(z)$ the odd ones. Thus the filter pair (h, g) can be written with the polyphase matrix $P(z)$ as

$$P(z) = \begin{bmatrix} h_e(z) & h_o(z) \\ g_e(z) & g_o(z) \end{bmatrix} \tag{3.10}$$

and the corresponding transform can be written as

$$\begin{bmatrix} r_1(z) \\ d_1(z) \end{bmatrix} = P(z) \begin{bmatrix} x_e(z) \\ z^{-1}x_o(z) \end{bmatrix} \tag{3.11}$$

Daubechies and Sweldens [DS98] proved that any polyphase matrix representing a wavelet transform can be decomposed in *primal* and/or *dual* lifting steps by applying the LU decomposition. In these lifting steps, new finite filter h^{new} and g^{new} are respectively evaluated as

$$h^{new}(z) = h(z) + s(z^2)g(z) \tag{3.12}$$

and

$$g^{new}(z) = g(z) + t(z^2)h(z) \tag{3.13}$$

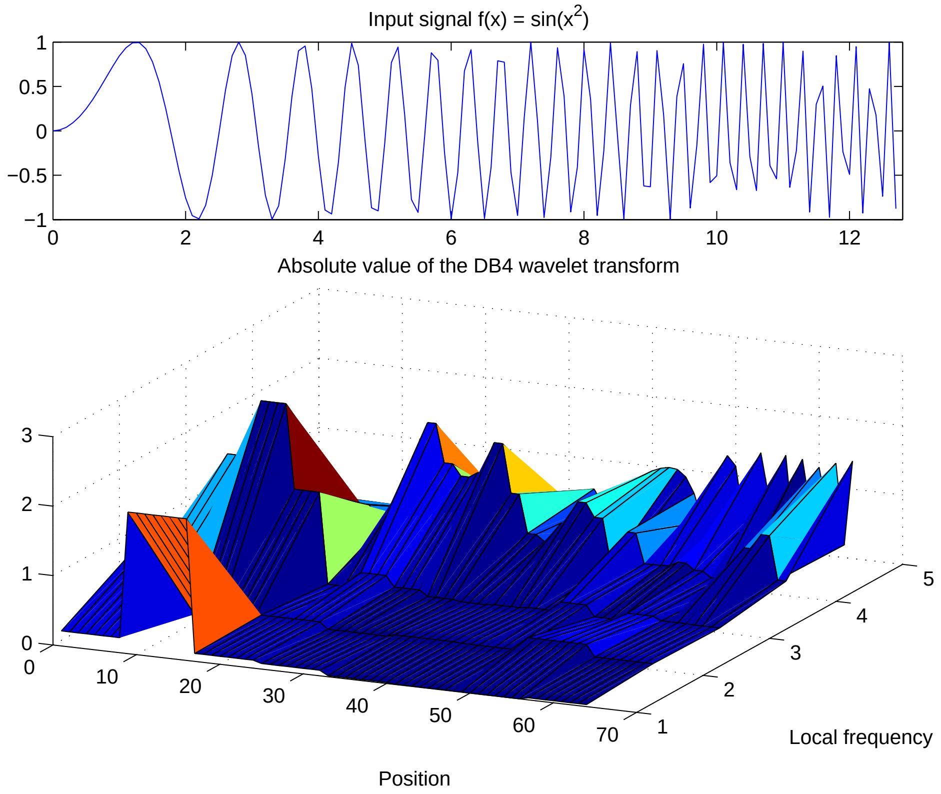

Figure 3.1: Example of local analysis with wavelet. The DB4 wavelet is used to analysis the input signal $y = \sin(x^2)$. Since low frequency values in the wavelet analysis are shared between high-frequency samples, it is necessary to interpolated them so that for each position in the signal domain all frequency values are shown. By doing this operation a result similar to the windowed DFT is obtained, an it is possible to see how the output of the local transform varies while the analysis window is shifted. In this case, the signal $y = \sin(x^2)$ increases its frequency and the output of the local analysis with the DB4 wavelet shows how the low frequency components decrease and the high-frequencies grow while the analysis window moves along the signal.

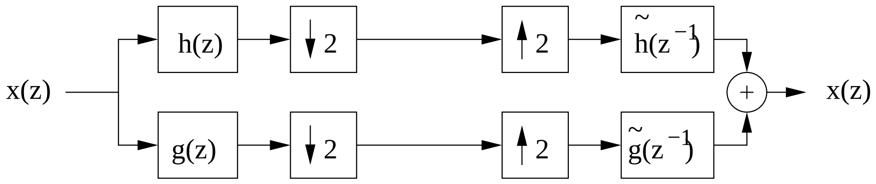

Figure 3.2: Basic filter bank for biorthogonal wavelet transform.

where $s(z)$ and $t(z)$ are Laurent polynomials. Thus the polyphase matrix can be written as

$$P^{new}(z) = \begin{bmatrix} 1 & s(z) \\ 0 & 1 \end{bmatrix} P(z) \ \texttt{or} \ P^{new}(z) = \begin{bmatrix} 1 & 0 \\ t(z) & 1 \end{bmatrix} P(z). \qquad (3.14)$$

By alternating these two steps, every polyphase matrix can be decomposed into the product of several triangular 2 × 2 matrixes and a diagonalization matrix. This decomposition has three main advantages:

- it reduces the computational requirements because $s_k(t)$ and $t_k(t)$ are often either scalar values or monomials, thus buffers can be reduced;
- since each step depends on the output of the previous stage, pipelining can be easily adopted to increase output speed;
- the inverse transform can be easily evaluated by inverting the steps and by swapping the input and output of each lifting step.

In Figure (3.3), the general block scheme of a lifted direct wavelet transform is shown.

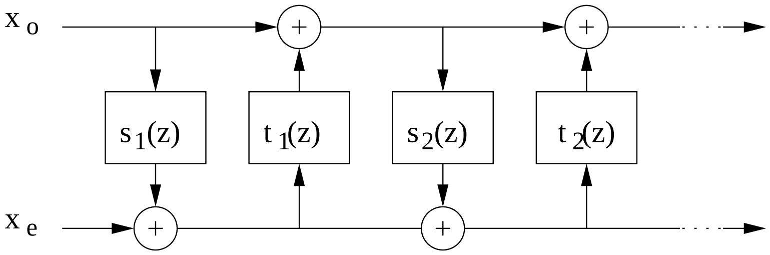

Figure 3.3: Lifted direct transform block scheme. By inverting the data flow, the scheme of the inverse transform is obtained.

Wavelets are used in several applications, from physics to engineering. For image and video coding, 2D and 3D wavelets are used to provide scalability. Since the wavelet transform consists of a couple of filters which separate low- and high-frequency components, it can be used for up- and down-sampling. In fact, by applying an orthonormal transform, the low-pass filtered image can be down-sampled without aliasing. Similarly, a zero-padded image can be fed to the inverse transform to obtain an upsampled image. Whenever the inverse transform is applied not only to the downsampled image but also to the high-frequency coefficient the original full resolution image is obtained.

An example of wavelet application for image coding is the JPEG2000 [TM02], where the reversible 5/3 and the non-reversible 9/7 wavelet transforms are used. The first wavelet is an integer-to-integer [AK00] reversible transform which guarantees perfect image reconstruction and thus it is used for lossless image compression. The 9/7 wavelet is a floating point transform, thus there is some flexibility in its implementation and it is meant to be used for lossy image coding.

Both transforms can be implemented by using the lifting scheme [AW01]. The 5/3 wavelet can be written as

$$d[n] = d_0[n] + \left\lfloor \frac{1}{2}\left(s_0[n+1] + s_0[n]\right) \right\rfloor \tag{3.15}$$

$$s[n] = s_0[n] + \left\lfloor \frac{1}{4}\left(d[n] + d[n-1]\right) + \frac{1}{2} \right\rfloor . \tag{3.16}$$

Similarly the 9/7 transform can be decomposed in

$$d_1[n] = d_0[n] - \alpha_0\left(s_0[n+1] + s_0[n]\right) \tag{3.17}$$

$$s_1[n] = s_0[n] - \alpha_1\left(d_1[n] + d_1[n-1]\right) \tag{3.18}$$

$$d_2[n] = d_1[n] + \alpha_2\left(s_1[n+1] + s_1\right) \tag{3.19}$$

$$s_2[n] = s_1[n] + \alpha_3\left(d_2[n] + d_2[n-1]\right) \tag{3.20}$$

$$s[n] = \beta_0 s_2[n] \tag{3.21}$$

$$d[n] = \beta_1 d_2[n] \tag{3.22}$$

where

$$\alpha_0 \approx 1.586134, \quad \alpha_1 \approx 0.052980, \quad \alpha_2 \approx 0.882911,$$
$$\alpha_3 \approx 0.443506, \quad \beta_0 \approx 0.812893, \quad \beta_1 = 1/\beta_0.$$

3.1.3 SNR scalability for predictive coding techniques

The generic block scheme of a scalable encoder is shown in Figure (3.4), where N quality layers are generated. The input signal x is initially sub-sampled to the lowest resolution and encoded as in traditional coding schemes. Successively, the signal reconstructed by the decoder is not only used for future prediction, but also for upper layers prediction. In this case it is up-sampled to match the upper layer resolution and it is subtracted from the input signal, thus obtaining the new prediction error.

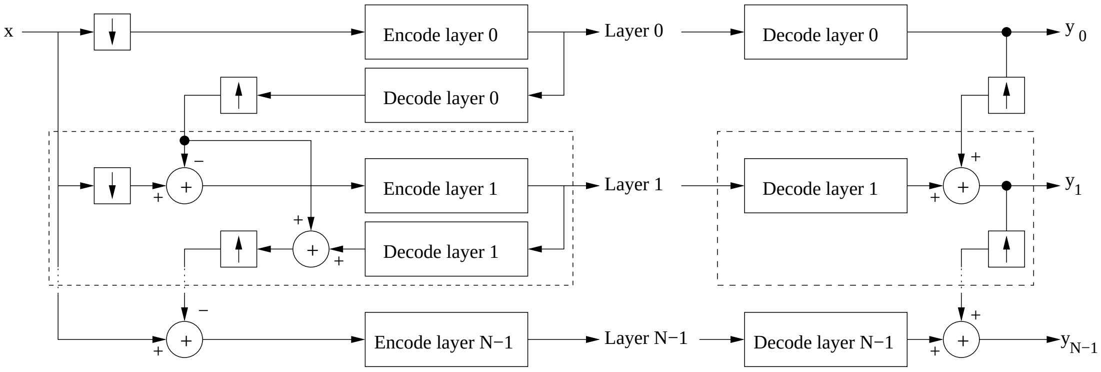

Figure 3.4: Generic scalable encoder block scheme. N quality layers are generated as one base layer, i.e. layer 0, and $N-1$ enhancement layers.

The dashed box holds the encoder and decoder for the generic enhancement layer. There can be as many layers as desired, even though in normal applications no more than three layers are used. In order to control the decoder drift, each refinement layer has to exploit the information decoded by the lower-quality layers. This approach is very flexible, because it can be similarly applied not only for spatial scalability but also for temporal and SNR scalability. Its major drawback is represented by inefficiency. In fact, all the enhancement layers are used as references, but prediction is performed only once at the base layer and it is optimized for that resolution, but it usually is not optimal for successive resolution. As an example, consider motion estimation in spatial scalability: if it is performed on a sub-sampled image the motion vector field will take into account less details than in the high-resolution case. Thus, motion vectors that minimize the energy of the residual information for low-quality signals will probably not be able to minimize the energy of the high-resolution signal and they will reduce efficiency. This problem cannot be solved by simply changing the resolution level used to perform motion estimation: motion estimation at full frame dimensions will consider details that will be lost in down-sampling, thus obtaining non-optimal prediction and base layer instability. The same applies both for temporal and SNR scalability. In the first case rescaling the motion vector field cannot lead to optimal prediction, while for SNR scalability by varying the quantization step size the residual energy changes and optimality is no longer guaranteed.

To solve this problem, prediction has to be performed layer by layer, so that efficiency does not decrease. In Figure (3.5), the scheme of an encoder providing two SNR resolutions is shown, where the base layer works as any common hybrid encoder. The enhancement layer exploits another prediction loop to further reduce the error signal energy. Even by adopting an additional prediction loop the scheme is not able to obtain the same performance of a non-scalable encoder. This gap is due to suboptimality of the second prediction loop, where is not possible to encode the quality difference using the same bitrate as the difference bitrate between a low-quality and high-quality single resolution encoder.

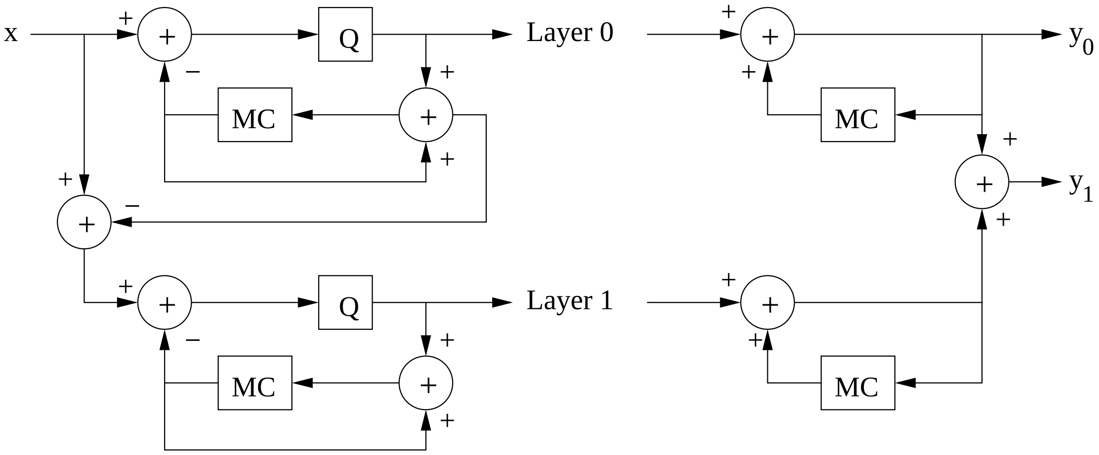

Figure 3.5: Two-loop encoder for SNR scalability. Layer 0 is the base layer, while layer 1 is the enhancement layer.

In fact, in the spatial case the various sub-sampled images are independent and can be individually selected. Similarly, in the temporal case images can be easily picked from the framebuffer. In case of SNR scalability the reconstructed images are not independent and prediction loops need to share them. This shared reference leads to a drift in the decoder when only the base layer or a subset of the enhancement layers are decoded. Even by hypothetically adopting several independent prediction loops as in the spatial and temporal case, drift cannot be avoided: quantization error is uncorrelated from the input signal and each layer error cannot be summed with those of the other layers to generate correct references.

Given the impossibility of having correct reference frames, three solutions are possible:

- *drift limitation*: a value D is added to the prediction error before quantization [MCO]. This approach assumes that the decoder is not aware of such compensation, and the proposed solution consists in evaluating the optimal D such that the quality of the base and enhanced layer is acceptable;

- *drift clipping*: the drift value is limited as soon as it reaches a maximum value D_{max}, which often is as big as the quantization step size. Identical drift clipping has to be applied at the decoder, which cannot ignore the correction as in the previous case. Optionally, the clipping rule can be optimized for the signal, but this solution requires the transmission of such rule before video transmission;

- *drift leaking*: the decoder drift is limited by multiplying it for a given coefficient α such that $0 \leq \alpha \leq 1$. By varying the value of this parameter, all the cases between drift free and unlimited drift can be represented.

These solutions are shown in Figure (3.6), where the encoder has been modified from the one in Figure (3.5) by arranging the two quantizers in a tandem configuration, obtaining a solution similar to FGS.

In general SNR scalability is not able to reach performances comparable to those of non scalable schemes. In fact, the unavoidable prediction mismatch at different quality levels reduces the coding efficiency of every coding algorithm.

3.1.4 SNR scalability for non predictive coding techniques

To exceed the limitation due to the inner structure of predictive coding techniques, several coding algorithms based on bitplane coding have been proposed.

The adoption of wavelets for image coding has brought to a new set of lossy and lossless compression algorithms. Exactly as in the hybrid coding scheme, transformed coefficients are quantized and encoded, but the main difference between these new algorithms and DCT-based techniques relies on the bigger input set of coefficients. In fact, the wavelet transform is applied to larger inputs than the DCT, which is usually applied to macroblocks of 16 × 16 pixels or smaller blocks, while the wavelet transform operates on the full image. Thanks to the bigger input size, coding algorithms do not need to perform quantization and entropy coding separately, but they can achieve jointly and efficiently both by doing bitplane encoding. To each encoded bitplane corresponds the reduction of 50% of the quantization step size, because an additional bit is added to the coefficients representation. To obtain coding efficiency, the intra- and inter-band correlation is exploited, because in the wavelet domain coefficients of the residual information tend to be self-similar between the decomposition layers: if a coefficient is null at a given decomposition level, the probability that

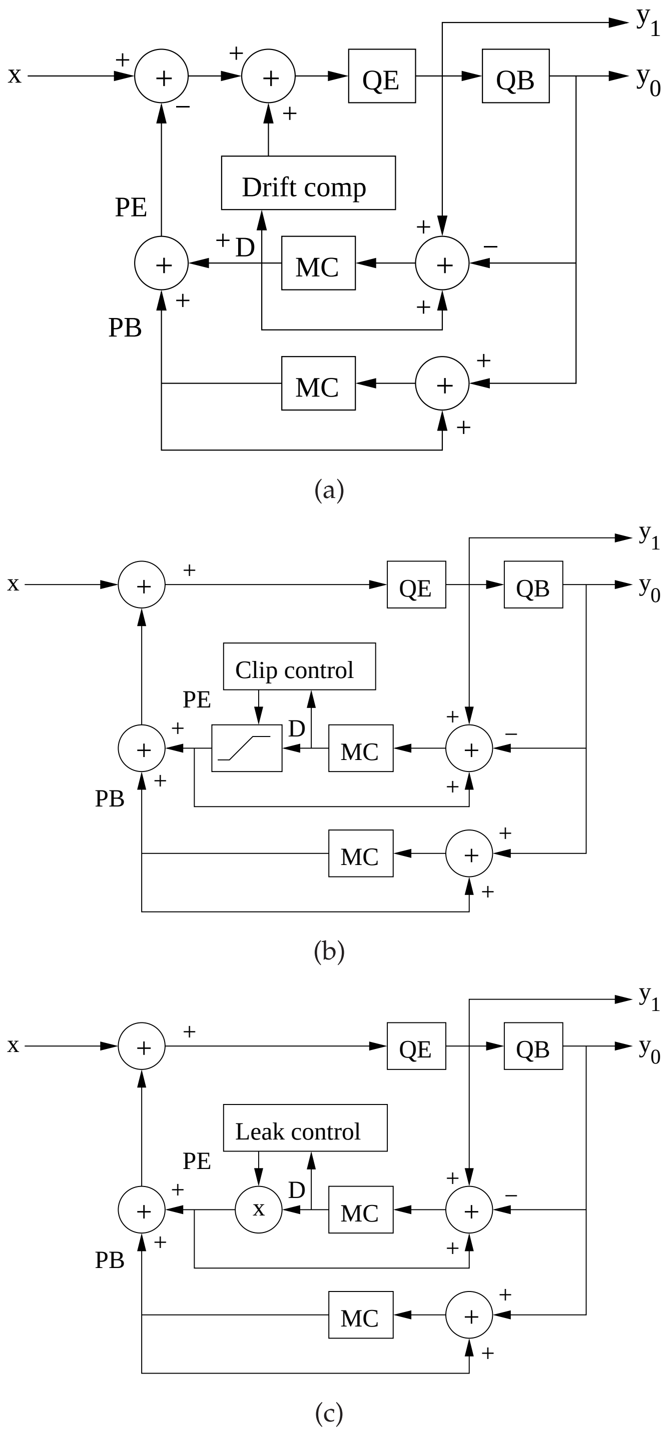

(a)

(b)

(c)

Figure 3.6: Drift control schemes for SNR scalability In (3.6(a)) drift compensation is adopted, in (3.6(b)) drift clipping is used and in (3.6(c)) drift leaking is adopted.

the corresponding pixels in higher frequency decomposition levels are zero is also high. Thus, algorithms obtain efficiency by exploiting this fact and model null and non null coefficients consequently.

The Embedded Zerotree Wavelet (EZW) algorithm, introduced by Shapiro [SCP93], was one of the first algorithms to show the full power of wavelet-based image coding. Embedded coding stands for a compression algorithm that allows progressive transmission of the image. Zerotrees are a structure that indicates that a coefficient in a band and all the coefficients corresponding to it in higher frequency decomposition levels are null, thus once the root of such tree is encoded there is no need to further spend bits to encode the tree internal nodes and leaves. The algorithm can be summarized in five steps:

1. Initialize: choose initial threshold, $T = T_0$, such that all transform values satisfy $|w(m)| < T_0$ and at least one transform value satisfies $|w(m)| \geq \frac{T_0}{2}$.

2. Update threshold: let $T_k = \frac{T_{k-1}}{2}$.

3. Significance pass: scan through insignificant values using baseline algorithm scan order. Each value $w(m)$ is tested as follows:

   ```
   if $|w(m)| \geq T_k$ :
     output sign of $w(m)$
   else :
     let $w_Q(m)$ retain its initial value of 0.
   ```

4. Refinement pass: scan through significant values found with higher threshold values T_j , for $j < k$ (if $k = 1$ skip this step). For each significant value $w(m)$, do the following:

   ```
   if $|w(m)| \in \left[w_Q(m), w_Q(m) + T_k\right)$ then :
     output bit 0
   else:
     output bit 1
     $w_Q(m) := w_Q(m) + T_k$ .
   ```

5. Loop: goto step 2.

The bit-plane encoding procedure can be continued for the desired number of bitplanes, i.e. to obtain quantized transform magnitudes $w_Q(m)$ which are as close as desired to the transform magnitudes $|w(m)|$. In case a given compression ratio is desired, it can be achieved by stopping the bit-plane encoding as soon as a given number of bits is exhausted. It is important to notice that the execution of the bit-plane encoding procedure can terminate at any point.

It is easy to see that after n loops, the maximum error between the transform values and their quantized counterparts is less than $\frac{T_0}{2^n}$. It follows that the error can be reduced to a value as small as wished by performing a large enough number of loops. If $w(m)$ are integers, after a $n = \log_2 \left(\max_m |w(m)|\right)$ steps compression is lossless, because all coefficients are represented at the same resolution used to elaborate them.

Wavelet transforms fit particularly well bit-plane encoding because wavelet transforms of images of natural scenes often have relatively few high-magnitude values, which are mostly found in the highest level subbands, i.e. in bands related to low frequencies. These high-magnitude values are first coarsely approximated during the initial loops of the bit-plane encoding, thereby producing a low-resolution, but often recognizable, version of the image. Subsequent loops encode lower magnitude values and refine the high magnitude values, adding further details to the image and refining existing details. Thus, progressive transmission is possible, and encoding/decoding can cease once a given bit budget is exhausted or a given error target is achieved.

In EZW, compression of embedded data is performed with zerotrees, which provide very compact descriptions of the position of insignificant coefficients. To define a zerotree, quadtrees have to be defined. A *quadtree* is a tree of locations in the wavelet transforms whose root is located at $[i, j]$ and whose children are at $[2i, 2j]$, $[2i + 1, 2j]$, $[2i, 2j + 1]$, $[2i + 1, 2j + 1]$. It includes the root, its children, the children of the root children and so on. In case all coefficients of the quadtree are zeros then it is said to be a *zerotree*.

In Figure (3.7) an example of Zerotrees is given. The first tree root has coordinates $[0, 1]$ and spans through four decomposition levels, while the second one begins in $[5, 3]$ and covers only two decomposition levels. Zerotrees are useful only if they occur frequently. Fortunately, with wavelet transforms of natural scenes, the multi-resolution structure of the wavelet transform produces many zerotrees, especially at high thresholds.

In EZW, the third step of the bitplane coding algorithm is modified as follows:

3 Significance pass: scan through insignificant values using baseline algorithm scan order. Test each value $w(m)$ as follows:

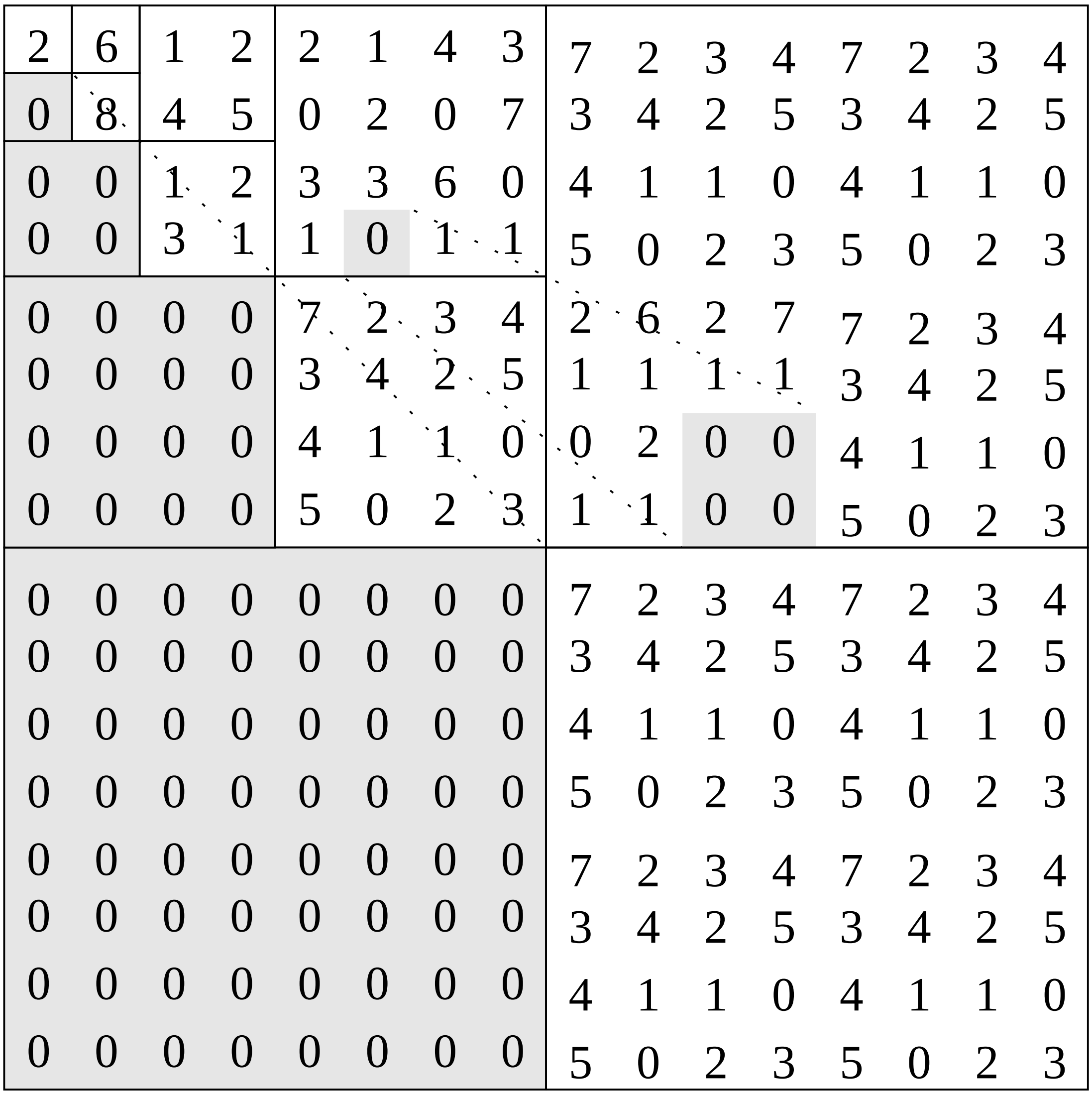

2	6	1	2	2	1	4	3	7	2	3	4	7	2	3	4
0	8	4	5	0	2	0	7	3	4	2	5	3	4	2	5
0	0	1	2	3	3	6	0	4	1	1	0	4	1	1	0
0	0	3	1	1	0	1	1	5	0	2	3	5	0	2	3
0	0	0	0	7	2	3	4	2	6	2	7	7	2	3	4
0	0	0	0	3	4	2	5	1	1	1	1	3	4	2	5
0	0	0	0	4	1	1	0	0	2	0	0	4	1	1	0
0	0	0	0	5	0	2	3	1	1	0	0	5	0	2	3
0	0	0	0	0	0	0	0	7	2	3	4	7	2	3	4
0	0	0	0	0	0	0	0	3	4	2	5	3	4	2	5
0	0	0	0	0	0	0	0	4	1	1	0	4	1	1	0
0	0	0	0	0	0	0	0	5	0	2	3	5	0	2	3
0	0	0	0	0	0	0	0	7	2	3	4	7	2	3	4
0	0	0	0	0	0	0	0	3	4	2	5	3	4	2	5
0	0	0	0	0	0	0	0	4	1	1	0	4	1	1	0
0	0	0	0	0	0	0	0	5	0	2	3	5	0	2	3

Figure 3.7: Example of two zerotrees in a four levels wavelet decomposition. Both trees have gray background, the root of the biggest tree has $[0,1]$ coordinates, while the root of the smallest one has coordinates $[5,3]$.

```
If $|w(m)| \geq T_k$, then
  Output the sign of $w(m)$
  Set $w_Q(m) = T_k$
Else if $|w(m)| < T_k$ then
  Let $w_Q(m)$ remain equal to 0
  If $m$ is at first level, then
    Output $Z$
  Else
    Search through quadtree having root $m$
    If this quadtree is a zerotree, then
      Output $R$
    Else
      Output $Z$ .
```

The symbol R indicates the root of a Zerotree, while Z denotes a zero which is not part of a Zerotree. As an example, the first step of EZW for data in Figure (3.7) is encoded by choosing $T_0 = 16$ and $T_1 = 8$ thus all coefficients divided by eight are null except the one in $[1,1]$. Since it is positive, a $+$ symbol it is emitted. Coefficient at $[0,0]$ is a single zero, while those at $[1,0]$ and $[0,1]$ are the roots of two Zerotrees spanning four decomposition levels. Following the scanning method proposed by Shapiro covers the values at $[2,2]$, $[3,2]$, $[2,3]$ and $[3,3]$, which are the roots of four Zerotrees covering three levels. Thus the output symbol sequence is

$$Z, R, R, +, R, R, R, R. \tag{3.23}$$

In the second step $T_2 = 4$ and the encoded output is

$$\begin{aligned}
&Z, +, R, \\
&Z, Z, +, +, \\
&Z, Z, Z, Z, \\
&Z, Z, +, Z, Z, R, Z, +, Z, Z, +, Z, R, R, Z, R, \\
&+, Z, Z, +, Z, +, Z, +, +, Z, Z, Z, +, R, Z, R, \\
&+, Z, Z, +, +, Z, Z, +, Z, +, Z, +, Z, +, Z, +, \\
&+, Z, +, Z, +, Z, Z, Z, +, Z, Z, Z, \\
&Z, +, Z, +, +, Z, Z, +, Z, Z, Z, Z, Z, +, Z, +, +, Z, +, Z \\
&+, Z, Z, +, +, Z, Z, +, Z, +, Z, +, Z, +, Z, +, +, Z, Z, Z, +, Z, Z, Z,
\end{aligned}$$

$$+, Z, Z, Z, +, Z, Z, Z, +, Z, Z, +, +, Z, Z, +, Z, +, Z, +, Z, +, Z, +,$$
$$+, Z, +, Z, +, Z, +, Z, 0 \tag{3.24}$$

Symbols R, Z, $+$ and $-$ can be further compressed by applying entropy coding while the 0 and 1 symbols can be directly written to the bitstream, especially when encoding the less significant bits, because they tend to be independent and equiprobable.

Most bitplane encoding algorithms for wavelets share the strategy of significance and refinement steps. Most differences lie in how these steps are encoded. For example, the SPIHT algorithm [SA96] is a refined version of EZW.

SPIHT stands for Set Partitioning In Hierarchical Trees, where *Hierarchical Trees* refers to the quadtrees, *Set Partitioning* refers to the way these quadtrees partition the wavelet transform values at a given threshold. By a careful analysis of this partitioning of transform values, Said and Pearlman were able to greatly improve the EZW algorithm performance.

The only difference between SPIHT and EZW is that SPIHT uses a different approach to encode the zerotree information. SPIHT uses a state transition model which describes how the locations of transform values move from one threshold to the next. Instead of coding the symbols R and Z output by EZW to mark locations, the SPIHT algorithm uses states I_R , I_V , S_R , and S_V and outputs code for state transitions such as $I_R \rightarrow I_V$, $S_r \rightarrow S_V$ and so on. These four states model how the coefficient values in each quadtree compare with the coding threshold. Since coefficients are correlated both with neighbor values in the same band and with those in other bands, the adoption of the state model is able to significantly increase the compression ratio.

Another example is given by Wavelet Different Reduction (WDR) [TWJ98] algorithm, Although WDR will not typically produce higher PSNR values than SPIHT, it can produce perceptually superior images, especially at high compression ratios. In WDR, the significance pass works on the information of the index of new non null coefficients and their sign, by saving the sign of the coefficient and the run between coefficients, i.e. the difference between the value of each coefficient index and its successor.

In the last years, the zerotree approach has been substituted by the adoption of arithmetic encoding and context modeling. The most famous standard based on this strategy is JPEG2000 [TM02]. In this standard, the quantized sub-bands are divided in *precincts*, rectangular regions in the DWT domain. Precincts usually are defined in order to hold the coefficients in several sub-bands that correspond to the same are of the image.

Precincts consist of *code-blocks*. Each code-block contains coefficients of only one sub-band and, with the exception of blocks located at image boundaries, has equal size. Finally each code-block is encoded with EBCOT, which is a bitplane coding algorithm that relies on an arithmetic encoder and a context modeling algorithm. Even though zerotree coding has been abandoned and the bitplane encoding algorithm has been evolved into a tree steps algorithm, namely Significance Propagation, Magnitude Refinement and Cleanup Pass, the base strategy of providing several image sizes with the DWT and several quality levels is still adopted in JPEG2000.

3.1.5 Temporal scalability techniques

Most of temporal scalability coding schemes can be easily implemented on coding algorithms because they require framebuffer reordering and are independent of B frames availability. In temporal scalability, the low-quality layer consists of a low framerate sequence, while the enhancement layers hold the frames necessary to increase the framerate.

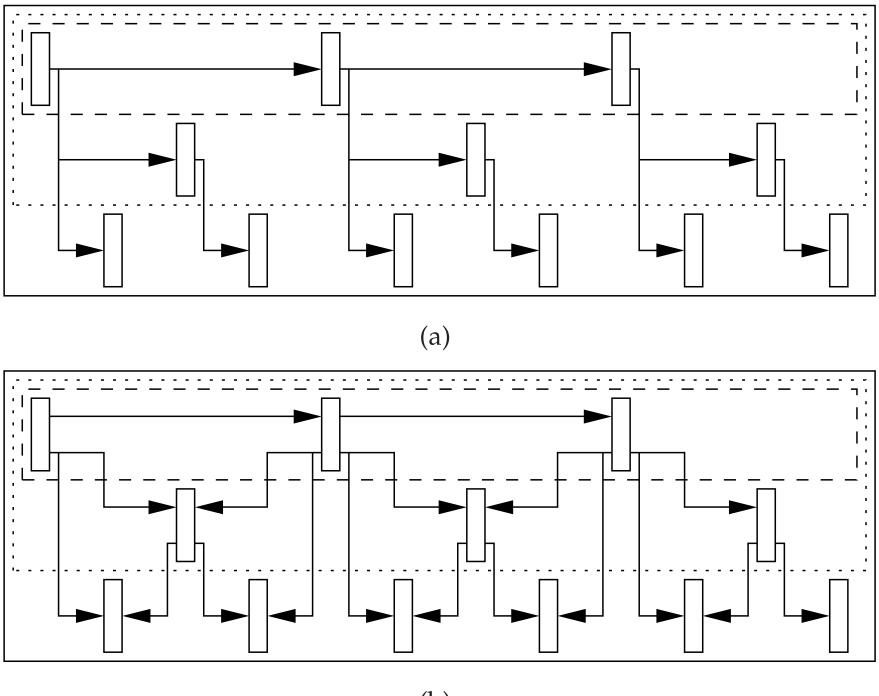

(a)

(b)

Figure 3.8: Temporally scalable coding schemes based on three layers hierarchic P decomposition, shown in (3.8(a)), and hierarchic B, presented in (3.8(b)). The low quality sequence is hold in the dashed boxes, the intermediate one is in the dotted boxes and the full quality sequence is surrounded by the continuous boxes.

In case only P frames are available, as shown in Figure (3.8(a)), the base layer is encoded as in non-scalable coding schemes, by predicting the currently encoded frame with the previous one. Enhancement layers change how prediction works: in fact, frames are not estimated from the previous one in the layer but by the temporally nearest frames, no matter which layer the frame belongs to. A similar strategy, shown in Figure (3.8(b)), is adopted in case also B frames are available: the base layer is encoded by using P frames, and the first enhancement layer consists of only B frames, which are encoded exactly as if they were encoded in a non-scalable encoder. Successive layers need to be modified, so that they can adopt a strategy similar to the P-only scalable video case. In this case B frames can have not only I and P frames as reference but also B frames, thus obtaining a structure denoted as B-frame pyramid or hierarchical-B structure.

The adoption of the B-frame pyramid introduces robustness to transmission errors without significantly increasing the required bitrate. In fact, on one hand the base layer encodes temporally far frames as P, thus the prediction error tends to have more energy than in the non-scalable case. On the other hand, this increased bitrate is compensated by the massive adoption of bi-predicted frames minimizes the prediction error, so finally the required bitrate is the same. Moreover, since B frames have two references and these references do not belong to the same layer unless they both are in the base layer, error concealment algorithm can deal with lost information by reducing the B prediction to a P-only one.

Another approach to temporal scalability is given by [KXP97] where a three dimensional wavelet transform is applied to the input sequence to encode it, either without or optionally with motion compensation. When motion estimation is not used, the encoder consists of a temporal analysis block followed by a spatial analysis block and a 3D SPIHT kernel. The division of the three dimensional wavelets into the temporal and spatial block is possible because three dimensional separable 9/7 bi-orthogonal Daubechies and 2 tap Haar filters are used, which can be decomposed into three mono-dimensional filters. Thus the first stage divides frames in low-pass frames, which hold the temporal average of the frames and high-pass frames, where the differences between frames are stored. The successive spatial block generates three different spatial resolutions. SNR scalability is finally provided by 3D SPIHT, an extension to the two dimensional Set Partitioning In Hierarchical Tress (SPIHT) coder [SA96].

An example of this coding scheme is shown in Figure (3.9), where four frames are decomposed into two temporal resolutions. At the lower framerate,

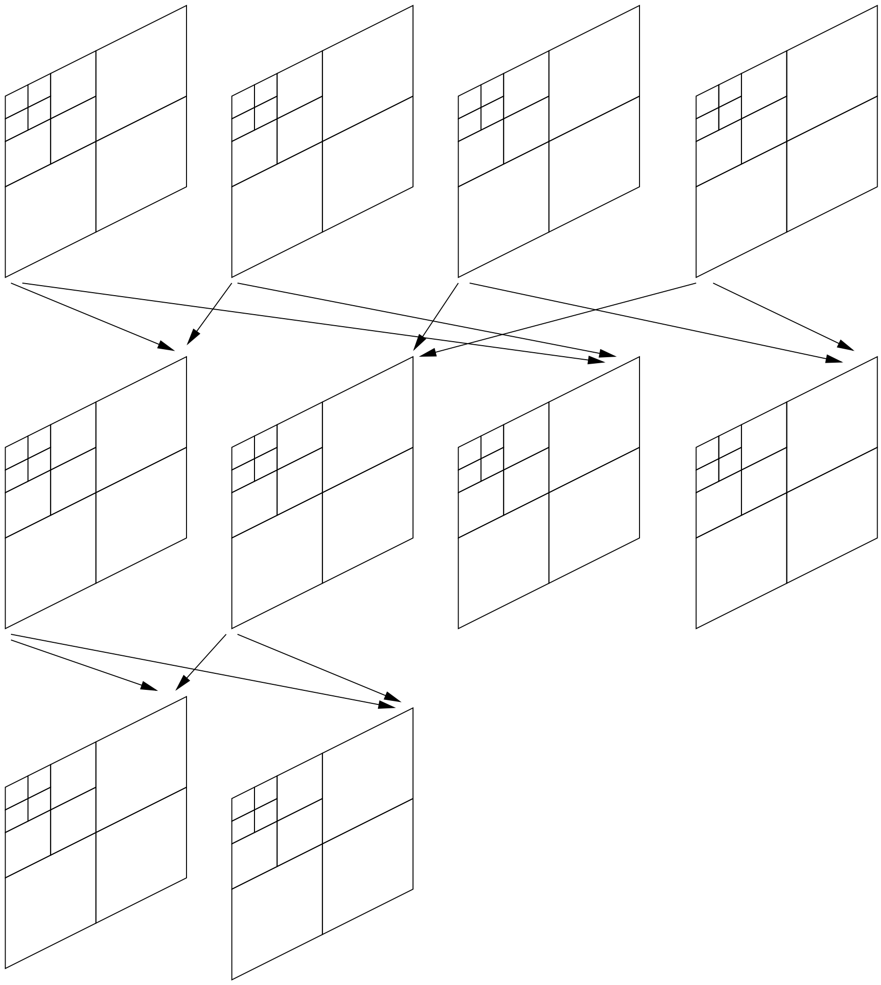

Figure 3.9: 3D wavelet-based coding scheme with two temporal quality layers and three spatial quality layers.

frames are the average of those of the original sequence. By using two more frames, the original sequences is reconstructed, adding the missing temporal details.

To further rise efficiency, motion estimation is necessary. By introducing it in a three dimensional wavelet scheme, the Motion Compensated Temporal Filtering (MCTF) is obtained, which can be denoted either as $2D + t$ or $t + 2D$ wavelet transform.

Since subband and wavelet transforms can be fully described by linear filter operations, they can be applied along motion trajectories. In case the motion vector field is homogeneous, each image pixels can be linked to another one in a previous frame. This situation is however extremely rare and in most pictures isolated areas are present, as well other zones where several vectors point to the same portion of the image. In the first case, areas are said to be *unconnected*, while in the second case they are sad to be *multiple connected*. In this two case it is not possible to immediately apply MCTF.

A solution to this problem was proposed by Ohm [Ohm91] in case of Haar filters. Two frames A and B can be transformed after motion compensation with a pair of non orthonormal Haar filters into a low-pass L and a high-pass H frame as

$$\begin{aligned} L(m,n) &= \frac{1}{2}B(m,n) + \frac{1}{2}A\left(m + \hat{k}(m,n), n + \hat{l}(m,n)\right) && (3.25) \\ H(m,n) &= A(m,n) - B\left(m + k(m,n), n + l(m,n)\right). && (3.26) \end{aligned}$$

The L frame is the motion compensated average of A and B, while H is their motion compensated difference. $[k, l]$ is the forward motion vector fields, while $[\hat{k}, \hat{l}]$ is the backward motion information. In case motion vectors are homogeneous, i.e. unique motion trajectories exist, then $[k, l]$ and $[\hat{k}, \hat{l}]$ are dependent. Whenever unconnected regions exists, they are embedded in L as

$$L(m,n) = B(m,n)\ , \tag{3.27}$$

while multiple connected zones are encoded in the high pass frame as prediction differences, i.e.

$$H(m,n) = A(m,n) - \hat{A}(m,n)\ . \tag{3.28}$$

By adopting this transform, operation are now fully invertible and perfect reconstruction is strictly possible when full-pixel accuracy of motion compensation is implemented. In case sub-pixel motion estimation is implemented lossy reconstruction is obtained, because subpixel estimation requires ideal interpolation both in analysis and synthesis steps, which is obviously not possible.

Successively Ohm [Ohm94] demonstrated that arbitrary methods of motion compensation can be used in MCTF and distortion can be kept small, provided that he interpolation filter profile is sharp enough.

Equations (3.25, 3.26) can be given a different interpretation. A and B frames can be seen as the even and odd polyphase components of the temporal axis transform. Suppose that exist A^* B^* which are univocally connected, that is

$$\begin{aligned} A^* &= A(m+\hat{k}, n+\hat{l}) && (3.29)\\ B^* &= B(m+k, n+l) && (3.30) \end{aligned}$$

where $k = -\hat{k}$ and $l = -\hat{l}$. Under this assumption the high-pass and low-pass frames can be written as

$$\begin{aligned} H(m,n) &= A(m,n) - B(m+k, n+l) && (3.31)\\ L(m,n) &= B(m,n) + \frac{1}{2}H(m+\hat{k}, n+\hat{l}) && (3.32)\\ &= \frac{1}{2}\left[B(m,n) + A(m+\hat{k}, n+\hat{l})\right] && (3.33) \end{aligned}$$

This equivalence allows to implements the MCTF with the lifting scheme, as shown in Figure (3.10). The main advantage of implementing MCTF as a lifting scheme is that it is no longer limited to full pel motion estimation for perfect reconstruction [PPB01].

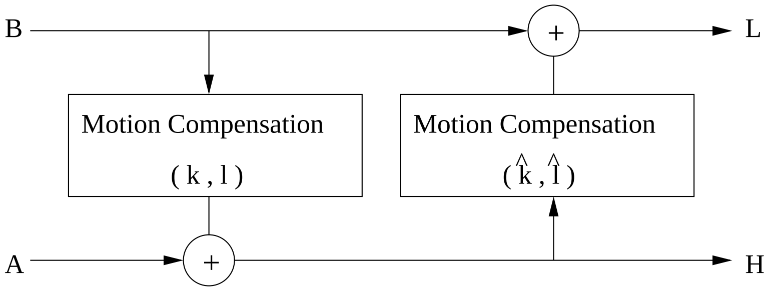

Figure 3.10: MCTF lifting scheme.

The hypothesis that $k = -\hat{k}$ and $l = -\hat{l}$ does not generally hold. Hence, motion compensation applied to H to generate L should be as close as possible to the inverse of the motion compensation used to obtain H from B, in order to reduce portions of the image unconnected or multiple connected. In case inverse motion compensation does not satisfy this requirement, ghosting artifacts appear in the low-pass frame and the results is not suitable any more for temporal scalability.

In typical block-based motion compensated coding schemes, the previous A and the high-pass H frames are considered fixed, while blocks float in the successive and low-pass frames B and L. This choice leads to the following consequences:

- unconnected pixels are those remaining undefined after inverse motion compensation. In this case their values is filled with those from the B in the equivalent positions;
- in case of multiple connected regions, it is necessary to specify the correct value.

As previously said, two coding schemes are available to implement 3D wavelet transform. In case spatial resolutions are evaluated before motion estimation, the $2D + t$, which is shown in Figure (3.11). This approach is characterized by better performance in terms of spatial and SNR scalability. Furthermore, adaptive processing for each spatial subband is possible.

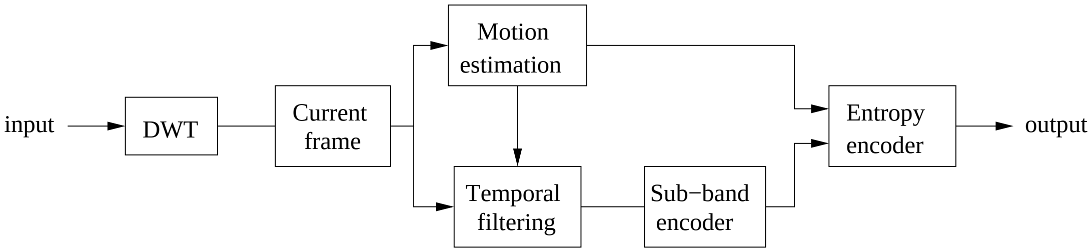

Figure 3.11: Motion compensated 3D DWT: $2D + t$ structure. Frames are initially decomposed into several spatial resolutions and successively temporal filtering is applied to add temporal scalability.

The major drawback of this scheme is the non-uniqueness of the motion vector field (a different motion vector field is necessary for each spatial resolution). To share a common motion vector field between all spatial resolutions, motion estimation needs to be performed before applying DWT, thus adopting the $t + 2D$ structure, as shown in Figure (3.12).

In this case temporal filtering is applied only to the biggest spatial resolution and temporal filtered frames are successively decomposed into the desired spatial resolutions. Although this approach has the advantage of sharing the same motion vector field between all resolutions, it is characterized by spatial

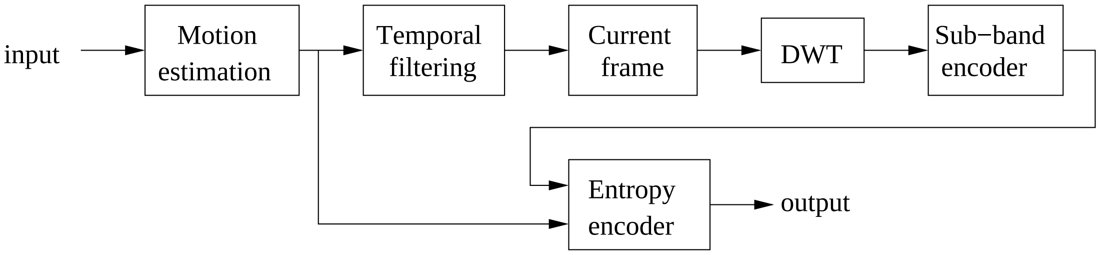

Figure 3.12: Motion compensated 3D DWT: $t + 2D$ structure. Temporal filtered frames are spatially decomposed in order to add spatial scalability to already enabled temporal scalability.

subband leakage, which reduces the image quality. By comparing these two schemes, is clearly appears how the second operation efficiency is degraded by the first one. In fact, the first transform can operate the original signal and obtain the optimal solution, but the second transform works on the transformed output and looses efficiency. Thus, in Figure (3.11) spatial scalability is good but temporal scalability is penalized and three motion vector fields are necessary. On the other hand, in Figure (3.12) temporal scalability and motion estimation come first, so motion vectors can be unique, and spatial resolutions quality is limited by subband leakage.

3.2 Protection enhanced scalable video coder

Multiple Description Coding aims to add reliability to video applications by dividing the input signal into several descriptions in order to reduce information loss and by estimating lost data exploiting the redundancy shared between the descriptions. Scalable Video Coding aims to compress video sequences at several quality levels, usually by exploiting spatial and temporal redundancy of the encoded sequence. Since MDC and SVC often perform similar operations, it is worth studying how MDC schemes can be applied to SVC in order to achieve robust scalable coders. In the last part of my Ph.D. program, I developed three MDC schemes to enhance SVC robustness and in this section I present the results I obtained [1].

In motion-compensated video codecs, temporal and spatial prediction is used to efficiently reduce the redundancy of the input video sequences. As

[1] This work was performed while visiting the Video Processing Laboratory at University of California, San Diego. This work was supported in part by a scholarship from the "Fondazione A. Gini" (Padova, Italy).

a consequence, temporally-predicted frames need valid references to be correctly reconstructed by the decoder. Whenever transmission errors occur, they do not only affect the currently decoded frame but also those depending on it, usually until an I frame is received.

Efficient Scalable Video Coding codecs are based on motion compensation, therefore they need to add protection to the produced bitstream as well as non scalable video codecs. Since many SVC schemes rely on a bitstream extractor which selects the desired information from the high-quality compressed bitstream, solutions based on Forward Error Correction (FEC) codes might not be always suitable. In fact, FEC codes are usually applied to matrix of packed packets, but in SVC the same portion of video can be saved in very different packets, depending on the desired size, framerate and quality. Thus, the more combinations are available, the harder is to pre-compute all the possible combinations and the corresponding encoded version. Because of the nature of these techniques, FEC codes and also Unequal Error Protection (UEP) cannot be evaluated once for all the available resolution and therefore they hardly fit SVC needs. Moreover, they are hard to adapt to the network conditions, which can often change, and whenever the most important information layer is lost, the received information is often useless.

Operations performed in scalable video codecs can be exploited also to generate descriptions. As a trivial example, the wavelet transform divides each quality level into three bands that can be grouped into descriptions. Also temporal scalability can be similarly exploited.

SVC can benefit from the adoption of MDC in several ways. In fact, MDC not only provides error resilience by exploiting the transmission channels diversity, but it can be used to provide finer scalability. As an example, traditional scalable video codecs provide scalability by temporally subsampling frames or by transmitting at different resolutions or qualities. With MDC the same resolution or the same framerate can be further divided and the decoder can decided to decode an approximation of a high-quality sequence instead of having to reproduce a low quality sequence. Moreover, by providing finer scalability other problems can be addressed, as for example handover and network adaptation. As an example, a mobile terminal equipped with a 802.11 network interface card and a GSM antenna receiving packets through GPRS/EDGE can exploit the features offered by SVC, but as it switches from the wireless LAN to the cellular network or vice versa it is subject to different packet loss patterns and the available bandwidth might require changing the frame rate, the frame size or the quality of the decoded sequence. In this case, a scalable video coder based on MDC might dynamically switch to fit at best to the network and guarantee the best quality of the decoded sequence.

The proposed encoder is based on motion compensation of wavelet-decomposed frames, and shares some bitstream syntax elements with H.264/AVC [WSBL03]. Unlike many SVC schemes, all blocks constituting the proposed encoder work in fixed-point arithmetic. Because of this reason, I renounced to implement the 9/7 wavelet.

Intra-coded frames are encoded using the Le Gall 5/3 wavelet transform to the image in order to obtain three spatial resolutions. The obtained image is immediately encoded by using the Embedded Zerotree Wavelet (EZW) [SCP93] algorithm. This algorithm was chosen instead of more efficient ones, because of its simplicity, since the interest is focused more on MDC than on Single Description Coding (SDC) performance.

In case of temporal prediction, as shown in Figure (3.13), inter-coded frames can be encoded as P or B, after having been decomposed using the 5/3 wavelet to obtain two levels. Temporal Multiple Description Coding can be enabled by connecting the Multiple Description Successive Temporal Approximation and Referencing (MDSTAR) algorithm block to the encoder. Motion estimation can be performed at the desired decomposition level, usually the intermediate or the top level. When the intermediate decomposition level is used, time is saved because motion compensation involves only an image that has one quarter of the pixels of the original image. When the top decomposition level is used better motion estimation is obtained for the full-size sequence and consequently higher compression ratio is reached.

After motion compensation, the residual information for each spatial resolution is evaluated and the three error signals are merged together with the Low-Band Correction (LBC) [Han04] algorithm to enhance reconstruction quality without increasing the required bandwidth. In this algorithm, the transformed coefficients of the residual information of a lower spatial resolution are used to replace the low band of the transformed coefficients of the upper resolution.

In the simple case of two spatial resolutions, if C_0 is the currently encoded frame at high spatial resolution, C_1 its sub-sampled version, R_0 and R_1 respectively the big and small reference frames and E_0 and E_1 the full size and the sub-sampled prediction errors, it is possible to write

$$E_0 = C_0 - R_0 \, . \tag{3.34}$$

Applying the down-sampling filter D to the previous equation we obtain

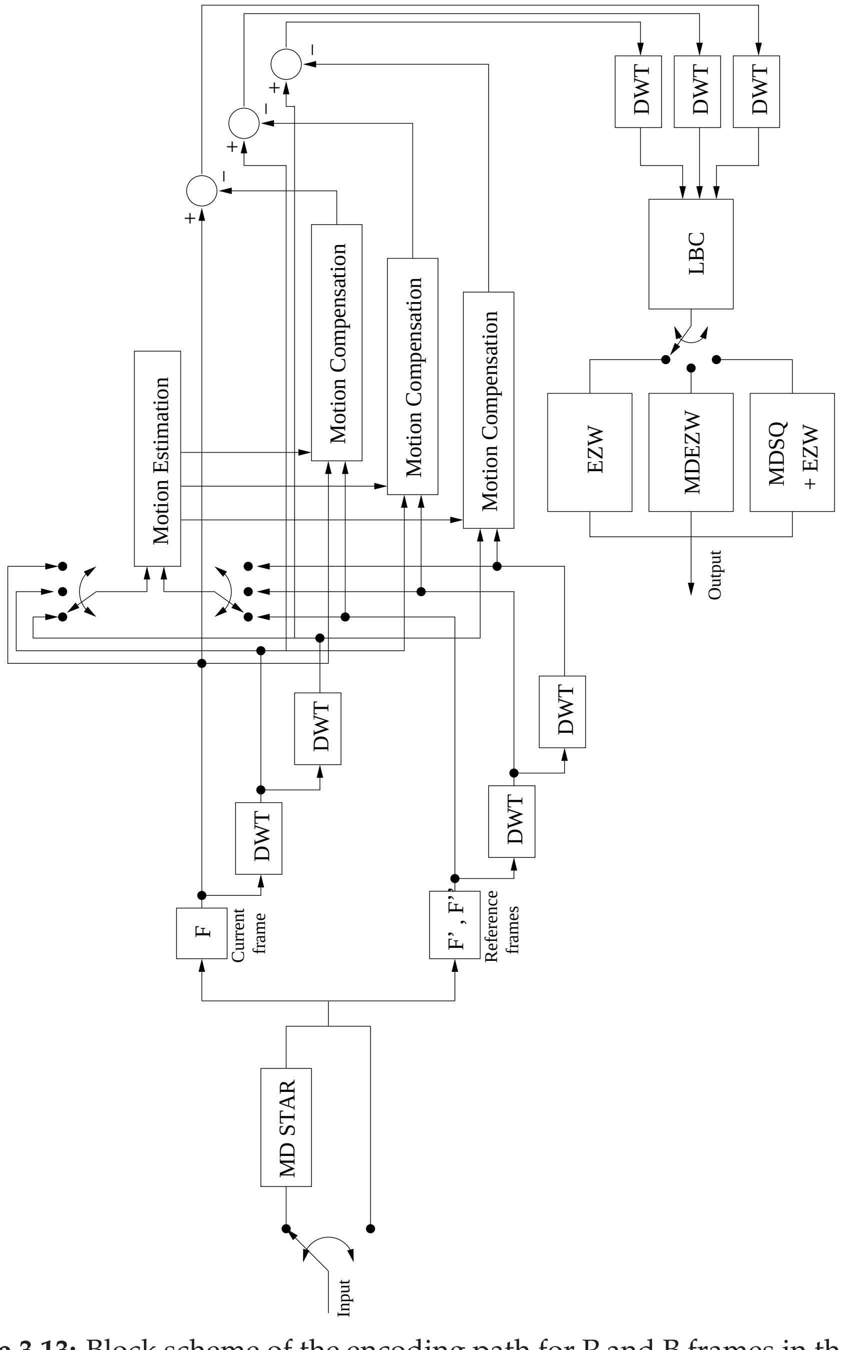

Figure 3.13: Block scheme of the encoding path for P and B frames in the proposed encoder. Predicted frames can be reordered with the MD-STAR algorithm to exploit temporal MDC. Successively, frames are decomposed into three levels by using DWT and motion estimation is performed at the desired decomposition level. The motion vector field is then appropriately scaled and used for each level motion compensation. The obtained residual informations are merged together by using DWT and the LBC algorithm. Finally EZW, MDEZW or EZW with MDSQ can be used to compress the residual information and generate the descriptions.

$$D(E_0) = D(C_0) - D(R_0) = C_1 - D(R_0) \ . \tag{3.35}$$

If the final prediction error signal E satisfies

$$E = E_0 - U(D(E_0)) + U(E_1) \tag{3.36}$$

and the down-sampling filter D and the up-sampling filter U are derived by bi-orthogonal wavelet filters, then in reconstruction the two residuals can be obtained as

$$E_1 = D(E) \tag{3.37}$$

$$E_0 = E - U(E_1) + U(D(E_0)). \tag{3.38}$$

This substitution allows better reconstruction quality for every spatial resolution than transmitting only part or all the residual information of the biggest spatial resolution. In fact, if only the residual information of the higher spatial resolution is used, artifacts may appear in the smallest sequence, because scaled motion vectors and small 4x4 pixels blocks can bring to a imperfect motion compensation and to visible blocking artifacts. A pictorial example of how LBC works in shown in Figure (3.14).

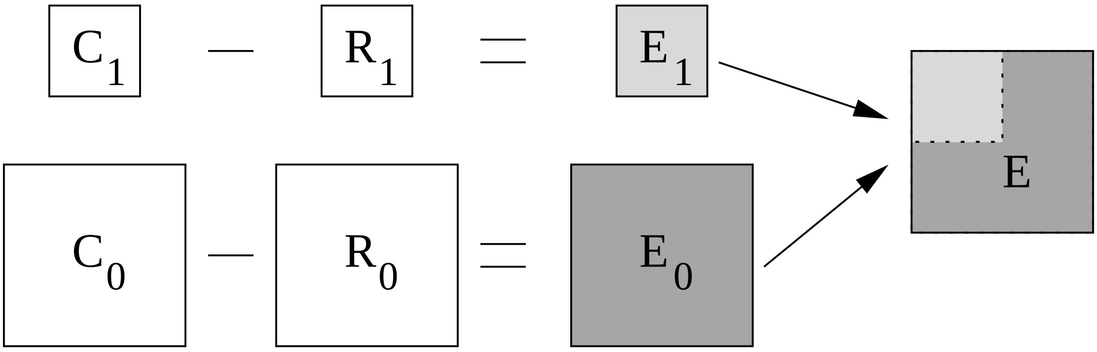

Figure 3.14: Low Band Correction for two decomposition levels.

Motion vectors are encoded as in H.264/AVC base profile. They are predicted using the median between the vectors of the left, upper and upper-right blocks and encoded exploiting the exp-golomb code, as specified in H.264/AVC Context Adaptive Variable Length Coding (CAVLC).

Finally, residual information can be encoded by using EZW or two variants I developed: Multiple Description EZW (MDEZW) and Multiple Description

Scalar Quantizer (MDSQ) based EZW. By adopting MDEZW spatial correlation is exploited to generate descriptions, dividing the bands imposed by the Discrete Wavelet Transform (DWT). In MDSQ-based EZW the residual information is quantized by a MDSQ and the two obtained descriptions are independently encoded by EZW. Although I never used two different MDC techniques at the same time, it should not be difficult to output four descriptions instead of two.

3.2.1 Spatial Multiple Description Coding

By excluding the MDSTAR algorithm and enabling the MDEZW [CN07] block, spatial MDC is enabled in the encoder.

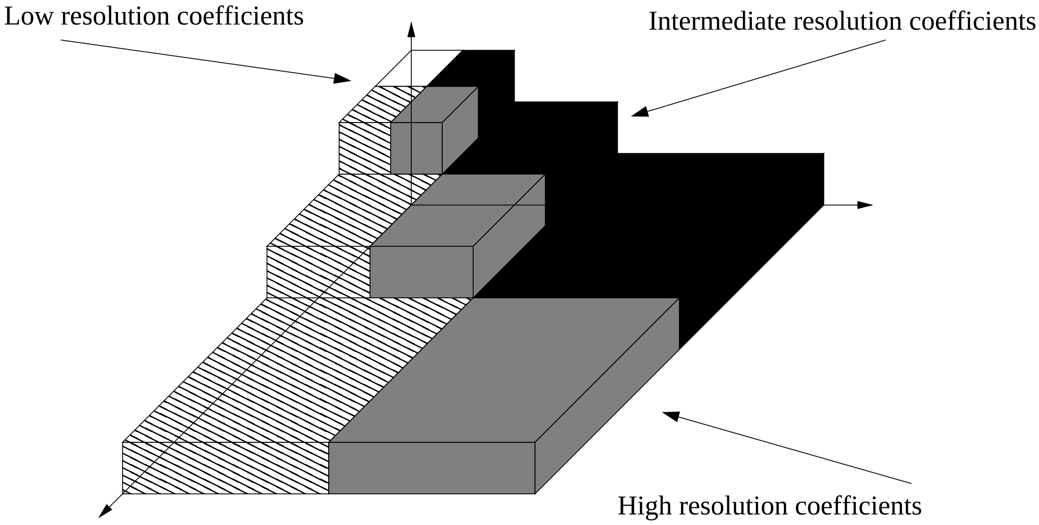
Low resolution coefficients
Intermediate resolution coefficients
High resolution coefficients

Figure 3.15: Multiple descriptions construction. Low-, intermediate- and high-resolution DWT-transformed coefficients are merged together as described in the LBC algorithm. Bands of the same color belong to the same description. The white low band is shared between all descriptions.

Spatial multiple descriptions are generated by splitting the output of the LBC block during EZW coding. Particularly, each decomposition layer is divided into three description exploiting the LH, HL and HH bands obtained from the wavelet transform. During tests, it was noticed how performance increased by not assigning the same subbands to the same description. In fact, by putting an LH, an HL and a HH band in each description the reconstruction quality increases. This came at a too high price in terms of introduced redundancy because it broke the structure of the zero-trees and therefore it was decided not to take advantage of this gain of half dB in PSNR. Motion vectors are duplicated on each description, because since they are encoded taking advantage of prediction, in case of transmission error, not only those relative to the lost description but all motion vectors are influenced by the wrong reconstruction. This can cause annoying artifacts, especially in this scheme, where the same motion vector field is shared between the available resolution: in the high resolution sequence motion vectors are doubled and therefore errors are much more visible. Although this choice requires more bandwidth, part of this requirement can be reduced thanks to motion vectors prediction and for high quality videos does not excessively increase redundancy, since most bits are used to encode the residual information. Figure (3.15) shows how coefficients from the three resolution images are merged together using LBC and descriptions are generated. Please note that in Figure (3.15) the vertical dimension is used only to ease bands grouping and does not correspond to any implemented functionality.

Since we require to be able to dynamically switch between the single description and multiple description approach, EZW coding has to be slightly modified. Instead of iteratively scanning the bands of each decomposition level, our implementation of EZW scans all the bands of each description. This gives the possibility of switching between one and three descriptions and in order to switch between resolution band scanning can be interrupted at the desired decomposition level.

I also tried to make the introduced redundancy tunable. I tried to insert some parity subbands to generate a fourth description used for parity checking, but it turned out that these additional bands cannot be efficiently encoded with EZW because their coefficients do not share the same inter- and intraband correlation. If redundancy tunability is needed, a better solution is given by copying some low bands on more than one description, or studying oversampled wavelets.

3.2.2 MDSQ-based Multiple Description Coding

As already shown in Section (2.7.1), the Multiple Description Scalar Quantizer (MDSQ) is an extension to the optimal Lloyd-Max scalar quantizer proposed by Vaishampayan [Vai93b], where the encoder sends the information over two different channels subject to a rate constraint. The receiver reconstructs the received source samples from the currently working channels. The optimal MDSQ minimizes the reconstructed signal distortion when both data chunks are correctly transmitted, while in case of only one description reception, reconstruction is characterized by fixed average distortion.

Since it is not always possible to change the cells of the quantizer, many MDC schemes relying on the MDSQ optimize only the reconstruction level, thus obtaining a suboptimal system. This problem is even more important in this coding scheme, because it works in fixed point and truncation errors would increase computational noise. Moreover, since the optimal MDSQ requires Voronoi cells whose boundaries are not bit-aligned as the cells imposed by the bitplane encoding algorithms, it was decided only to apply the index assignment algorithms.

Simulation results were disappointing. In fact, if the number of diagonals is big, than the side decoders cells size is such that reconstruction quality in case of transmission error is too low to be acceptable. Cells are so big that quantization is too aggressive and noise destroys the visual information. Following a paper of Sun and Dai [SD], we tried to reduce the number of diagonals to reduce cells size and therefore quantization noise. By reducing the number of diagonal in the assignment matrix we got good reconstruction quality but the introduced redundancy raised quickly. In fact, by using less diagonal in the assignment matrix the output signals become more correlated, and in the case proposed by Sun and Dai the precision of the obtained descriptions has only one bit less then the original one and therefore the required bitrate corresponds to encoding the image twice, skipping only the less significant bitplane.

●	●					
	●	●				
		●	●			
			●	●		
				●	●	
					●	●

Figure 3.16: Assignment matrix proposed by Sun and Dai. By using only two diagonals, the first seven bits are in practice replicated.

For this reasons, after having run some tests to measure the introduced redundancy, it was decided to focus on other MDC schemes and consider MDSQ not a valid solution for SVC schemes.

3.2.3 Temporal Multiple Description Coding

By connecting the Multiple Description Successive Temporal Approximation and Referencing (MDSTAR) block [CN], temporal MDC can be enabled in the proposed encoder.

In MDSTAR, frames are first partitioned into even and odd. Successively, the obtained sequences are independently encoded with the Successive Temporal Approximation and Referencing (STAR) [Han03] algorithm. In STAR, temporal scalability is obtained by doubling the number of frames in each temporal level by dyadically decomposing them. Frames are selected by subsequently visiting the levels of the binary tree obtained by the decomposition. Depending on the availability of the reference frames, the current frame can be encoded either as P or B. When the STAR algorithm is applied to the split frames independently, it is possible to identify couples of frames, one in each description, which are adjacent in the original sequence. Since these frames are highly correlated, for each frame it is possible to store the motion vector field obtained by the motion estimation performed by using the other frame as reference. Whenever a transmission error occurs, the lost frame can be estimated by applying the motion vector field to the relative frame in the other description. An example of how MDSTAR works is given in Figure (3.17), where the sequence dyadic decomposition is shown. The two descriptions hold either the frames filled with a pattern or with a color and one of the two I initial frames.

The partitioning process has a major drawback in case of many temporal decomposition levels: if the decomposition levels are more than three, then frames in the low framerate layer are badly spaced, and the reconstructed sequence consists of very far couples of near frames. In this case it is not possible to produce a smooth enough playback of the sequence. As a solution for this specific case, the Multiple Description version of STAR has to be modified so that the roots of the trees imposed by the dyadic decomposition are not located in adjacent frames but they have a distance of

$$\frac{2^{l-1}}{2} \pm 1$$

frames, where l is the number of decomposition levels. In fact, when in each description are obtained l decomposition levels then each binary tree holds

$$\sum_{n=0}^{l-1} 2^n$$

frames and the distance in terms of frames between the root of the tree and the successive decomposition level frames is equal to 2^{l-1}. As a consequence

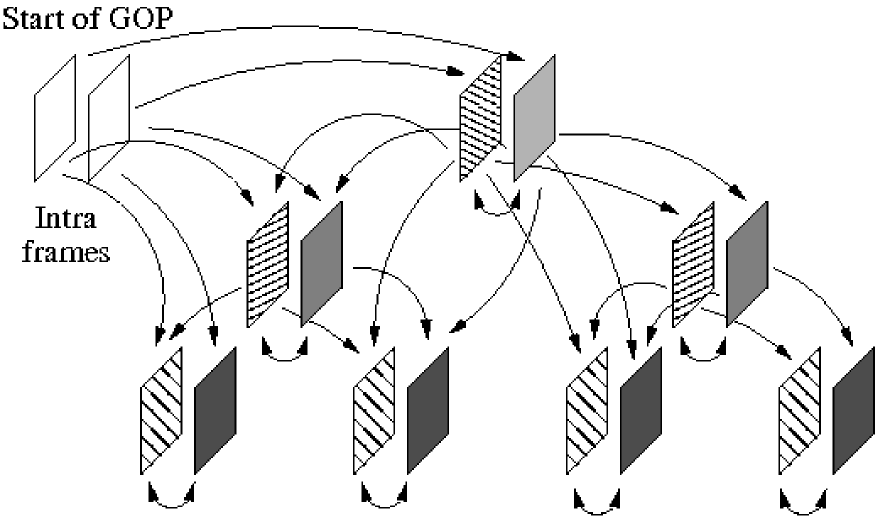

Figure 3.17: Example of Multiple Description STAR algorithm application for three temporal decomposition levels and 16 frames GOP. The star algorithm is independently applied to even and off frames. Redundancy is introduced by evaluating the additional motion vector fields and optionally encoding some bitplanes of the residual information of neighbor frames.

offsetting the trees roots of $\frac{2^{l-1}}{2} \pm 1$ frames, the frames of a decomposition level will be close to those of the successive decomposition layer in the other description and therefore the maximum spread between the frames will be achieved, because of the dyadic decomposition. The ± 1 term takes into account the fact that the frames indexes must be integer.

Redundancy tunability can be introduced by varying the search range in motion estimation between frames couples and by encoding some bitplanes of the difference signal. However, by adjusting these parameters quality does not significantly increases. In fact, if the input sequence has a limited motion vector field, quality does not change by increasing the search range upon a critical range. If motion estimation is accurate, then introducing more redundancy by encoding some bitplanes of the residual information might not be justified by quality, especially in case of few transmission errors.

An upper bound to the introduced redundancy for each frame can be estimated as

$$m_r \cdot m_c \cdot v_m \cdot 2 \cdot l(r) \tag{3.39}$$

bits, where m_r and m_c are the number of macroblocks per row, v_m the number of vectors per macroblock and per column and $l(r)$ is the maximum length

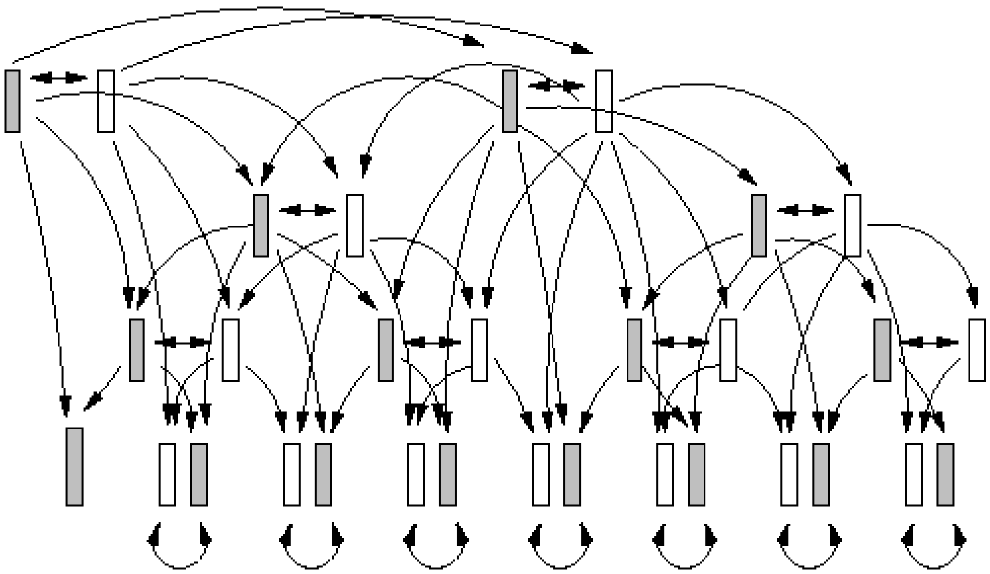

Figure 3.18: Example of Multiple Description STAR algorithm application for four temporal decomposition levels with equally spaced frames.

in bits necessary to encode one motion vector component by using the CAVLC syntax to encode `se` syntax elements. $l(r)$ is 3 for a search range of one pixel, 5 for a three pixel search range, 7 for a seven pixel search range and so on, as it can be easily seen in the CAVLC specification.

This estimate does not take into account the fact that by splitting even and odd frames motion compensation loses efficiency because reference frames are far from the encoded one. This is not considered an error, because the STAR algorithm separates the input frames by applying a dyadic decomposition and therefore the temporal distance does not really change and the motion compensation efficiency does not change.

3.2.4 Experimental Results

In the previous chapter we adopted as test scenario the loss of a single frame in one description to test the PSNR behavior. This scenario was realistic only in case of low-bitrate transmissions, but by applying MDC to SVC this scenario became inappropriate, thus, we decided to applied the so called Error Patterns for Internet Experiments.

Since performance of the MDSQ-based approach was poor, only spatial and temporal multiple description coding were investigated.

Test conditions

Error Patterns for Internet Experiments [Wen99], are provided to test the schemes in case of unreliable transmission, in case of 3%, 5%, 10% and 20% packet error rate. They have been obtained performing some experiments on the Internet backbone to provide up-to-date information about the packet loss characteristics. The conclusions drawn out of those experiments can be summarized as follows:

- There are virtually no bit errors in IP/UDP packets;
- No relationship can be observed between the packet size and the packet loss rate;
- No relationship can be observed between the bitrate and the packet loss rate;
- Packet losses typically occur randomly or in very short bursts like two or three packets;
- Packet loss rates are dependent on the connection;
- Packet loss rates are dependent on the time of day.

These patterns consist of 10000 characters with a value larger than ’0’, plus whitespace characters. When interpreting the patterns, any whitespace characters should be ignored. Each non-whitespace character reflects the delay category of a single packet. The delay can be calculated by subtracting the ASCII-value of ’0’ from the character reflecting the delay of a packet. The resulting number should be multiplied by 10 to reflect the delay in milliseconds. A value of ’1’, for example reflects between 0 and 10 ms delay, a value of ’5’ reflects 41-50 ms delay.

File	Pattern	Average Delay	Loss	Loss150	Loss200
3	ubc35	125 ms	3.3%	3.8%	3.4%
5	ucla194	141 ms	5.6%	5.7%	5.7%
10	ubc12	160 ms	11.5%	19.7%	13.2%
20	ubc92	160 ms	20.8%	30.0%	22.7%

Table 3.1: Statistical information for Error Patterns for Internet Experiments

In Table (3.2.4) the statistical information about the four proposed patterns is shown, where Loss is the packet loss rate (all packets marked as ’0’ in the error patter file), Loss150 is the packet loss rate when assuming all packets are lost that arrive later than 150% of the average delay and Loss200 is similar to Loss150, but assuming 200% of average delay. Loss150 and Loss200 can be optionally used for a (very much) simplified simulation of the RTP buffer management.

During the evaluation of these new test conditions, extremely long packet loss bursts of more than 100 packets were rarely observed. Error patterns containing such extremely long network stalls were not used for any assessment beyond the packet loss probability calculation, as they render multimedia communication useless. The most likely reaction of a user in such cases would be to 'hang up, and dial again'. It is unclear, whether these results represent backbone behavior, or whether they were caused by some form of extremely high local network utilization, e.g. due to batch backup runs or automatic software updates in the involved LANs, but they show how the assumption in [PA97] and [Per99] of error bursts corrupting the transmission are not verified.

3.2.5 Spatial Multiple Description Coding

Since MDEZW generates three descriptions by truncating the scanning process of each bitplane, it is able to efficiently protect the bitstream without introducing noticeable redundancy. In fact, by not only setting to zero the coefficients relative to other descriptions but also by truncating the scanning process, it is able to generate the description for the residual information without duplicating any information but the motion vector field. This substantially does not require many bits since it is differentially encoded as in H.264/AVC, and the LL wavelet band in the smallest decomposition level. Since the number of decomposition layers can be much higher than the number of spatial resolution, the LL band only has a few pixels.

In Figures (3.19, 3.20) the Redundancy Rate-Distortion (RRD) region for 4CIF sequences is represented, showing the achievable PSNR by introducing some redundancy. Results are the same for all the tested sequences, such as "*crew*" or "*soccer*". In these two figures, the RRD region was evaluated under the 5% and 20% packet loss scenario respectively using 6 decomposition levels in MDEZW.

In case smaller sequences are used, worse results can be achieved. In fact, each time a decomposition level is added redundancy is approximately reduced of up to 75%. This happens because by adding an adjunctive level, the shared LL band is further split and only one quarter of its coefficients are shared between the descriptions. Clearly, in order to obtained the same redun-

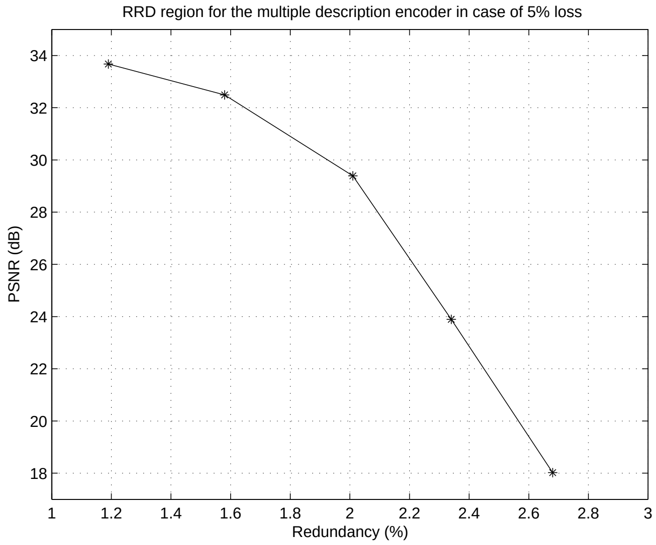

Figure 3.19: Redundancy Rate-Distortion regions for the multiple description encoder in case of 5% packet loss probability for 4CIF sequences sequence using 6 decomposition levels in MDEZW. Since redundancy is not a degree of freedom in this scheme, each point is a complete RRD region for a given number of bitplanes encoded. Drawn lines show the PSNR and redundancy vary by changing the number of encoded bitplanes.

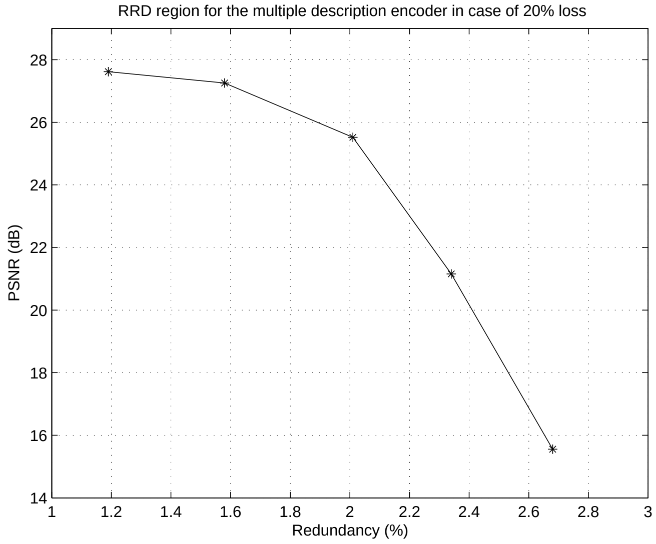

Figure 3.20: Redundancy Rate-Distortion regions for the multiple description encoder in case of 20% packet loss probability.

dancy additional decomposition levels have to be added and in case of information loss less data is available for reconstruction, leading to worse quality. Thus, the number of decomposition levels is a trade-off, because the less coefficients are shared the more fragile the coding scheme becomes.

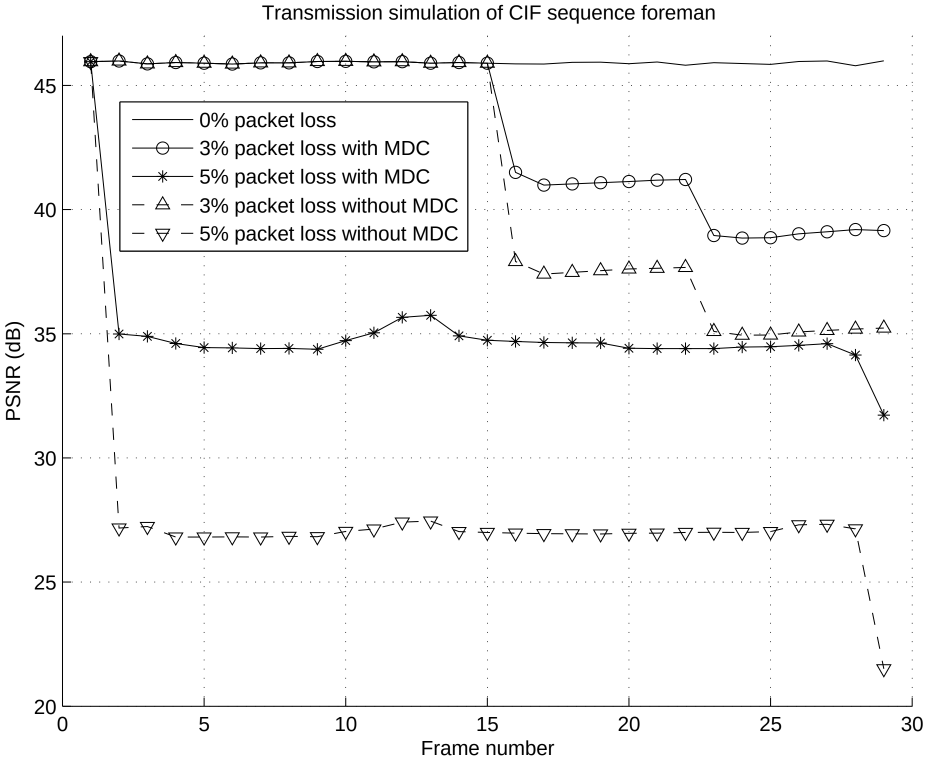

Figure 3.21: Comparison of the decoded sequence quality for 0%, 3% and 5% packet loss probability using SVC and MDC schemes and the *"foreman"* CIF sequence.

It is important to notice that this coding scheme does not allow the user to choose the amount of redundancy introduced, and therefore RRD region consists of only one point. The drawn lines in these figures show how the introduced redundancy and the PSNR of the reconstructed sequence change by varying the number of encoded bitplanes. The more bitplanes yield higher quality of the reconstructed sequence and at the same time fewer redundancy because it consists only of the motion vector field.

The quality of the decoded sequence was compared at the receiver in the single and multiple description cases, assuming that in case of packet loss in the single description decoder the frame is discarded. For the single description encoder each packet consists of one frame, while for the single encoder,

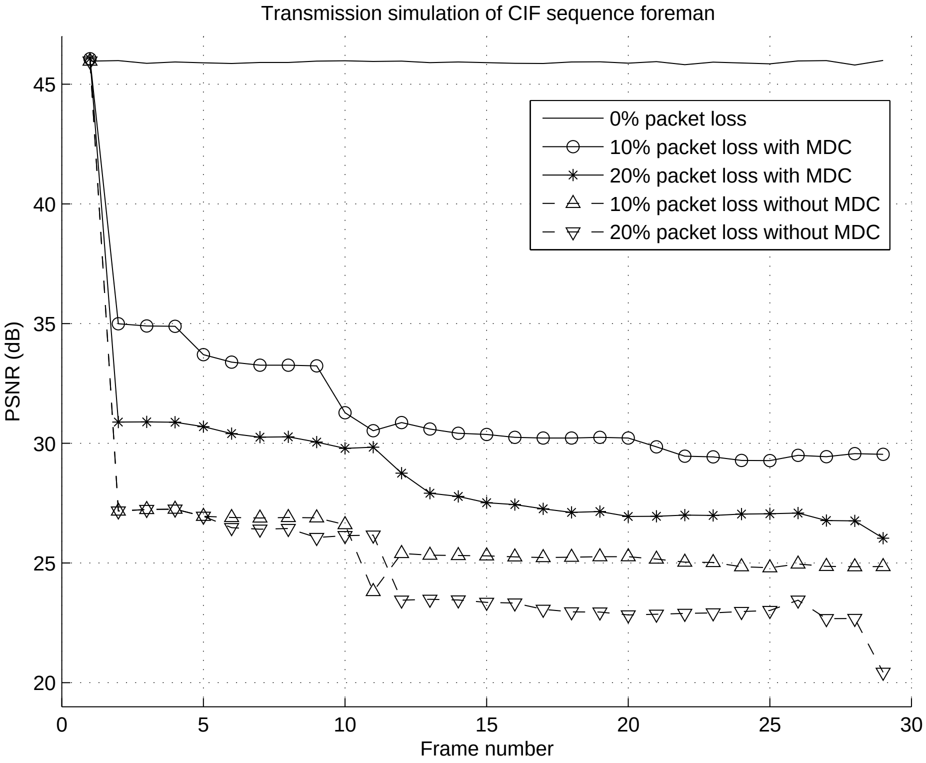

Figure 3.22: Comparison of the decoded sequence quality for 0%, 10% and 20% packet loss probability using SVC and MDC schemes and the “*foreman*” CIF sequence.

each packet hold one frame description. Since single description packets are approximately as big as three multiple description packets, the probability of packet loss in case of SVC is three times the probability of loosing one packet during MDC. In Figures (3.21, 3.22) the comparison results of SVC and MDC are shown for the proposed packet loss patterns using the *"foreman"* CIF sequence coding seven bitplanes.

An example of what the distortion looks like is shown in Figure (3.23), where the decoded sequence *"foreman"* is reported after having lost five packets. Each packet loss corresponds to some coefficients of the residual signal having value of zero, therefore the introduced artifacts are very similar to those affecting images lossy compressed by interrupting the bitplane encoding before all the coefficients bits have been properly encoded.

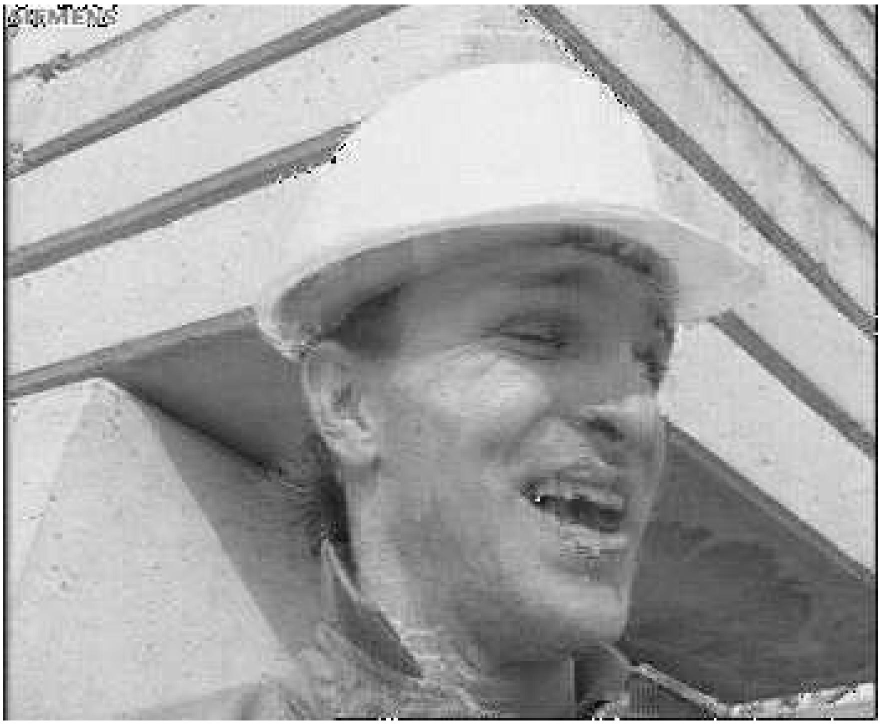

Figure 3.23: Example of video corruption after five transmission errors for MDEZW. The introduced distortion is similar to the artifacts obtained in image compression by truncating the bitplane encoding before all coefficients have been compressed at the resolution necessary for lossless encoding.

Keeping in mind the small amount of introduced redundancy, it can be concluded that the achieved result is positive. In fact, by qualitatively comparing this scheme with those developed for the H.264/AVC encoder, not only this scheme offers good protection requiring only very small redundancy, but at the same time it can be easily integrated into SVC schemes, because of its simplification and minimal modification of the EZW algorithm.

3.2.6 Temporal Multiple Description Coding

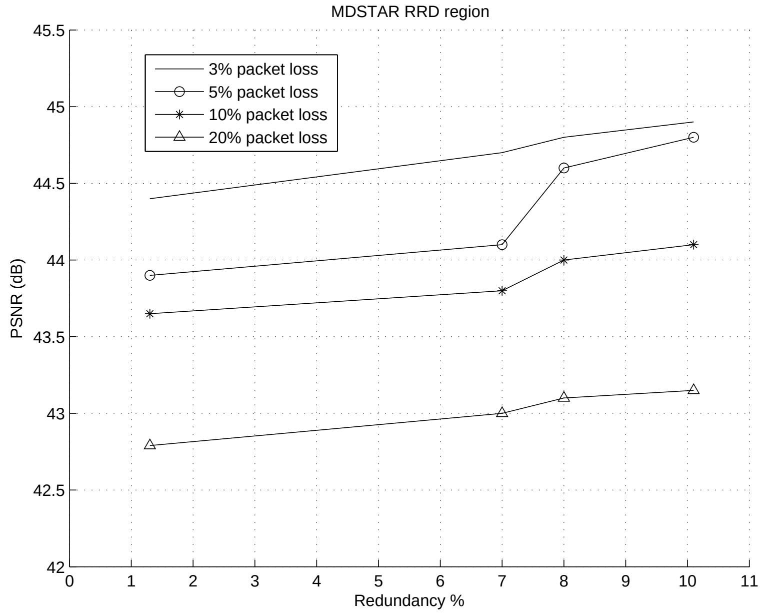

Figure 3.24: Redundancy Rate-Distortion for the "*foreman*" CIF sequence. The average PSNR of the decode sequence afflicted by transmission error is plotted against the introduced redundancy for 3%, 5% 10% and 20% error probability.

The first test for MDSTAR was the evaluation of the RRD region. The amount of redundancy cannot be easily tuned, as it can appear. In fact, what makes Equation (3.39) an upper bound is the fact that motion vectors are predictively encoded and therefore increasing r does not always increase the bits necessary to hold $l(r)$. If the input sequence has an uniform motion vector field the introduced redundancy is significantly smaller and does not change by varying r. Since redundancy consists of only a few bits if compared to the total bitstream, redundancy can be further and better tuned by storing not only the motion vector field between the couples of frames, but also some bitplanes of the residual information from motion estimation.

As tests have shown, the RRD region is in practice flat, and it only varies of portions of dB when adding several bitplanes in the information that links frames in each couple. Obviously, the reconstruction quality is dependent from the percentage of lost packets, so in Figure (3.24) the four regions corresponding to the four Error Patterns are shown. The flatness of such regions led to the choice of not including any additional bitplanes in the successive tests.

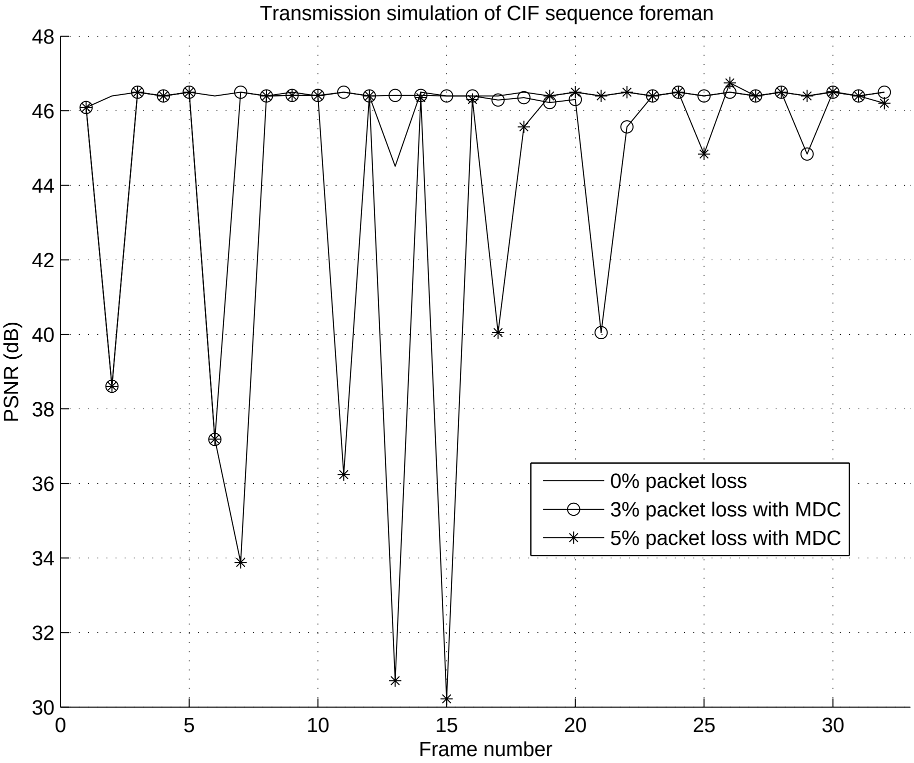

Figure 3.25: Transmission simulation if the *"foreman"* CIF sequence compressed with the MDSTAR algorithm. In this case the 3% and 5% error patterns are used.

Figures (3.25, 3.26) show how the PSNR of the *"foreman"* sequence at CIF resolution varies in case of errors. In Figure (3.25) the 3% and 5% error patterns are used, while in Figure (3.26) 10% and 20% packet loss probabilities are used. All tests evince that PSNR losses are not homogeneous, but significantly varies from frame to frame. The flickering quality is due to the even and odd frames separation and dyadic decompositions.

In fact, even and odd separation is the main reason for alternating quality frames, but the dyadic decomposition explains why errors afflict only a few frames and do not span the successive frames. In the hierarchic decomposition, most errors corrupt frames in the binary tree of the affected frame. Moreover, since in the dyadic decomposition B frames are massively used, if the currently decoded frame has one corrupted reference, the unaffected one smoothes the reconstruction errors because they are averaged for prediction.

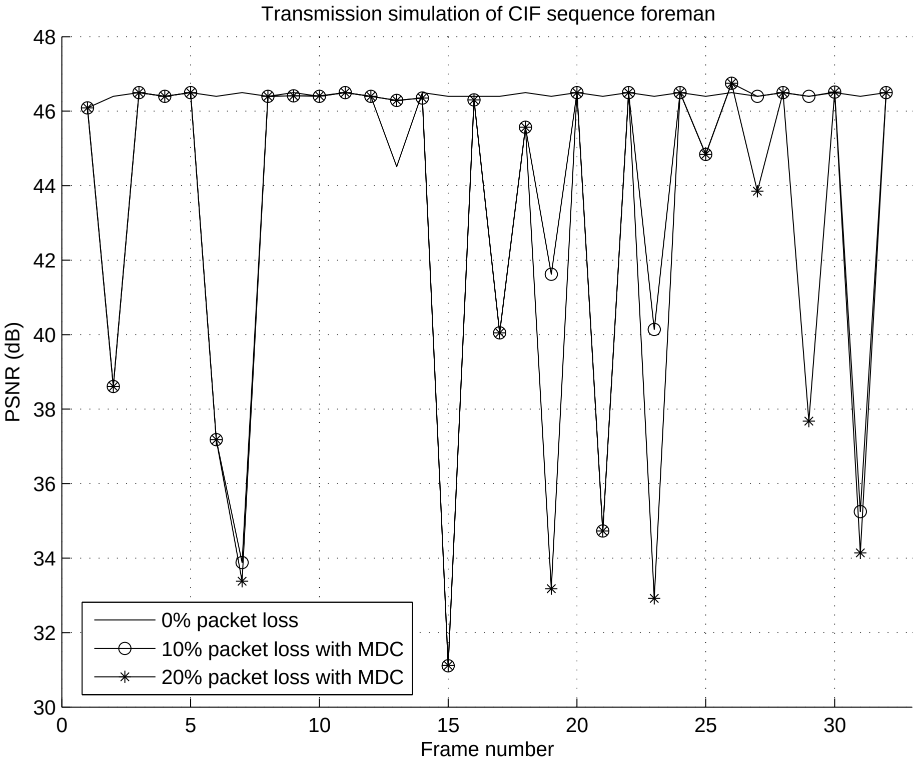

Figure 3.26: Transmission simulation if the *"foreman"* CIF sequence compressed with the MDSTAR algorithm. In this case the 10% and 20% error patterns are used.

The only case when errors propagate on successive decomposition tree happens when the root of the tree is corrupted. In fact, the tree root is used to predict as P the next tree root, thus errors can propagate. To contrast this, two solutions are available:

- increasing the number of decomposition levels. Each time a temporal decomposition level is added, the number of roots is halved, as the probability of corruption of such frames is reduced. This strategy does not directly stop distortion propagation, but the levels number can be jointly chosen with the GOP size, so that the maximum tolerable distortion can be obtained.
- save additional residual bitplanes only for trees roots. This prevents error propagation. If all the residual information is encoded errors are stopped, but usually not all the bitplanes are necessary, especially when

prediction is efficient. Moreover, if a tree root is corrupted and errors corrupt its reconstruction, even the successive root can be reconstructed by motion-compensating the correctly received roots in the other descriptions.

Figure (3.27) is a final example, where the eleventh, thirteenth and fifteenth frames of the "*foreman*" sequence are respectively shown in 3.27(a), 3.27(b) and 3.27(c). The sequence transmission is flawless, wit the exception of the thirteenth frame, which is lost. Since the error originates in the thirteenth frame and redundancy consists only of the motion vector field, in 3.27(b) the blocking artifacts due to the mere motion compensation can be seen. The eleventh frame is encoded as B from the ninth and thirteenth frames and therefore in 3.27(a) distortion is reduced by bidirectional motion compensation. The fifteenth frame in 3.27(c) is encoded as P frame using the thirteenth frame as reference and decoder drift increases because of the bad-quality reference.

3.2.7 Comparison between the spatial and temporal approaches

MDEZW and MDSTAR have opposite characteristics that make them hard to use together, as it was hoped at the beginning of the Protection Enhanced Scalable Video Encoder.

The spatial approach is extremely light in terms of computational overhead, because no additional operation is required if compared to the single description encoder. Further more, prediction is not altered by switching from the single description to the multiple description encoder, so the bitstream extractor or an hypothetical relay server can dynamically switch from the SD to the MD configuration and vice-versa, depending on the channels statistics. Therefore, theoretically is possible to execute the first version on the encoder in real-time, given an appropriate optimization of the code.

Contrarily, MDSTAR involves several additional operation of motion estimation and compensation. Even the coding order is different, so it is not possible is dynamically switch from the single description to the multiple encoder, but the compressed bitstream have to be separately generated. This is the reason why MDEZW and MDSTAR cannot be work together in real-time in a scalable encoder.

By comparing the corresponding Redundancy Rate-Distortion regions, it can be seen that in both algorithms the introduced redundancy is small, but MDSTAR is able to better exploit it. In fact, for a comparable amount of redundancy, it clearly appears that the mean output quality of MDSTAR is superior

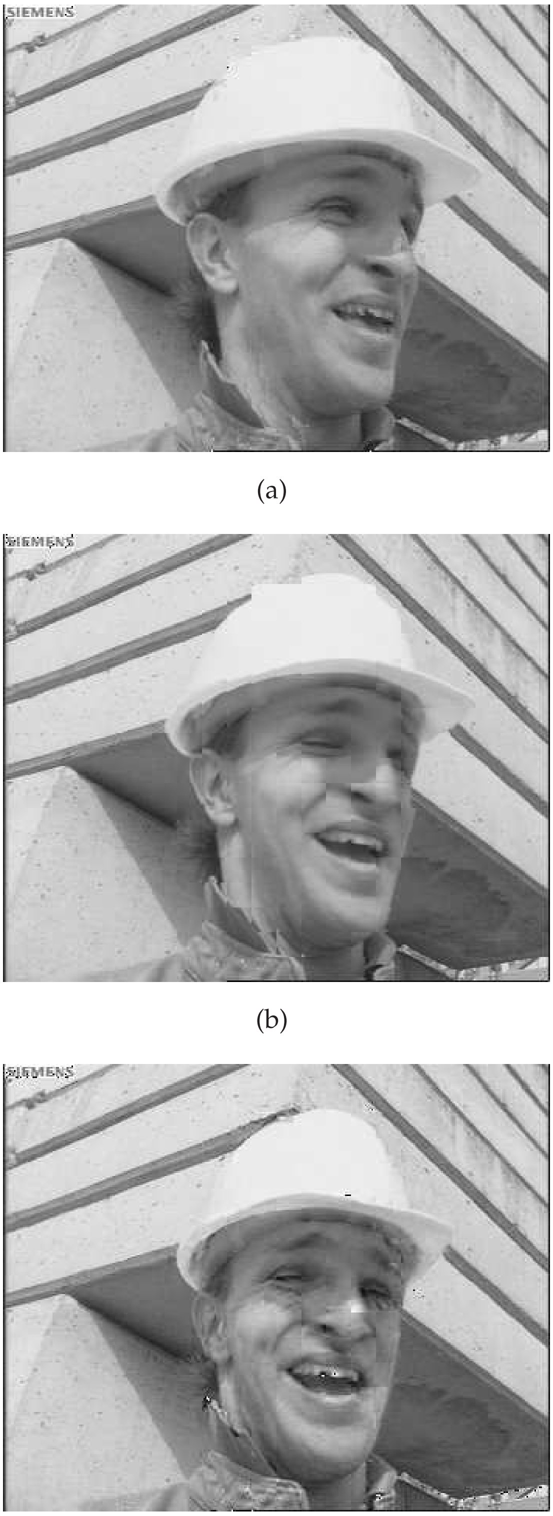

(a)

(b)

(c)

Figure 3.27: Example of introduced distortion in case of transmission error for MDSTAR.

to MDEZW, as the transmission simulation confirm. On the other hand, the computational requirements of MDSTAR make it hard to adopt it, because of all the necessary motion compensation operation at the decoder, which can be a mobile device with reduced computational resources, and also because the dyadic decomposition introduces a significant decode delay that requires to store in the frame buffer many more frames then MDEZW. The latter, event tough offers less protection to errors, can be nearly implemented for free in terms of CPU and memory. Thus, it is the candidate for future applications to scalable video coding for future distributed applications, such P2P video streaming.

As final remark, qualities of MDEZW and MDSTAR are summarized in Table (3.2.7).

	MDEZW	**MDSTAR**
Exploited correlation	spatial	temporal
Efficiency	good	good
Computational Cost	low	high
Tunability	no	yes
Switchable between SDC and MDC	yes	no

Table 3.2: Qualitative comparison of MDZW and MDSTAR.

Chapter 4

Conclusions

The topic of this thesis is reliable transmission of non-scalable and scalable video. Among several different strategies, Multiple Description Coding is a joint source channel technique which aims to add robustness by dividing the input signal in subsampled portions and by sending them over distinct channels, in order to exploit the channel diversity. One main characteristic of Multiple Description Coding is the fact that joint source channel coding is mainly focused on source coding and possible signal division strategies are chosen starting from the coding scheme and not from the channel statistics, as other joint source channel solutions do.

With the exception of implementing it as pre- and post-processing operations, application of Multiple Description Coding is in general hard, especially when these techniques are added to an already existing coding standard.

This is the case of H.264/AVC, where schemes based on spatial or temporal input subsampling can be easily implemented but can lead to misfunction. In fact, spatial subsampling breaks Intra prediction, while temporal subsampling reduces motion compensation efficiency because it forces motion estimation on temporally far frames. Other schemes cannot be implemented as pre- and post-processing blocks, so they require heavy changes in the encoder source code. Even the solution based on a Multiple Description Scalar Quantizer, which eventually was implemented as a lookup table, required a deep study of the code before being able to implement it. The worst case was the Motion-Compensated Multiple Description Video coding, which required several thousands of lines of code to fit the JVT reference encoder.

In the scalable video case, application of MDC was easier, because some coding strategies were decided by keeping into account the encoder design and the generated descriptions. As an example, the Le Gall 5/3 wavelet was chosen because it is the optimal trade-off between computational complexity and output quality of the Single Description and Multiple Description cases. Wavelets with longer filters were under examination, because by increasing the filter size the correlation of the wavelet coefficients rises, thus making possible to introduce an estimation of lost coefficients. The major drawback of this approach was the reduction of the compression ratio and of the output quality of the single description decoder, because long filters tend to degrade edges sharpness in the frames, so eventually it was chosen not to pursue this strategy.

Only by adding support to Multiple Description Coding during standards definition, as it happened for other tools such as Data Partitioning and Flexible Macroblock Ordering in the H.264/AVC standard, it will be possible to apply these techniques. Fortunately, emerging scenarios in Scalable Video Coding and Peer-to-Peer video streaming over non-homogeneous networks seem to be the suitable environment where these techniques will be fully exploited.

Future steps in Multiple Description Coding research applied to Scalable Video Coding will aim to increase compression efficiency and redundancy tunability. The first goal will be addressed by enhancing motion compensation and by substituting EZW with arithmetic encoding. Hopefully, better management of the introduced redundancy in spatial MDC will be obtained by adopting new overcomplete wavelet transforms, whose additional bands will be used as parity check bands that can be efficiently compressed. Finally, directional wavelets can be further investigated to rise compression ratios.

Bibliography

[Ahl85] R. Ahlswede. The rate-distortion region for multiple descriptions without excess rate. *IEEE Transactions on Information Theory*, 31(6):721–726, 1985.

[AK00] M.D. Adams and F. Kossentini. Reversible Integer-to-Integer Wavelet Transforms for Image Compression: Performance Evaluation and Analysis. *IEEE TRANSACTIONS ON IMAGE PROCESSING*, 9(6), 2000.

[Apo00] J. Apostolopoulos. Error resilient video compression through the use of multiple states,. *Proc. IEEE Int. Conf. Image Processing*, 3:352–355, 2000.

[Apo01a] J. Apostolopoulos. Reliable video communication over lossy packet networks using Multiple State Encoding and path diversity. In *IEEE VCIP 2001*, January 2001.

[Apo01b] J. Apostolopoulos. Unbalanced Multiple Description video communication using path diversity. In *Proc. of International Conference on Image Processing, ICIP 2001*, Thessaloniki, Greece, October 2001.

[AW01] MD Adams and R. Ward. Wavelet transforms in the JPEG-2000 standard. *Communications, Computers and signal Processing, 2001. PACRIM. 2001 IEEE Pacific Rim Conference on*, 1, 2001.

[BRTV04] R. Bernardini, R. Rinaldo, A. Tonello, and A. Vitali. Frame based multiple description for multimedia transmission over wireless networks. In *Proc. of 7th Int. Symp. WPMC*, volume 2, pages 529–532, Abano Terme, Italy, July 2004.

[CCD$^+$06] O. Campana, A. Cattani, A. De Giusti, S. Milani, N. Zandonà, and G. Calvagno. Multiple Description Coding Schemes for the

H.264/AVC Coder. In *Proc. of the International Conference on Wireless Reconfigurable Terminals and Platforms (WiRTeP)*, pages 217–221, Rome, Italy, April 2006.

[CDSY98] AR Calderbank, I. Daubechies, W. Sweldens, and B.L. Yeo. Wavelet transforms that map integers to integers. *Appl. Comput. Harmon. Anal*, 5(3):332–369, 1998.

[CM04] O. Campana and S. Milani. A Multiple Description Coding Scheme For The H.264/AVC Coder. In *Proc. of the International Conference on Telecommunication and Computer Networks IADAT-tcn2004*, pages 191–195, San Sebastian, Spain, December 2004.

[CN] O. Campana and T. Nguyen. A Temporal Multiple Description Coding Based Scalable Video Codec.

[CN07] O. Campana and T. Nguyen. Protection Enhanced Scalable Video Coding. In *Proc. of the 15th European Signal Processing Conference (EUSIPCO 2007)*, Poznan, Poland, September 2007.

[CT06] T. M. Cover and J. A. Thomas. *Elements of Information Theory*. Wiley-Interscience New York, 2006.

[DIS91] ISO DIS. 10918-1. *Digital Compression and Coding of Continuous-tone Still Images (JPEG), CCITT Recommendation T*, 81, 1991.

[DMW03] H. Schwarz D. Marpe and T. Wiegand. Context-based adaptive binary arithmetic coding in the H.264/AVC video compression standard. *IEEE Transactions on Circuits and Systems for Video Technology*, 13(7):620–636, 2003.

[DS98] I. Daubechies and W. Sweldens. Factoring wavelet transforms into lifting steps. *Journal of Fourier Analysis and Applications*, 4(3):247–269, 1998.

[EF95] S. Eckart and C. Fogg. ISO/IEC MPEG-2 software video codec. *Proc. SPIE*, 2419:100–118, 1995.

[GC82] Abbas A. El Gamal and Thomas M. Cover. Achievable rates for multiple descriptions. *IEEE Transactions on Information Theory*, IT-28(6):851–857, November 1982.

[Ger79] A. Gersho. The channel splitting problem and modulo-PCM coding. *Bell Labs Memo for Record (not archived)*, October 1979.

[GK98] V.K. Goyal and J. Kovacevic. Optimal multiple description transform coding of Gaussian vectors. *Proc. IEEE Data Compression Conf*, pages 388–397, 1998.

[GKAV98] VK Goyal, J. Kovacevic, R. Arean, and M. Vetterli. Multiple description transform coding of images. *Image Processing, 1998. ICIP 98. Proceedings. 1998 International Conference on*, 1, 1998.

[Goy01a] Vivek K. Goyal. Multiple description coding: Compression meets the network. *IEEE Signal Processing Magazine*, 8(5):74–93, September 2001.

[Goy01b] Vivek K. Goyal. Single and Multiple Description Transform Coding with Bases and Frames. In *Proc. of SIAM*, 2001.

[Gra95] A. Graps. An introduction to wavelets. *IEEE Computational Science and Engineering*, 2(2):50–61, 1995.

[GVT98] VK Goyal, M. Vetterli, and NT Thao. Quantized overcomplete expansions in IR N: analysis, synthesis, and algorithms. *IEEE Transactions on Information Theory*, 44(1):16–31, 1998.

[Han03] W. J. Han. Successive Temporal Approximation and Referencing (STAR) for Improving MCTF in Low End-to-end Delay Scalable Video Coding. *ISO/IEC JTC 1/SC 29/WG11 M10308*, December 2003.

[Han04] W. J. Han. Responses of call for proposal for scalable video coding. *ISO/IEC JTC 1/SC 29/WG11 MPEG2004/M10569/ S*, March 2004.

[HPCH07] H.C. Huang, W.H. Peng, T. Chiang, and H.M. Hang. Advances in the scalable amendment of H.264/AVC. *IEEE Communications Magazine*, 45(1):68–76, 2007.

[Jay81] N.S. Jayant. Sub-sampling of a DPCM speech channel to provide two “self-contained” half-rate channels. *Bell Syst. Tech J.*, 60(4):501–509, April 1981.

[Kai74] JF Kaiser. Nonrecursive digital filter design using the I 0-sinh window function. *Proc. IEEE Int. Symp. Circuits Syst*, 3:20–23, 1974.

[KL01] C. Kim and S. Lee. Multiple description coding of motion fields for robust video transmission. *IEEE Transactions on Circuits and Systems for Video Technology*, 11(9):999–1010, September 2001.

[KXP97] B.J. Kim, Z. Xiong, and W.A. Pearlman. Very low bit-rate embedded video coding with 3D set partitioning in hierarchical trees (3D SPIHT). *IEEE Transactions on Circuits and Systems for Video Technology*, 1997.

[Li01] W. Li. Overview of fine granularity scalability in MPEG-4 video standard. *Circuits and Systems for Video Technology, IEEE Transactions on*, 11(3):301–317, 2001.

[LJL$^+$03] P. List, A. Joch, J. Lainema, G. Bjntegaard, and M. Karczewicz. Adaptive deblocking filter. *IEEE Transactions on Circuits and Systems for Video Technology*, 13(7):614–619, 2003.

[Mal89] SG Mallat. A theory for multiresolution signal decomposition: the waveletrepresentation. *Pattern Analysis and Machine Intelligence, IEEE Transactions on*, 11(7):674–693, 1989.

[MCO] C. Mayer, H. Crysandt, and J.R. Ohm. Bit plane quantization for scalable video coding. *Proc. SPIE Visual Communications and Image Processing02*, pages 1142–1152.

[Mil80] Stewart E. Miller. Fail-safe transmission without standby facilities. Technical report, Bell Labs, Tech. Rep. TM80-136-2, August 1980.

[Mil83] Stewart E. Miller. Fail-safe transmission system, January 1983.

[MWG05] D. Marpe, T. Wiegand, and S. Gordon. H.264/MPEG4-AVC Fidelity Range Extensions: Tools, Profiles, Performance and Application Areas. *Image Processing, 2005. ICIP 2005. IEEE International Conference on*, 1, 2005.

[Ohm91] JR Ohm. A hybrid image coding scheme for ATM networks based on SBC-VQ and tree encoding. *Proceedings of the Fourth International WorkshopPacket Video, Kyoto, August*, pages 2–1, 1991.

[Ohm94] J.R. Ohm. Three-dimensional subband coding with motion compensation. *IEEE Transactions on Image Processing*, 3(5):559–571, 1994.

[Ohm05] J.R. Ohm. Advances in Scalable Video Coding. *Proceedings of the IEEE*, 93(1):42–56, 2005.

[oII96] Joint Video Team (JVT) of ISO/IEC MPEG and ITU-T SG 15. Draft recommendation h.263 "video coding for low bitrate communication". In *Joint Video Team (JVT) of ISO/IEC MPEG & ITU-T VCEG (ISO/IEC JTC1/SC29/WG11 and ITU-T SG16 Q.6)*, June 1996.

[OS75] AV Oppenheim and RW Schafer. Digital signal processing. *Research supported by the Massachusetts Institute of Technology, Bell Telephone Laboratories, and Guggenheim Foundation. Englewood Cliffs, NJ, Prentice-Hall, Inc., 1975. 598 p.*, 1975.

[OWVR97] M.T. Orchard, Y. Wang, V. Vaishampayan, and A.R. Reibman. Redundancy rate-distortion analysis of multiple description coding using pairwise correlating transforms. *Proc. IEEE Int. Conf. Image Processing*, 1:608–611, 1997.

[Oza80] L. Ozarow. Source-Coding Problem with Two Channels and Three Receivers. *BELL SYS. TECH. J.*, 59(10):1909–1921, 1980.

[PA97] Fernando Pereira and Thierry Alpert. MPEG-4 video subjective test procedures and results. *IEEE Transactions on Circuits and Systems for Video Technology*, 7(1):32–51, 1997.

[Per99] F. Pereira. MPEG-4 testing and evaluation procedures document, DOC. ISO. Technical report, IEC JTC1/SC29/WG11, 1999.

[PPB01] B. Pesquet-Popescu and V. Bottreau. Three-dimensional lifting schemes for motion compensated videocompression. *Acoustics, Speech, and Signal Processing, 2001. Proceedings.(ICASSP'01). 2001 IEEE International Conference on*, 3, 2001.

[Rec90] H. Recommendation. 261: Video codec for audiovisual services at p x 64 kb/s. *CCITT White Book*, 1990.

[Ric03] Ian E. G. Richardson. *H.264 and MPEG-4 video compression: video coding for the next-generation multimedia.* Wiley, Chichester, 2003.

[RJW$^+$02] Amy R. Reibman, Hamid Jafarkhani, Yao Wang, Michel T. Orchard, and Rohit Puri. Multiple-description video coding using motion-compensated temporalprediction. *IEEE Transactions on Circuits and Systems for Video Technology*, 12(3):193–204, 2002.

[RMR$^+$04] R. Bernardini, M. Durigon, R. Rinaldo, L. Celetto, and A. Vitali. Polyphase spatial subsampling multiple description coding of video streams with H264. In *Proceedings of ICIP*, volume 5, pages 3213–3216, Singapore, October 2004.

[RWS05] J. Reichel, M. Wien, and H. Schwarz. Joint Scalable Video Model JSVM-3 Annex S. *JVT-P202, Poznan, Poland, July*, 2005.

[SA96] A. Said and W. A.Pearlman. A New, Fast, and Efficient Image Codec Based on Set Partitioning in Hierarchical Trees. *IEEE Transactions on Circuits and Systems for Video Technology*, 6(3):243–250, 1996.

[SCP93] J. M. Shapiro, D. S. R. Center, and N. J. Princeton. Embedded Image Coding Using Zerotrees of Wavelet Coefficients. *IEEE Transactions on Signal Processing*, 41(12):3445–3462, 1993.

[SD] Y. Sun and Q. Dai. Multiple Description Image Codec for Error Prone Channels.

[SR] M. Standard and ISO Recommendation. IEC-11172-2 (1993). *No Author. No Place of Publication*, pages 89–129.

[TM02] D. S. Taubman and M. Marcellin. *Jpeg 2000: Image Compression Fundamentals, Standards and Practice*. Kluwer Academic Publishers, 2002.

[TWJ98] J. Tian and RO Wells Jr. Embedded Image Coding Using Wavelet Difference Reduction. *Wavelet Image and Video Compression*, pages 289–301, 1998.

[Vai93a] PP Vaidyanathan. *Multirate systems and filter banks*. Prentice-Hall, Inc. Upper Saddle River, NJ, USA, 1993.

[Vai93b] Vinay Anant Vaishampayan. Design of Multiple Description Scalar Quantizers. *IEEE Transactions on Information Theory*, 39(3):821–833, May 1993.

[VK95] M. Vetterli and J. Kovačevic. *Wavelets and subband coding*. Prentice-Hall, Inc. Upper Saddle River, NJ, USA, 1995.

[Wed03] T. Wedi. Motion compensation in H.264/AVC. *IEEE Transactions on Circuits and Systems for Video Technology*, 13(7):577–586, 2003.

[Wen99] S. Wenger. Proposed error patterns for internet experiments. *ITU-T Study Group 16 H.263+ Video Experts Group*, 15, 1999.

[WOVR01] Y. Wang, MT Orchard, V. Vaishampayan, and AR Reibman. Multiple description coding using pairwise correlating transforms. *Image Processing, IEEE Transactions on*, 10(3):351–366, 2001.

[WSBL03] T. Wiegand, G.J. Sullivan, G. Bjntegaard, and A. Luthra. Overview of the H.264/AVC video coding standard. *IEEE Transactions on Circuits and Systems for Video Technology*, 13(7):560–576, 2003.

[Zam99] R. Zamir. Gaussian codes and Shannon bounds for multiple descriptions. *IEEE Transactions on Information Theory*, 45(7):2629–2636, 1999.

[ZB87] Zhen Zhang and Toby Berger. New Results in Binary Multiple Descriptions. *IEEE Transactions on Information Theory*, 33(4):502–521, 1987.

[ZMD05] N. Zandonà, S. Milani, and A. De Giusti. Motion-Compensated Multiple Description Video Coding for the H.264/AVC Standard. In *Proc. of IADAT International Conference on Multimedia, Image Processing and Computer Vision*, pages 290–294, Madrid, Spain, March 2005.